Optical signal processing for space division multiplexed systems

Joseph Slim

▶ **To cite this version:**

Joseph Slim. Optical signal processing for space division multiplexed systems. Optics [physics.optics]. Université de Rennes, 2021. English. NNT : 2021REN1S004 . tel-03223184

HAL Id: tel-03223184

https://theses.hal.science/tel-03223184v1

Submitted on 10 May 2021

HAL is a multi-disciplinary open access archive for the deposit and dissemination of scientific research documents, whether they are published or not. The documents may come from teaching and research institutions in France or abroad, or from public or private research centers.

L'archive ouverte pluridisciplinaire **HAL**, est destinée au dépôt et à la diffusion de documents scientifiques de niveau recherche, publiés ou non, émanant des établissements d'enseignement et de recherche français ou étrangers, des laboratoires publics ou privés.

UNIVERSITÉ DE RENNES 1

THESE DE DOCTORAT DE

L'UNIVERSITE DE RENNES 1

ECOLE DOCTORALE N° 596
Matière, Molécules, Matériaux
Spécialité : *Photonique*

Par

Joseph SLIM

Optical signal processing for space division multiplexed systems

Thèse présentée et soutenue à Lannion, le 17 février 2021
Unité de recherche : Unité Mixte de Recherche n°6082 Institut FOTON

Rapporteurs avant soutenance :

Karsten Rottwitt	Professeur des universités / Technical University of Denmark
Esben Ravn Andresen	Maître de conférence HDR / Université de Lille

Composition du Jury :

Président :	Monique Thual	Professeure des universités / Université de Rennes 1
Examinateurs :	Julien Fatome	Ingénieur de recherche / Université de Bourgogne
Dir. de thèse :	Christophe Peucheret	Professeur d'Université / Université de Rennes 1
Co-dir. de thèse :	Mathilde Gay	Ingénieur de recherche / Institut Foton - CNRS UMR 6082

Table of contents

Acknowledgments

I would like to thank Christophe Peucheret and Mathilde Gay for their support to complete this work. I would also like to thank Kamal Hussain, Alberto Parini, Paulo Ferreirinha de Almeida and Amiri Sultani Mziray for helpful discussions. A very special thanks to Patrice Feron, Olivier Durand, Olivier Berder, Monique Thual and Pascal Besnard.

List of Acronyms

AOSP all-optical signal processing

BS Bragg scattering

CW continuous wave

DMD differential mode delay

DSP digital signal processing

DSF dispersion-shifted fiber

EDFA erbium-doped fiber amplifier

FMF few-mode fiber

FWHM full-width at half maximum

FWM four-wave mixing

GER gain extinction ratio

GVD group velocity dispersion

IGV inverse group velocity

MCF multicore fiber

MDM mode-division multiplexing

MI modulation instability

MIMO multiple-input multiple-output

MMF multimode fiber

NLSE nonlinear Schrödinger equation

OEO optical-to-electrical-to-optical

PC phase conjugation

PDM polarization-division multiplexing

PSA phase-sensitive amplification

PSFC phase-sensitive frequency conversion

QAM quadrature amplitude modulation

QPSK quadrature phase shift keying

SDM space-division multiplexing

SMF single-mode fiber

SM-NE single-mode nonlinear element

SNR signal-to-noise ratio

SPM self-phase modulation

TDM time-division multiplexing

WDM wavelength-division multiplexing

XPM cross-phase modulation

ZDW zero-dispersion wavelength

Summary in French

Depuis l'invention des fibres optiques, l'évolution de leur capacité de transmission ne cesse d'augmenter. Plusieurs percées technologiques telles que l'amélioration de la fabrication des fibres, ont permis de développer des fibres à faible perte, et les amplificateurs à fibre dopée à l'erbium ont permis une amplification optique à large bande. Toute cette croissance a soulevé des défis pour trouver de nouvelles technologies pour étendre la capacité des réseaux. Historiquement, cette croissance a été soutenue par l'exploration de plusieurs techniques de multiplexage, comme le multiplexage en longueur d'onde, multiplexage en polarisation, multiplexage temporel et modulation d'amplitude.

Selon la théorie de Shannon, la capacité d'un canal de communication s'étend linéairement avec la bande passante du canal et logarithmiquement avec le rapport signal sur bruit. Ainsi, l'augmentation de la puissance du signal augmente le rapport signal sur bruit et réduit l'impact du bruit, et il n'y a pas de capacité maximale tant que la puissance du signal peut être augmentée. Cependant, dans un réseau optique typique, l'augmentation de la puissance d'une fibre optique augmente l'impact de la non-linéarité de la fibre. Et les fibres optiques présentent le phénomène non linéaire effet Kerr, qui introduit des distorsions qui augmentent avec la puissance du signal. Cela impose finalement une limite à la puissance du signal qui peut être utilisée, et la quantité d'informations transmises peut être limitée en raison de leur limite de capacité non linéaire, qui dépend des propriétés physiques de la fibre.

Les réseaux optiques actuels sont basés sur des fibres monomodes, dont nous ne sommes pas très loin d'approcher leur limite de capacité non linéaire. Bien qu'une approche alternative consiste à installer davantage de fibres monomodes en parallèle, des solutions alternatives doivent être envisagées pour la prochaine génération de systèmes de communication optique. En augmentant le rayon du cœur d'une fibre monomode, le nombre de modes supportés par la fibre augmente et la fibre peut être appelée fibre multimode. Ces fibres permettent la propagation de la lumière sur plusieurs trajets, et elles pourraient être considérées comme une solution efficace pour augmenter la capacité. En particulier, une dimension supplémentaire qu'est l'espace, peut être exploitée dans ces fibres pour transmettre des informations supplémentaires, conduisant au multiplexage spatiale qui consiste à utiliser des fibres multicœurs, ou des fibres légèrement multimodes. Dans les fibres multicœurs, les cœurs individuels de la fibre sont utilisés comme canaux indépendants pour transmettre les données. Et dans les fibres légèrement multimodes, la fibre supporte un petit nombre de modes, et ces

modes sont utilisés comme canaux indépendants pour transmettre les données, et cette technique de multiplexage est connue sous le nom de multiplexage modale.

La conversion des informations d'un signal vers un autre canal est l'une des fonctions essentielles du traitement du signal, qui peut être classée en deux catégories: électrique et tout optique. Dans le domaine électrique, les signaux optiques doivent être convertis en signaux électriques et traités dans le domaine électrique avant d'être reconvertis dans le domaine optique. Dans ce cas, le nombre de dispositifs optoélectroniques nécessaires augmente avec le nombre de modes de la fibre. Et plus le nombre de modes augmente, plus la complexité électronique augmente. C'est là que l'optique entre en jeu. Certaines fonctionnalités pourraient être exécutées plus efficacement directement dans le domaine optique, ce qui est connu par le traitement du signal tout-optique, comme la conversion de longueur d'onde, où la lumière contrôle la lumière par des effets non linéaires, à travers un dispositif non linéaire, et sans revenir à l'électronique.

Dans ce cas, les modes d'une fibre légèrement multimode peuvent être démultiplexés dans des fibres monomodes non linéaires, de sorte que le traitement tout-optique puisse être réalisé individuellement dans chacune d'eux, avant de les multiplexer à nouveau. Cependant, les multiplexeurs traditionnels incluent beaucoup de pertes lors de la combinaison des modes, qui augmentent avec le nombre de modes de la fibre. Une autre solution possible est d'utiliser des lanternes photoniques, où il n'est pas nécessaire d'effectuer un multiplexage et un démultiplexage en mode strict, car les photoniques lanternes excitent une combinaison linéaire de modes et permettent une transition sans perte du multimode au monomode. Mais la solution la plus simple serait toujours d'utiliser une seule fibre non linéaire multimode pour effectuer un traitement du signal tout-optique pour tous les modes simultanément. Pour ce faire, une meilleure compréhension des interactions multimodes non linéaires entre les modes est souhaitable, ce qui est le but de ce travail.

Le mélange à quatre ondes est un effet non linéaire qui peut être considéré comme un outil pour implémenter des fonctions de traitement du signal tout-optique. Il peut être réalisé dans des matériaux optiques non linéaires, où de nouvelles fréquences appelées idler sont générées. Par exemple, en considérant trois champs optiques, deux pompes et un signal, l'interaction non linéaire produit une nouvelle onde appelée idler par mélange à quatre ondes, qui amène les paires de photons à transférer l'énergie des fréquences des pompes aux fréquences du signal et de l’idler. Ceci est connu sous le nom de mélange à quatre ondes non dégénéré. Si les deux

fréquences des pompes coïncident, le processus est appelé mélange à quatre ondes dégénéré. Dans ce cas, une seule pompe puissante et un signal, produisent un idler par mélange à quatre.

Un mélange à quatre ondes significatif ne se produit que si les deux conditions de mélange à quatre ondes sont satisfaites. La première condition est la conservation de l'énergie, et elle définit l'espacement des fréquences entre les ondes en interaction. La deuxième condition est l'accord de phase, qui peut être exprimée à partir des constantes de propagation des ondes en interaction, et l'idler généré par mélange à quatre ondes dépend de l'accord de phase, qui doit être suffisamment petit pour obtenir un idler fort.

Lorsque toutes les ondes en interaction se propagent sur le même mode à l'intérieur de la fibre, le processus de mélange à quatre ondes peut être appelé mélange à quatre ondes intramodal. Et ce processus est généralement appelé instabilité de modulation. Son accord de phase dépend seulement sur la dispersion du second ordre. Cela signifie que pour avoir un accord de phase complet, la fibre doit avoir une dispersion du second ordre nulle.

Lorsque toutes les ondes en interaction se propagent sur différents modes à l'intérieur de la fibre, le processus de mélange à quatre ondes peut être appelé mélange à quatre ondes intermodal. Les deux principaux processus de mélange à quatre ondes intermodal sont généralement connus par conjugaison de phase et de diffusion de Bragg. Leur accord de phase dépend de la dispersion du second ordre, ainsi que de la dispersion du premier ordre, contrairement au cas intramodal précédent. Cela signifie que pour obtenir un accord de phase intermodal, la fibre doit avoir de petites différences de dispersion de premier ordre et de dispersion de second ordre entre les deux modes, de sorte que les deux termes dans l'équation d'accord de phase puissent être annulés.

Le mélange à quatre ondes entre différentes ondes peut être étudié en utilisant l'équation de Schrödinger non linéaire qui décrit la propagation dans les fibres optiques. Lorsque plus d'un mode se propage dans la fibre, le système devient plus compliqué, puisque les mélanges à quatre ondes intramodal et intermodal se produit simultanément entre les modes dans ce cas. Ainsi, les trois processus d'instabilité de modulation, de conjugaison de phase et de diffusion de Bragg se produisent en même temps et peuvent s'influencer mutuellement. Afin de montrer toutes les interactions possibles entre les ondes, l'équation de Schrödinger non linéaire multimode est utilisée. Dans ce cas, le nombre de coefficients non linéaires augmente avec le nombre de modes. Cependant, si nous calculons ces coefficients non linéaires, nous constatons que beaucoup d'entre eux sont identiques en raison de la forme spécifique de l'équation de l'aire

effective. De plus, certains d'entre eux sont moyennés à zéro, du fait de la symétrie des modes. Ces simplifications permettent de simplifier l'équation non linéaire de Schrödinger, qui nécessite des solutions numériques pour être résolu.

Une façon de le résoudre consiste à utiliser la méthode de ‘‘split-step Fourier method’’ en définissant deux opérateurs, dispersion et non-linéarité. La dispersion est considérée dans le domaine fréquentiel et la non-linéarité dans le domaine temporel. Et l'équation est alternativement résolue en fréquence et en temps. Par exemple, une fibre peut être divisée en un grand nombre de petits segments, et le split-step peut être appliquée dans chacun d'eux. Le champ optique se propage d'abord à la moitié de la distance du premier segment, où seule la dispersion est considérée. Ensuite, le champ est multiplié par le terme non linéaire au plan médian, puis le champ se propage dans l'autre moitié où seule la dispersion est à nouveau considérée. Le même raisonnement peut être appliqué pour le cas monomode et le cas multimode, sauf que dans le cas multimode le nombre d'équations augmente en fonction du nombre de modes, ainsi que le nombre d'opérateurs de dispersion et de non-linéarité.

Le Chapitre 1 décrit la motivation et l’objectif de la thèse. Dans le Chapitre 2, la théorie nécessaire pour décrire la propagation des ondes électromagnétiques dans les fibres multimodes est brièvement revue. Les phénomènes linéaires, ainsi que les phénomènes non linéaires tels que l'auto-modulation de phase, la modulation de phase croisée et le mélange à quatre ondes sont décrits. La propagation multimode basée sur l'équation de Schrödinger non linéaire multimode est décrite, ainsi que la méthode split-step pour la résoudre. Dans le Chapitre 3, la conception d’une fibre légèrement multimode qui permet de traiter les modes simultanément et indépendamment est présentée. En utilisant l'effet non linéaire de mélange à quatre ondes intramodal, des effets non linéaires tels que la conversion de longueur d'onde, la conversion de fréquence sensible à la phase et l'amplification sensible à la phase ont été étudiés. Dans le Chapitre 4, les interactions non linéaires entre les différents modes ont été étudiées en utilisant le mélange à quatre ondes intermodale. La conception d’une fibre légèrement multimode plus flexible qui permet de briser la condition principale imposée par le mélange à quatre ondes intermodale a été présentée. La fibre permet de réduire la contrainte de séparation ente les fréquences, et la réalisation des interactions non linéaires entre les ondes portées par différents modes d’une manière plus flexible.

1 Introduction

1.1 Motivation

Optical fibers form today the backbone of optical networks through all the planet, bringing people closer together than ever, and building a modern globalized world, due to their abilities of transporting modulated light over long distances with low attenuation and over a large bandwidth. An incredible progress and growth in optical communication systems has been seen, achieving a spectacular success thanks to low-loss silica based optical fibers, namely single-mode fibers (SMFs). Four decades ago, almost all communication systems relied in general on the transmission of information over electrical cables. Since its invention in the 1960s [1], optical fibers have reshaped terrestrial telecommunication systems with hundreds of thousands of kilometers of cables interconnected around the globe, providing the global communication networks. The ever-growing number of users and machines connected to the Internet and its associated applications, high-definition video, cloud-based services, mobile data [2, 3, 4] are the reason behind the growth of the capacity of optical communications. It is also expected that in the near future, more advanced technologies will have a contribution as well, concluding that the capacity limits of the communication infrastructure will be reached soon.

All this exponential growth urged the need to increase the capacity of SMFs, and raised the challenges to find new technologies to expand the capacity of the networks, in order to avoid a capacity crunch [5]. This growth has been sustained historically by exploring several innovative technologies of information multiplexing as shown in Figure 1.1, using different degrees of freedom or dimensions of a light beam in an SMF (wavelength, time, amplitude and phase, polarization). For instance, the wavelength is used for wavelength-division multiplexing (WDM), where each wavelength carries an independent data channel. The time is used for time-division multiplexing (TDM) by aggregating multiple low-speed data channels into high-speed data streams, while the amplitude and phase of an optical field are used for advanced multi-level quadrature amplitude modulation (QAM), and the polarization is used for polarization-division multiplexing (PDM) to double the channel capacity.

The technological implementation of WDM yield to a capacity growth by expanding the number of WDM channels, together with the occupied bandwidth of the erbium-doped fiber amplifiers (EDFAs) that enabled broadband optical amplification. The bandwidth of the amplifiers was fully occupied after the introduction of the systems with several hundreds of Gb/s. Increased efficiency in the use of spectrum led to further increases in capacity, resulting in an increased spectral efficiency. The use of PDM signals led to further increases in spectral efficiency, by transmitting two independent signals on the two polarization of light.

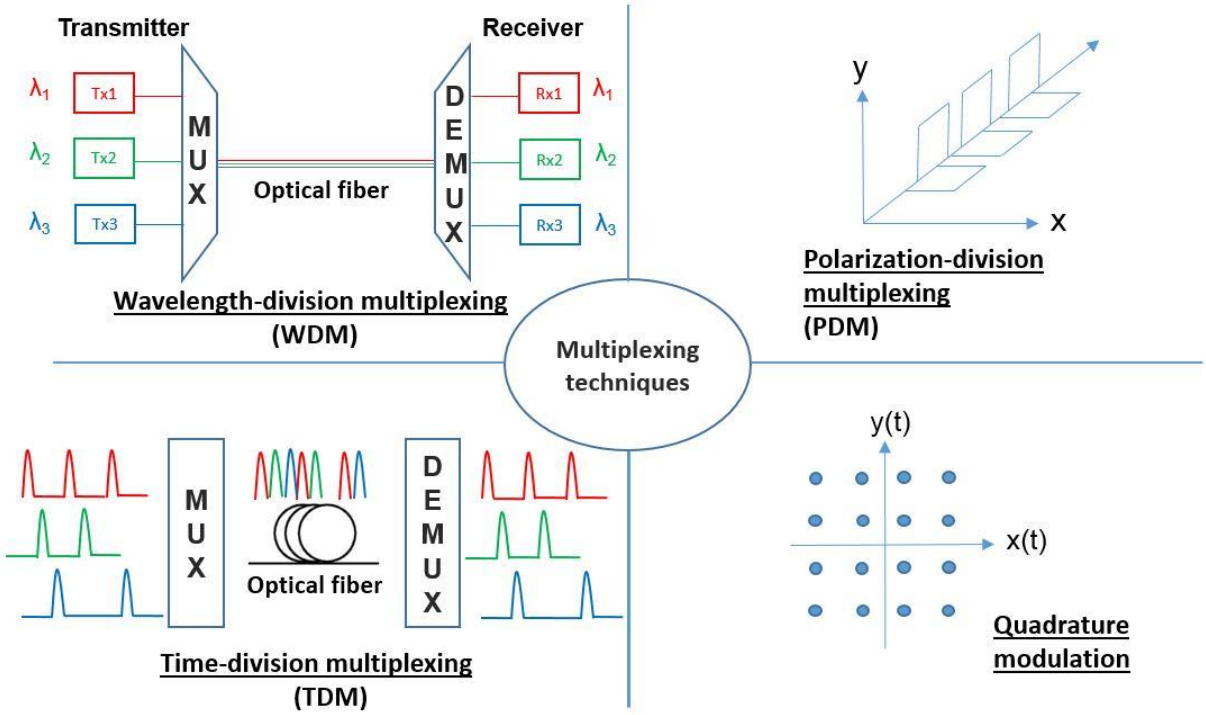

Figure 1.1: Physical dimensions (wavelength, time, amplitude and phase, polarization) with their corresponding multiplexing techniques.

Today's systems use multilevel modulation to increase the spectral efficiency, such as quadrature phase shift keying (QPSK) and QAM together with coherent detection enabling the decomposition of the phase and the amplitude. However, the use of more complicated signaling symbol arrangements reduces the systems tolerance to noise. According to Shannon's theory of channel capacity, the capacity of a communication channel scales linearly with the bandwidth of the channel, and logarithmically with the signal-to-noise ratio (SNR) [6]. Thus increasing the signal power increases the SNR and reduces the impact of noise, and there is no maximum capacity as long as the signal power can be increased. However, in a typical optical network, increasing the power in an optical fiber increases the impact of fiber nonlinearity.

In linear transmission systems, the major limitation is caused by additive noise [7], and the spectral efficiency can be raised by increasing the power of the transmitted signal. However, silica based optical fibers differ from other transmission media as they exhibit the nonlinear phenomenon Kerr effect [8], that introduces distortions that increase with the signal power. This eventually imposes a limit on the signal power that may be used, and a certain threshold not to exceed. Thus, the quantity of transmitted information in optical fibers can be limited due to their nonlinear capacity limit, that depends on the fiber physical properties such as loss and nonlinear coefficients and dispersion. Therefore, low performance of the system is expected as the signal power increases, where the maximum spectral efficiency can be reached before nonlinear signal distortions become dominant.

As the current backbone optical networks are exclusively based on SMFs, the studies on their nonlinear capacity-limits have indicated that we are not very far from approaching this limit [9, 10, 11], which means that achieving a further increase in spectral efficiency becomes more and more challenging. Although an alternative approach is to install more SMFs in parallel as a short term solution, alternative solutions must be considered for next generation of optical communication systems. Fiber supporting multiple spatial modes that allow more than a single path for the propagating light has gained significant attention over the past years [12]. There are different types of fibers supporting multiple spatial modes, that might be considered as an efficient solution to increase the capacity. In particular, an additional dimension that is space, has not been exploited yet. It could be exploited in these fibers to carry additional information, leading to the so called multiplexing technology space-division multiplexing (SDM) [13, 14]. SDM relies on the spatial distribution of optical fields, and it consists in using multicore fibers (MCFs) [15, 16] or few-mode fibers (FMFs) [17, 18], where individual cores of a MCF, or spatial modes of an FMF based on mode-division multiplexing (MDM), are used as independent channels to transmit the data.

As the increased number of frequency channels in a SMF increases the total intensity followed by detrimental nonlinear effects, the power in SDM systems can be distributed across a larger spatial region in MCFs or FMFs which leads to a reduced intensity, and hence nonlinear effects impact. Figure 1.2 shows cross-sections of fibers supporting multiple spatial modes. Figure 1.2 (a-b) show MCFs with different number of cores each supporting one fiber mode, and separated by the same distance in a hexagonal grid. These fibers allow to increase the capacity proportionally to the number of cores. Depending on the design, the cores of a MCF can be independent cores, or coupled cores. Independent cores allow independent transmission

channels in the fiber. This type of fibers can be designed with a core separation sufficiently large to reduce linear coupling between them. This in turns limits the spatial density of cores in the fiber. Alternatively, heterogeneous cores that reduce crosstalk can be used [19]. However, coupled-core MCFs allow strong coupling between cores, and the data initially launched in each core of the fiber, exit the fiber from multiple cores. Hence, multiple-input multiple-output (MIMO) digital signal processing (DSP) is required in this case to recover back the data [20]. Coupled-core MCFs allow a larger density of cores. It has also been shown that coupling between the cores of a MCF leads to lower nonlinear signal degradation [21].

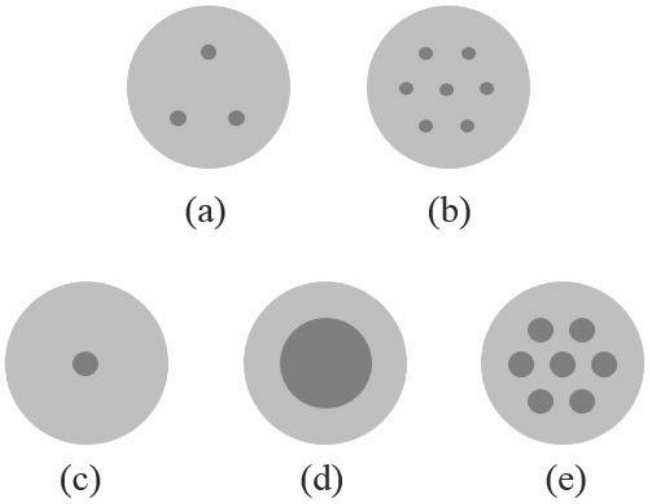

Figure 1.2: Cross-sections of fibers supporting spatial multiplexing. (a) 3-core, (b) 7-core, (c) few-mode fiber, (d) multimode fiber and (e) multicore-multimode fiber.

The number of spatial modes guided in an optical fiber increases with the core diameter. Therefore, by increasing the core size of a SMF, the number of the spatial modes supported by the fiber increases. If the fiber core supports a few number of spatial modes, the fiber can be called FMF. Such a fiber core is shown in Figure 1.2(c), and these fibers have gained a significant interest in the last years, as they can be efficient to use for SDM systems. If the fiber core supports a large number of spatial modes, the fiber can then be called multimode fiber (MMF), and is depicted in Figure 1.2(d). Similarly, the modes in a MMF can be uncoupled and coupled. For the case of uncoupled modes, the fiber can be designed with sufficiently different propagation constants between its spatial modes in order to suppress linear coupling, under ideal conditions [22]. When designing uncoupled-mode MMF or uncoupled-core MCF, the main challenge is to fabricate fibers with large spatial density of modes, and prevent linear mode coupling. For the case of coupled-mode MMFs, there is no need to impose restrictions

on the design and suppress linear mode coupling, as MIMO techniques can be applied to recover the data. However, the modes of MMF spatially overlap each other during the propagation, in contrast to MCFs. This in turns leads to nonlinear interaction between the modes, which will be the main focus of this work. Figure 1.2(e) shows a combination of a MCF and a MMF where it is possible to further increase the capacity.

In Figure 1.3, a schematic of a SDM transmission system is shown. Transmitters generate optical signals that are subsequently multiplexed onto different wavelengths and different spatial paths in the cores of a MCF, or the modes of a MMF. As SDM systems require development of special fibers supporting multiple spatial modes, they require as well spatial mode multiplexers and demultiplexers. Different multiplexing techniques have been proposed in order to couple signals from SMF into a MCF or a MMF. For instance, a number of SMFs can be adiabatically tapered together so that the core distances between the SMF cores fit the core distances of the MCF [23]. Achieving the SMF-MCF connection can be made as well through a 3D waveguide of glass or polymer in which light-guiding cores are inscribed with a short-pulse laser [23]. Another way of coupling in MCFs based on a system of lenses via free space from one fiber facet to another has been proposed [23].

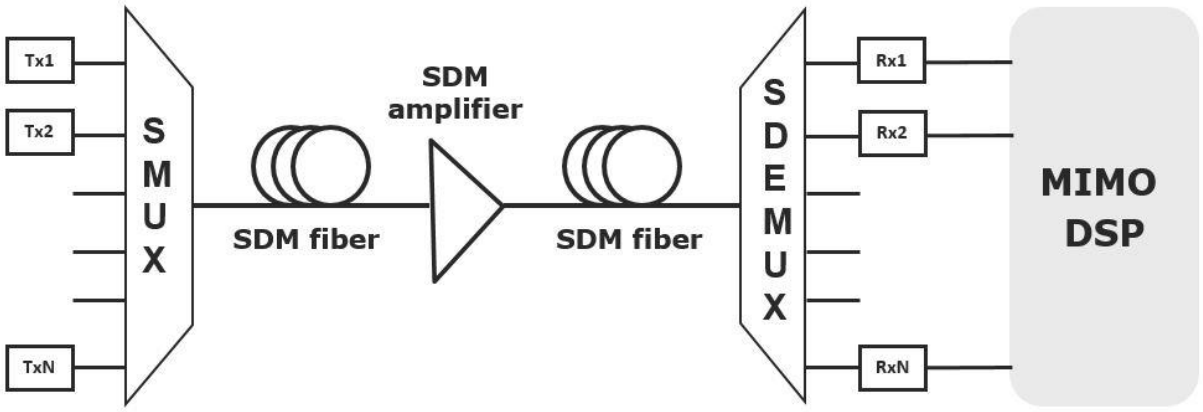

Figure 1.3: Schematic of SDM transmission system based on MIMO DSP.

As for the coupling between SMF-MMF, the most common type consists in exciting the individual modes in a MMF using phase-plates to convert beams of a SMF to field distributions similar to the MMF modes [24], which inserts losses. Silicon photonic integrated mode multiplexer has been presented with large loss as well [25]. Compact fiber grating coupler on silicon optical techniques with low loss has been demonstrated [26]. Moreover, multiple spot signal launch based on low-loss mode coupler has been proposed [27], it excites different spatial

locations of the fiber with spatially separated spots. Interestingly, photonics lanterns allow to merge different SMFs into one MMF through adiabatic taper, achieving thus lossless transition from MMF to SMF by exciting a linear combination of modes [28]. As for demultiplexing, same multiplexing techniques can be used.

A SDM system requires SDM optical amplifiers. Different amplification techniques have been proposed for transmissions over MCFs and MMFs. In particular, it has been shown that MCFs with erbium-doped cores can amplify multiple spatially separated channels, by individually pumping the cores [29], or by pumping the cladding [30]. EDFAs for SDM in FMFs have been demonstrated as well [31]. As mentioned earlier, when coupling between the modes occurs during the transmission, MIMO DSP is required on the output signals recovered by the receivers to equalize the coupling. Given that SDM requires different components to be implemented (transmitters, amplifiers, receivers and a transmission medium), the energy consumption and possible cost reductions effectiveness of SDM transmission system should be quantified compared to single-mode systems [32].

While the capacity increase was mostly sustained by advances on optical and electrical systems, mainly by improving the fiber quality and the transmitters-receivers electronics, the conflict between network capacity and the general concept of noise (linear and nonlinear distortions) in optical fiber communication will always be challenging, as it limits the reach between the two locations of a link. Thus, the signal always needs to be rebuilt using repeaters, which is known as regeneration. In this case, the signal is received and generated again using repeaters that operate through optical-to-electrical-to-optical (OEO) conversion. This consumes large amount of power, as repeaters are expensive components in terms of financial cost and energy consumption. The invention of EDFAs led to a revolution in optical communication systems [33], when optical fibers were doped with rare-earth elements to perform optical amplification and compensate the attenuation losses. The improvement was mainly due to removed need of expensive repeaters and OEO conversions, as well as efficient amplification of many wavelengths at the same time.

While nonlinearities are identified as the major limitation of transmission over silica based fibers, silica fibers have led to the advent of new field of nonlinear fiber optics, where several nonlinear effects were demonstrated, including stimulated Brillouin scattering and Raman scattering [34, 35] and Kerr-effect [36]. It is however believed that nonlinearities can be exploited to perform some processing functionalities more efficiently directly in the optical domain, a set of techniques known as all-optical signal processing (AOSP) [37]. The

femtosecond response time of nonlinearities in optical materials can be used to process and manipulate the signals, and thanks to the second-order $\chi^{(2)}$ and third-order $\chi^{(3)}$ susceptibilities, different devices have proved to be useful for optical signal processing, such as semiconductor optical amplifiers [38], highly nonlinear fibers [39], silicon waveguides [40], chalcogenide waveguides [41], periodically poled lithium niobate waveguides [42] and photonics crystals [43]. Several functionalities can be performed in these nonlinear devices, where optical signals can be processed directly in the light domain while eliminating the need of OEO conversions, such as all-optical regeneration [44, 45].

Moreover, functionalities and applications such as dispersion compensation [46], wideband comb regeneration [47], demultiplexing [48], optical sampling [49] and low-noise amplification [50] based on parametric effects have been demonstrated. Optical parametric amplifiers have received notable attention due to the need of amplification outside the erbium band, which allows as well to reduce the noise over conventional EDFAs, and subsequently increase the propagation distance. Wavelength conversion is another interesting AOSP functionality that increases the flexibility of dynamic wavelength-routed network [51], where the information carried on one signal could be transferred to another wavelength channel. Figure 1.4(a) shows an electrical wavelength conversion scheme when OEO conversions are required, and Figure 1.4(b) shows an AOSP wavelength conversion when eliminating OEO. AOSP has received notable attention due to its capability of increasing the capacity of optical networks by making use and exploiting nonlinear effects that are actually detrimental to optical transmission systems, while avoiding OEO conversions.

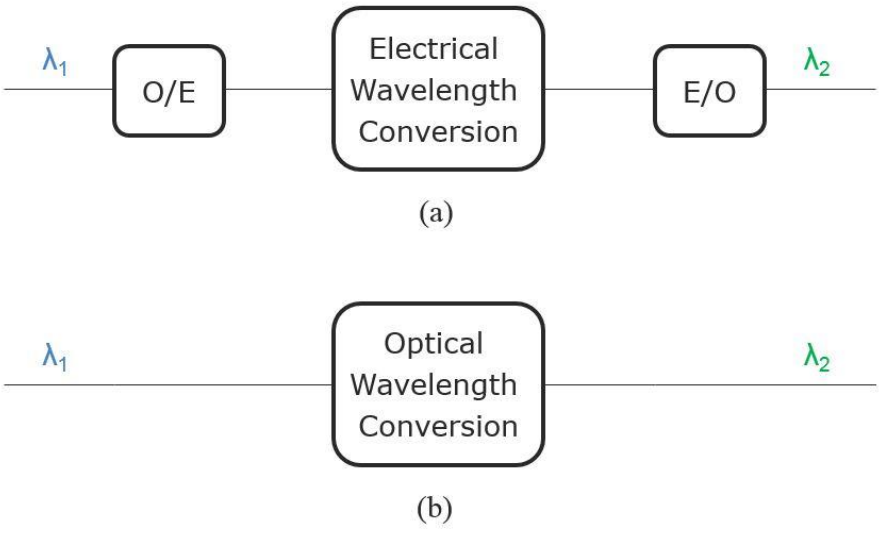

Figure 1.4: (a) Electrical wavelength conversion and (b) all-optical wavelength conversion.

1.2 Research Aims

AOSP has been proven to provide different functionalities in optical fiber communication. However, since a fiber capacity crunch is looming and SDM is being investigated as potentially being a lower cost solution and reduced management complexity, it is then necessary to investigate whether AOSP functionalities can be adapted to this context. In the following, the example of wavelength conversion in MDM will be considered.

Therefore, converting the information on a signal to another channel is one of the essential functions in signal processing, that can be classified in two categories: electrical and all-optical. In the electrical domain, optical signals have to be converted to electrical signals and processed in the electrical domain before being converted back to the optical domain as the scheme shown in Figure 1.4(a). This process known as OEO has some disadvantages such as power consumption and slower response time of optoelectronic/electronic devices comparing to AOSP, that has the capability to perform wavelength conversion faster with large bandwidth thanks to ultrafast nonlinear effects such as the Kerr effect.

Furthermore, wavelength conversion in MDM systems is quite different from that of single mode cases. As shown in Figure 1.5(a), OEO requires several pairs of transmitters and receivers that increase according to the number of modes of the FMF. Moreover, the unavoidable random mode mixing during the propagation in the fiber requires DSP to unwrap the scrambled modal information, thus complicating the MDM-OEO system significantly more than the single mode-OEO system.

This is where optical methods might be more advantageous, by directly processing the optical signals. In fact, in AOSP area, light controls light by nonlinear effects, through a nonlinear device, without going back through electronics. In this case, the modes of an FMF can be demultiplexed into single-mode nonlinear elements (SM-NE) in a first step, so that wavelength conversion can be performed individually in each one, before multiplexing them again for further transmission as shown in Figure 1.5(b). However, mode multiplexers suffer from mode combining losses, that scale with the number of modes of the fiber. Another possible solution is to use photonic lanterns [52], where there is no need to perform strict mode multiplexing and demultiplexing. Photonic lanterns excite a linear combination of modes and allow lossless transition from multimode to single mode (Figure 1.5(c)).

However, the easiest and most simplified method would always be to use a single multimode nonlinear fiber to perform wavelength conversion for all modes simultaneously (Figure 1.5 (d)), which will be one of the purposes of this work. In order to do so, a better understanding of nonlinear multimode interactions is desirable.

An important observation and common point regarding SDM can be noticed. That is, SDM always offers to reduce management complexity of the systems. For instance, and in terms of transmission capacity as discussed earlier, the capacity of an N mode MMF could be made comparable to that of N SMFs, making it more favorable to use a single MMF instead of N SMFs, thus reducing the complexity of the systems. Similarly, if AOSP can be performed in a single fiber for all the modes simultaneously, SDM may then be considered as one long term cost effective solution for optical networks.

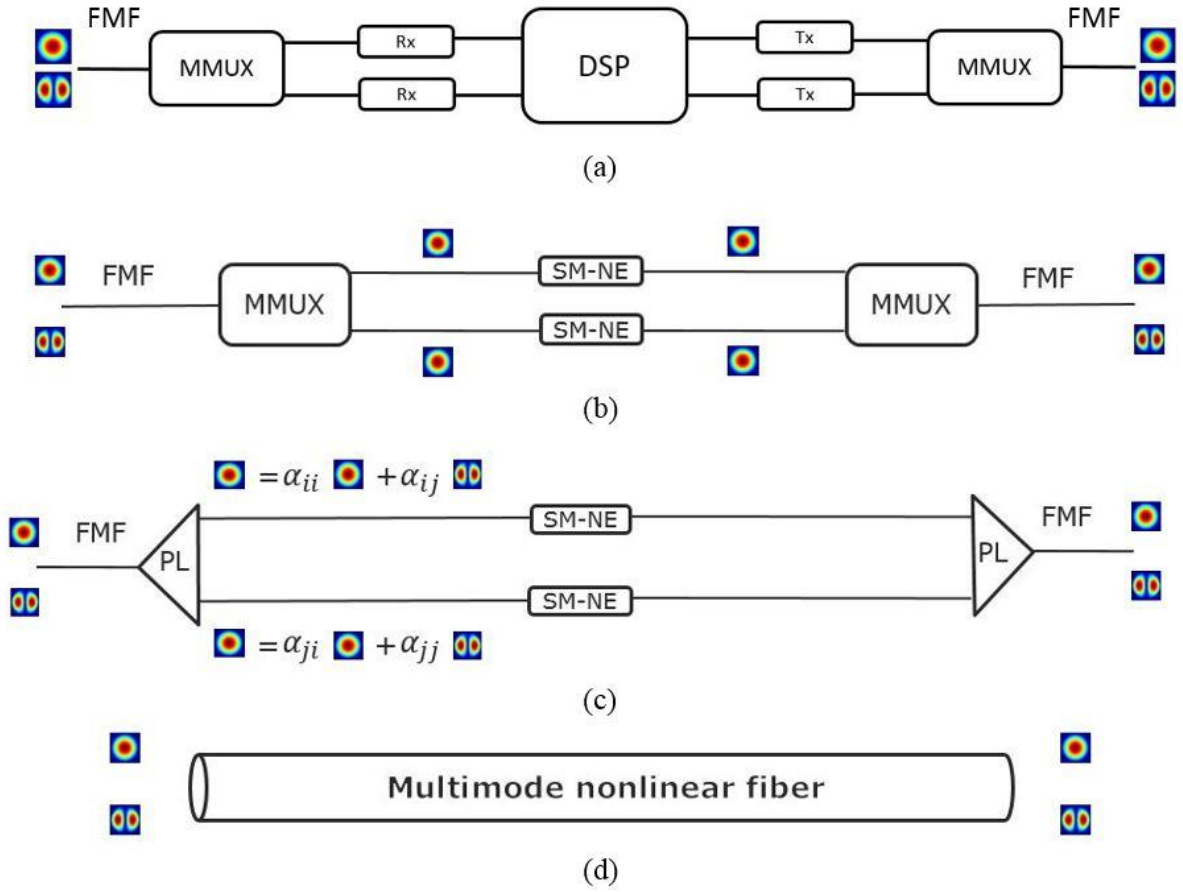

Figure 1.5: (a) signal processing through electrical domain, requiring OEO conversions when the two modes LP_{01} and LP_{11} are considered, (b) signal processing in optical domain using SM-NE, (c) signal processing in optical domain by replacing mode multiplexers with photonic lanterns and (d) ideal solution of signal processing in a single multimode nonlinear fiber. Rx: receive; Tx: transmit; DSP: digital signal processing; FMF: few-mode fiber; MMUX: mode multiplexer; SM-NE: single-mode nonlinear element; PL: photonic lanterns.

While nonlinear effects have been vastly investigated and exploited in SMFs [8], they were given comparatively little attention in MMFs. Despite the fact that nonlinear effects were first observed in FMFs [53], their impact on multiple spatial modes propagating in FMFs is still an area with many unknowns, as less is known about their interactions in this case. Furthermore, they have found applications in FMFs such as few-mode Raman amplifiers [54], optical switching [55], supercontinuum generation [56, 57], wavelength conversion [58], as well as parametric amplification [59] given that all data channels transmitted over different spatial modes need to be processed simultaneously.

Four-wave mixing (FWM) is one nonlinear effect that is particularly attractive in order to implement AOSP functionalities, including parametric amplification and wavelength conversion [60, 61, 62]. It can be performed in nonlinear optical materials that show a third-order susceptibility, where new frequencies, called idlers, are generated, depending on the allocation of input frequencies. The efficiency of FWM processes depends on the fulfillment of the phase matching condition, that depends on the dispersion properties of the fiber modes. In FMFs, two different types of FWM exist, known as intramodal FWM and intermodal FWM.

In the intramodal case, the interacting waves are all carried by the same spatial mode. In order to have efficient intramodal FWM processes on multiple modes in the same FMF, the phase matching condition should be satisfied for all the modes simultaneously. Several FMFs have been designed for the purpose of simultaneously achieving efficient parametric amplification [63, 64, 65] on multiple modes by tailoring the refractive index of the fiber in a way to obtain close values of the zero-dispersion wavelengths (ZDWs) for all the modes, while shifting them to the C-band. Furthermore, high values of inverse group velocity (IGV) differences between the modes are needed to prevent undesired intermodal processes. Although a number of fibers have been designed for this purpose, their fabrication is challenging due to fabrication tolerance issues. Furthermore, commercially available FMFs have different dispersion properties for the different supported modes, which prevent the phase matching condition from being simultaneously satisfied for all the modes over a large bandwidth. As a result, such simultaneous intramodal processes remain to be experimentally demonstrated. Alternatively, the use of photonic lanterns has been proposed, for example, to simultaneously wavelength-convert signals carried by all the modes supported by the transmission FMF as the scheme shown in Figure 1.5(c). In such a scheme, photonic lanterns are used to convert MDM signals into single mode tributaries, followed by parallel single-mode wavelength conversions and single-to-multimode conversion [66]. The scheme is however cumbersome, and the ideal

solution would be to simultaneously perform FWM wavelength conversion for all the modes in a single multimode nonlinear fiber.

Intermodal FWM between different spatial modes, has been observed for the first time in the 1970's by Stolen et al. [67], and has since been investigated in a number of studies [68, 69, 70, 71, 72, 73, 74], revived by the ongoing interest on MDM. Two main intermodal FWM processes can occur in an FMF, referred to as phase conjugation (PC) and Bragg scattering (BS). In contrast with intramodal FWM, the phase matching condition for intermodal FWM depends not only on the group velocity dispersion (GVD) of the modes, but also on their IGVs. Ensuring phase matching in the intramodal case thus requires operating near the ZDW, whereas, in the intermodal case, phase matching can be fully satisfied in the presence of large GVD. This has been reported in a number of experiments where intermodal FWM was found to be phase-matched over a specific frequency separation between the interacting waves carried by different modes [75, 76, 77], which limits the bandwidth of the conversion efficiency. While several FMFs have been designed to achieve large conversion bandwidths and high conversion efficiencies of multiple intramodal FWM processes in the same fiber [64, 65], designing an FMF that allows large intermodal FWM bandwidths for both PC and BS processes simultaneously seems to be more complicated. Nevertheless, a step-index MMF was proposed for bandwidth enhancement of the PC process when modes LP_{01} and LP_{02} are employed [78], and a graded-index MMF was proposed for bandwidth enhancement of the BS process when modes LP_{01} and LP_{11} are employed [79].

Accordingly, the objective of this work is to perform all-optical wavelength conversion by FWM nonlinear effect. The objective is divided into two goals: intramodal goal and intermodal goal, and they both require a specific fiber design. The fiber designed for the intramodal goal is to process the modes of the fiber simultaneously and independently, using the intramodal FWM nonlinear effect. However, the fiber designed for the intermodal goal is to broaden the bandwidth of interaction between the different modes of the fiber, thus broadening the bandwidth of conversion efficiency of the intermodal FWM nonlinear effects, known as PC and BS processes.

1.3 Outline

In Chapter 2, the theory needed to describe the propagation of electromagnetic waves in MMF is briefly reviewed. Linear phenomena, as well as nonlinear phenomena such as self-phase modulation (SPM), cross-phase modulation (XPM) and FWM are recalled from the literature. The multimode propagation based on the multimode nonlinear Schrödinger equation (NLSE) is discussed, as well as the split-step Fourier method used for solving it. In Chapter 3, we present the design of an FMF, that allows to process the modes simultaneously and independently. Using the intramodal FWM nonlinear effect, mode-independent nonlinear effects such as wavelength conversion, phase-sensitive frequency conversion (PSFC) and phase-sensitive amplification (PSA) were investigated. In Chapter 4, nonlinear interactions between different modes will be studied based on intermodal FWM. We present a more flexible design of an FMF that allows to break the main condition imposed when performing intermodal FWM. The fiber allows to reduce the constraint of limited frequency separation, and relax the detuning range between the interacting waves carried by different modes.

2 Wave Propagation in Optical Fibers

2.1 Optical Fibers

Optical fibers consist of the three parts: core, cladding and coating. The core is surrounded by the cladding, and its refractive index n_1 is greater than that of the cladding n_2. The coating exists just for mechanical protection and does not affect the light guiding. Optical fibers are usually made of silica (SiO_2) glass, and the refractive index profile is controlled by the concentration and distribution of dopants, such as germania (GeO_2). Figures 2.1(a-b) show cross sections and refractive index profiles of standard single mode and multimode step-index fibers. In a step-index optical fiber, the refractive index of the core n_1 is constant, and it undergoes an abrupt change at the core-cladding interface. The phenomenon that governs the propagation is total internal reflection, where light is guided due to the difference in refractive index between the core and cladding. Figure 2.1(c) shows the refractive index profile of a graded-index MMF. The refractive index of the core in this type of fiber is not constant, but it follows a certain function as it decreases gradually as a function of the radial distance from the center of the fiber, while the refractive index of the cladding remains usually constant. Graded-index MMFs have an advantage over step-index MMFs, which is their ability to limit modal dispersion, because the total reflection happens at an angle before the ray reaches the core-cladding interface, thus the rays follow a sinusoidal path which increases their velocities.

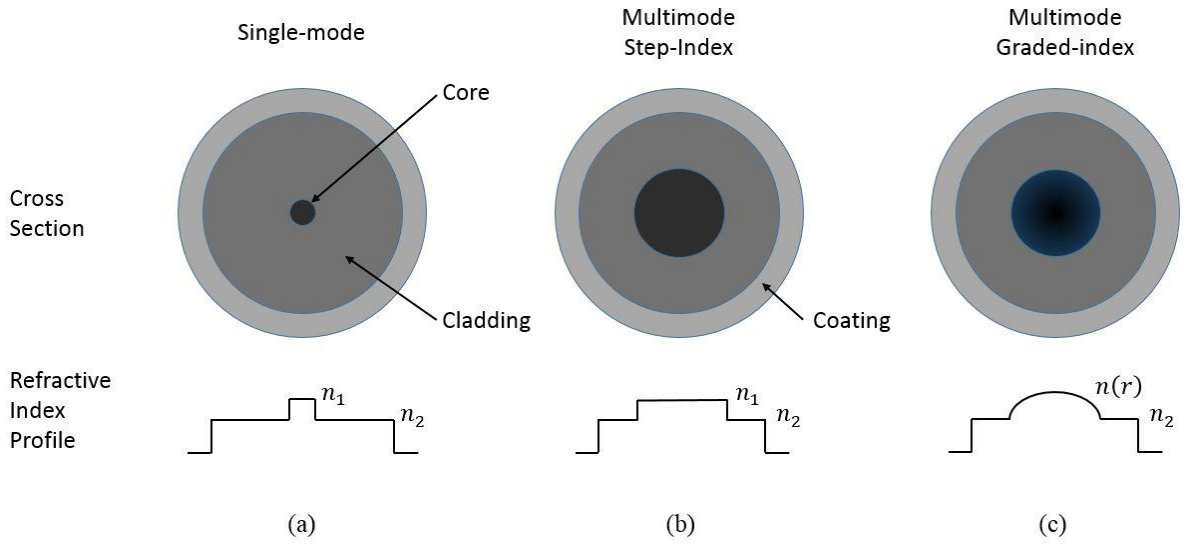

Figure 2.1: Cross section and refractive index profile of a (a) single-mode fiber, (b) step-index multimode fiber and (c) graded-index multimode fiber.

2.1.1 Fiber Modes

An optical fiber is a circular waveguide, where the propagation of optical fields is governed by Maxwell's equations. Therefore, electromagnetic waves should be considered in cylindrical coordinate system (r, ϕ, z), where the electric field **E** and magnetic field **H** can be written as

$$\mathbf{E}(r, \phi, z, t) = E(r, \phi) \exp[j(\omega t - \beta z)] \tag{2.1}$$

$$\mathbf{H}(r, \phi, z, t) = H(r, \phi) \exp[j(\omega t - \beta z)] \tag{2.2}$$

with ω as the frequency, β the propagation constant, and t is time. $E(r, \phi)$ and $H(r, \phi)$ are the transverse distribution of the electric and magnetic fields, respectively. The optical fields that propagate in optical fibers can be represented as guided modes, where each mode has a field distribution and a propagation constant. More specifically, the modes are the solution of the wave equation in cylindrical coordinates, that is solved by satisfying specific boundary conditions [8]. Considering an optical fiber with n_1 the refractive index of the core and n_2 the refractive index of the cladding, the modes propagating can be classified using two integers ν and m. The m value is called the radial mode number and represents the number of radial nodes that exist in the field distribution. The ν value is called the angular mode number, and represents the number of angular nodes that exist in the field distribution. The fiber modes are characterized by their effective indices n_{eff} and their propagation constants given by $\beta = n_{eff} k_0$, in the range

$$k_0 n_1 > \beta > k_0 n_2 \tag{2.3}$$

where k_0 is the free space propagation constant defined as $k_0 = \omega/c = 2\pi/\lambda$, with c as the velocity of light and λ is the wavelength of the optical field oscillating at the frequency ω.

In the case of *weakly guiding approximation* ($\Delta n = n_1 - n_2 \ll 1$), the core and the cladding indices can be approximated as identical ($n_1 \approx n_2$). In this case, the modes are degenerate and called linearly polarized modes ($\text{LP}_{\nu\text{m}}$). Figure 2.2 shows the intensity distributions of several modes of an optical fiber.

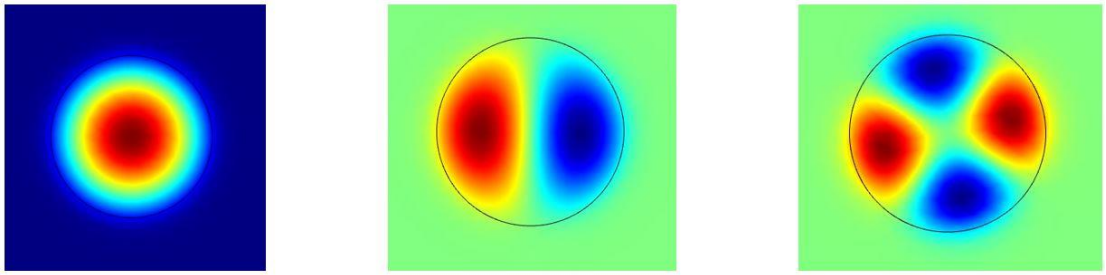

Figure 2.2: Intensity distribution of three exemplary linearly polarized modes, (a) the fundamental mode LP_{01}, (b) LP_{11} mode and (c) LP_{21} mode.

It should be noted that the solutions of the wave equation are denominated as TE, TM, HE and EH. These modes are called the true modes of the fiber. When $\nu = 0$, the propagating modes are called TE (transverse electric) or TM (transverse magnetic). The TE modes have no electric field along the longitudinal axis, and the TM modes have no magnetic field along the longitudinal axis. These transverse modes have no azimuthal structure $(\nu = 0)$. However, when $\nu \neq 0$, the propagating modes HE or EH are called "hybrid" modes, and they exist only for $\nu \geq 1$, therefore they have azimuthal structure. While TE and TM modes have no electric and magnetic field along the longitudinal axis, hybrid modes have both electric and magnetic field along the longitudinal axis. They are called HE or EH according to the dominating electric or magnetic field, and they appear in a two-fold degeneracy as even and odd modes with a $\pi/2$ phase difference.

It is usually difficult to solve the characteristic equation for the hybrid modes after applying the boundary conditions, whose solutions determine the propagation constant [8]. However, many simplification occurs if the *weakly guiding approximation* is adopted. In this case, TE_{0m} is degenerate with TM_{0m}. Similarly, $HE_{\nu+1,m}$ modes and $EH_{\nu-1,m}$ modes are degenerate. Therefore, with the help of the superposition principle for modes with equal propagation constants and under the *weakly guiding approximation*, it is possible to translate the modes into $LP_{\nu m}$ modes. Accordingly, different combinations of degenerate true modes can be linearly combined. For instance, Figure 2.3 shows the combination of the two modes TE_{01} and HE_{21} that leads to a mode whose transverse intensity distribution consists in two lobes that is linearly polarized, and defines the structure of the mode LP_{11}^{odd}.

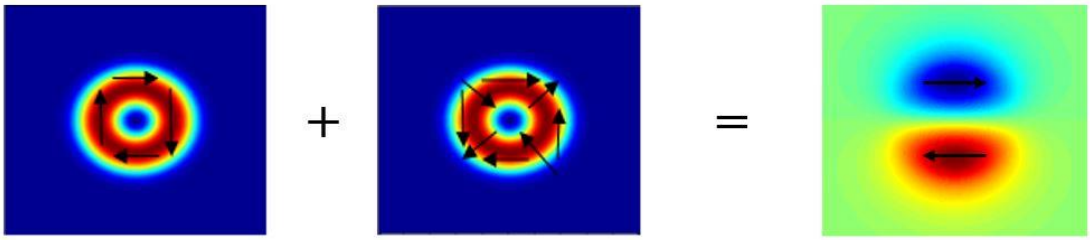

Figure 2.3: The superposition of the TE_{01} and odd HE_{21} modes that leads to the odd LP_{11} mode. Arrows denote polarization.

The designation and construction of the LP modes are summarized in Table 1.1:

Combination of True Modes	**LP Modes**	**Total Degeneracy**
$\mathbf{HE_{1m}}$ **(even)** $\mathbf{HE_{1m}}$ **(odd)**	LP_{0mx} $(\nu = 0)$ LP_{0my}	2
$\mathbf{HE_{2m}}$ **(odd) +** $\mathbf{TE_{0m}}$ $\mathbf{HE_{2m}}$ **(even) -** $\mathbf{TM_{0m}}$ $\mathbf{HE_{2m}}$ **(even) +** $\mathbf{TM_{0m}}$ $\mathbf{HE_{2m}}$ **(odd) -** $\mathbf{TE_{0m}}$	LP_{1max} LP_{1may} $(\nu = 1)$ LP_{1mbx} LP_{1mby}	4
$\mathbf{HE_{\nu+1,m}}$ **(odd) +** $\mathbf{EH_{\nu-1,m}}$**(odd)** $\mathbf{HE_{\nu+1,m}}$**(even) -** $\mathbf{EH_{\nu-1,m}}$**(even)** $\mathbf{HE_{\nu+1,m}}$**(even)+** $\mathbf{EH_{\nu-1,m}}$ **(even)** $\mathbf{HE_{\nu+1,m}}$ **(odd) -** $\mathbf{EH_{\nu-1,m}}$ **(odd)**	$LP_{\nu max}$ $LP_{\nu may}$ $(\nu \geq 2)$ $LP_{\nu mbx}$ $LP_{\nu mby}$	4

Table 1.1: Superposition of true vector modes that leads to linearly polarized modes.

All LP modes are a linear combination of different true fiber modes, except for LP_{0m} that are just composed of HE_{1m} modes. Each mode exists in two orthogonal polarizations. Therefore, the modes LP_{0m} have a degeneracy of two. However, besides the two orthogonal polarizations that the mode LP_{11} can have, two orthogonal field distributions can be obtained by a rotation of $\pi/2$, and the mode LP_{11} distributions are usually referred to as LP_{11a} and LP_{11b}, where a and b are the orientation of the mode. Thus there are four degenerate LP_{1m} modes (two orientations of the lobes, each with two possible polarizations). Similarly, the modes having an azimuthal number $\nu \geq 2$ have a degeneracy of four.

An important parameter used to characterize the guided modes in an optical fiber is the normalized frequency number (V) that is given by

$$V = \frac{2\pi a}{\lambda}\sqrt{n_1^2 - n_2^2} \tag{2.4}$$

where a is the radius of the core. The normalized frequency is useful for determining the cutoff conditions, as well as other parameters such as the total number of allowed modes, hence, it provides an answer whether a given mode will propagate in the fiber or not. Therefore, the normalized frequency should be chosen first when designing a fiber with a given number of modes.

The normalized propagation constant b is used to characterize the mode guiding strength, and is defined as

$$b = \frac{\beta^2 - k_0^2 n_2^2}{k_0^2(n_1^2 - n_2^2)} \tag{2.5}$$

Figure 2.4 shows the normalized propagation constant b as a function of the normalized frequency V for a few of the lower-order modes LP_{vm}. The cutoff condition is used, when a given mode cease propagating if V becomes smaller than a specific number. For example, the propagation of the mode LP_{11} is not allowed in the fiber when V becomes smaller than 2.405. However, the mode LP_{01} that is called fundamental mode or HE_{11} mode, has no cutoff condition because it is always allowed, and every fiber supports this mode.

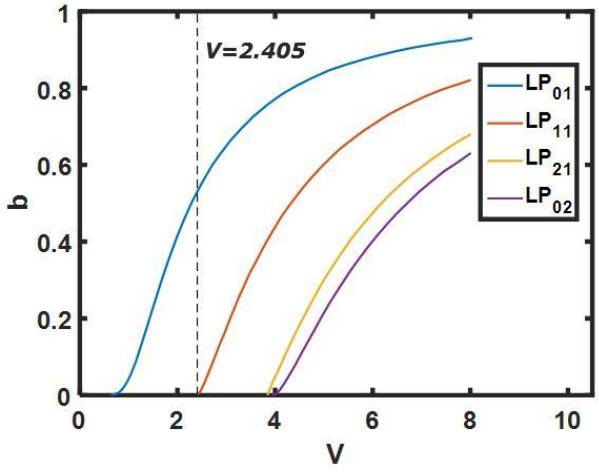

Figure 2.4: Normalized propagation constant b as a function of V for a few propagation modes, where cut-off condition for single mode propagation occurs for V < 2.405.

2.1.2 Fiber Losses

Transmitted optical signals through optical fibers suffer from attenuation due to loss occurring from different factors. Attenuation then plays an important role in determining the maximum transmission distance between the transmitter and the receiver. If P_{in} is the power launched at the input of a fiber of length L, the transmitted power P_{out} at the output will be given by

$$P_{out} = P_{in}\, e^{-\alpha L} \tag{2.6}$$

where α is the attenuation coefficient. The ratio of the output to the input power in a length unit of propagation is usually used to describe fiber loss rather than using the attenuation coefficient α. Thus, the ratio can be given by

$$\alpha_{dB} = -\frac{10}{L} log \frac{P_{out}}{P_{in}} \tag{2.7}$$

Fiber losses usually depend on the wavelength, illustrated in Figure 2.5, which shows the loss spectrum of a standard silica SMF as a function of wavelength. The attenuation depends from several factors, it is mainly caused by material absorption and Rayleigh scattering, as well as fiber imperfections due to fabrication techniques. The OH^- ion from water vapor in the glass leads to high absorption peaks at 1.24 μm and 1.38 μm. However, the elimination of water in fibers has reduced and almost removed the OH^- peaks. Losses occurring from splices and connectors contribute to the attenuation of the signal as well.

Attenuation must be compensated by optical amplification, such as EDFAs that are commonly used for compensating attenuation losses. Considering the attenuation losses as a function of the wavelength, three transmission windows can be identified. The first window ($0.8 - 0.9$ μm), has a high attenuation ($\approx$ 3 dB/km). The second window ($1.28 - 1.33$ μm), with a reasonable attenuation (0.33 dB/km), and the minimum dispersion. The third window ($1.525 - 1.625$ μm) is widely used, because it has the lowest loss. In the work conducted in the following chapters, AOSP will be performed in the third window known as C band, in the range $1.530 - 1.565$ μm.

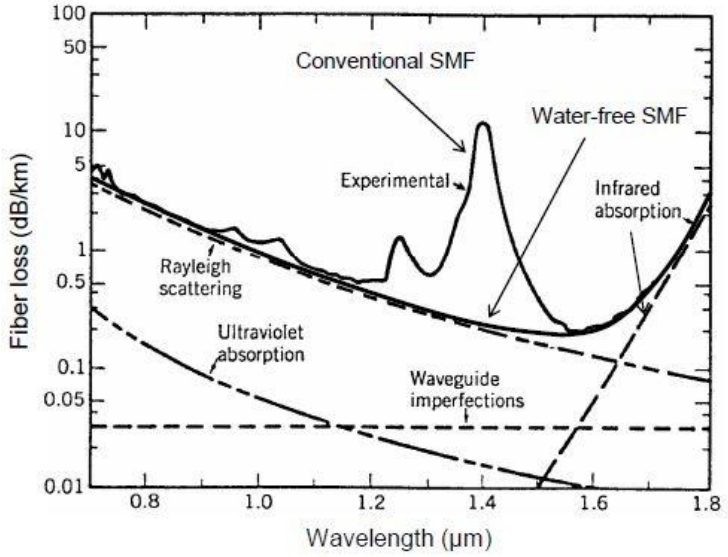

Figure 2.5: Loss spectrum of a standard single mode fiber (From Ref. [80]).

2.1.3 Dispersion

Dispersion is one of the main parameters in optical fibers that affects the distortion of the signal information as it propagates along the fiber in communication systems. Therefore, maintaining a low dispersion is of a big importance. There are different types of dispersion: material dispersion, waveguide dispersion and modal dispersion. The material dispersion manifests through the variations of the refractive index of the fiber material with respect to the wavelength, as different spectral components of a pulse travel at different speeds given by $c/n(\lambda)$, leading to the deformation and broadening of the pulse. Variations of the refractive index with respect to the wavelength can be described by the Sellmeier equation given by [81]

$$n(\lambda) = \left[1 + \sum_{i=1}^{3} \frac{A_i \lambda^2}{(\lambda^2 - \lambda_i^2)}\right]^{1/2} \tag{2.8}$$

where λ is the wavelength, A_i and λ_i are the Sellmeier coefficients. Refractive index and dispersion characteristics can then be presented as a function of the dopant concentration [8, 82]. The propagation constant β depends on the frequency of each mode of the fiber, which leads to waveguide dispersion. The cumulated effect of material and waveguide dispersion is referred to as chromatic dispersion or intramodal dispersion. While the material dispersion is a given material property, the contribution of the waveguide dispersion depends on the fiber design parameters such as the core radius or core-cladding index difference, which makes it

possible to alter the waveguide dispersion. For instance, the ZDW can be shifted in the vicinity of 1.55 μm by changing the shape of the fiber's refractive index profile, as will be shown in later chapters. Those fibers are called dispersion-shifted fibers (DSF). Moreover, considering a SMF that supports two orthogonally polarized modes propagating on the fundamental mode; the two modes should have identical propagation constants. However, in actual fibers with random and involuntary birefringence, a small difference between the propagation constants of the two modes occurs. Therefore, this difference between the two propagation constants of the modes contributes to the pulse spreading, which is known as polarization mode dispersion.

All the intramodal dispersion mechanisms described above exist in SMFs. They can also exist in MMFs where more than one mode propagates. Therefore, they can be applied for all the modes. Furthermore, an additional type of dispersion exists in MMFs, that is the modal dispersion. It can also be called intermodal dispersion, due to the variation of the effective index from mode to mode. This type of dispersion does not exist in SMFs, because it occurs as a result of the different modes associated with different values of β, hence, having different group velocity.

The effect of dispersion is considered by representing the modal propagation constant $\beta^{(p)}(\omega)$ of a mode p, using a Taylor series expansion around a center frequency ω_0, given by:

$$\beta^{(p)}(\omega) = n(\omega)\frac{\omega}{c}$$
$$= \beta_0^{(p)} + \beta_1^{(p)}(\omega - \omega_0) + \frac{\beta_2^{(p)}}{2}(\omega - \omega_0)^2 + \frac{\beta_3^{(p)}}{6}(\omega - \omega_0)^3 + \cdots, \qquad (2.9)$$

with

$$\beta_m = \left(\frac{d^m\beta}{d\omega^m}\right)_{\omega=\omega_0} \qquad (m = 0,1,2,\dots) \qquad (2.10)$$

where c is the speed of light in vacuum, β_1 is the IGV and β_2 is the GVD or the second order dispersion. The envelope of an optical pulse moves at the group velocity $v_g = 1/\beta_1 = c_0/n_g$, with n_g the group index, while β_2 is responsible for pulse broadening. The differential mode delay (DMD) between two modes p and q is defined as the variation of the group delay per unit length between them, and is given by

$$\mathrm{DMD}_{p,q} = \frac{1}{v_{g,p}} - \frac{1}{v_{g,q}} \qquad (2.11)$$

The dispersion parameter D is commonly used instead of β_2, and they are both related by the following relation

$$D = \frac{d\beta_1}{d\lambda} = -\frac{2\pi c}{\lambda^2}\beta_2 \tag{2.12}$$

The dispersion D is usually expressed in ps/km/nm, while β_2 is expressed in s^2/m. The coefficients of the Taylor series in Equation (2.9) that represent higher order dispersion terms are also used to calculate the effects of dispersion, and are given by

$$\beta_3 = \left(\frac{\lambda}{2\pi c}\right)^2 (\lambda^2 S + 2\lambda D) \tag{2.13}$$

$$\beta_4 = -\left(\frac{\lambda}{2\pi c}\right)^3 (\lambda^3 C + 6\lambda^2 S + 6\lambda D) \tag{2.14}$$

where S is the dispersion slope, and C is the dispersion curvature.

As mentioned previously, the dispersion D is the combination of the material dispersion D_M and the waveguide dispersion D_W, $D = D_M + D_W$. Considering a standard SMF, Figure 2.6 shows both material and waveguide dispersion (D_M and D_W), along with the total dispersion D. It can be realized that the ZDW of the fiber is around 1310 nm. Therefore, the pulse broadening effect can be eliminated when operating at/near the ZDW.

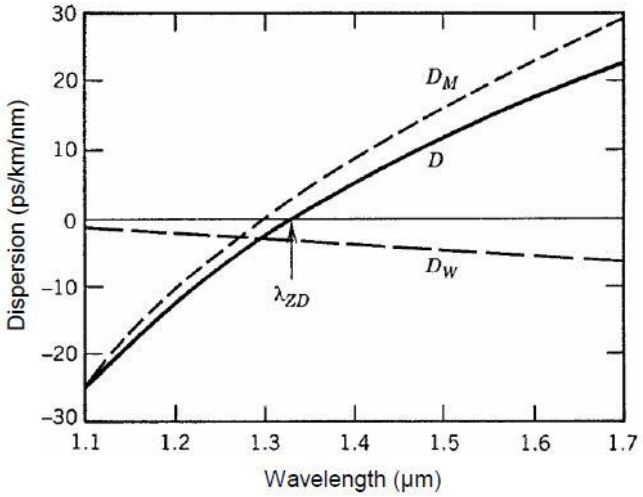

Figure 2.6: Material dispersion D_M, waveguide dispersion D_W and total dispersion D for a standard SMF (From Ref. [80]).

By modifying the index profile of the fiber that depends on the fiber design parameters, the ZDW can be shifted towards 1550 nm. When $D < 0$ ($\beta_2 > 0$), the fiber is said to exhibit normal dispersion, and anomalous dispersion when $D > 0$ ($\beta_2 < 0$), where the two regions are

separated by the ZDW. In the normal dispersion regime, high frequency components of an optical pulse travel slower than low frequency components of the same pulse, and the opposite occurs in the anomalous dispersion regime. The two dispersion regimes affect the behavior of the nonlinear effects in the fiber. For instance, solitons [8] may appear when operating in the anomalous regime.

2.1.4 Dispersion-altered Fibers

Considering a SMF, the dispersion vanishes at a wavelength of $1310\ nm$, however, the lowest attenuation occurs at the most widely used wavelength of $1550\ nm$. Optical amplification using EDFAs operate in the range of $1530\ nm$ to $1610\ nm$, where large dispersion occurs. Therefore, different index profiles of optical fibers were designed to improve the dispersion performance around $1550\ nm$, by manipulating the index profile and the geometry of the fiber. Some of these fibers are known as dispersion-shifted fibers, dispersion-flattened fibers and dispersion compensating fibers.

In the dispersion shifted fibers, the ZDW is shifted to the lowest attenuation region, that is around $1550\ nm$ [83], where low dispersion can be achieved over a narrow range. Multiclad fibers with step or graded cores are used to design dispersion-shifted fibers [84, 85]. In this thesis, we will focus on this type of fibers in our designs, where an example of the index profile is shown in Figure 2.7(a), while other choices are possible.

The low dispersion wavelength range can be extended in the case of the dispersion-flattened fibers [86]. The index profile of the fiber can be manipulated in a way to obtain several ZDWs in the wavelength range of operation. Multiclad fibers with double, triple and quadruple-clad fibers can be used to design dispersion-flattened fibers, as shown in Figure 2.7(b).

As for dispersion compensating fibers, they are used to compensate the cumulative dispersion in the fiber [87, 88]. Considering a regular SMF that has a dispersion value of around $+16\sim17\ \mathrm{ps/(nm.km)}$ at the wavelength 1550 nm, the cumulated dispersion after a long distance may be of considerable magnitude. For instance, for a $10\ \mathrm{km}$ fiber length, the cumulative dispersion will be $+160\sim170\ \mathrm{ps/nm}$. In order to compensate this amount of dispersion, a splicing dispersion compensating fiber can be added to the link with a specific length calculated according to the previous initial fiber, and that exhibits large negative

dispersion to cancel out and reduce the total dispersion to around $0\ \mathrm{ps/(nm.km)}$, as shown in Figure 2.7(c).

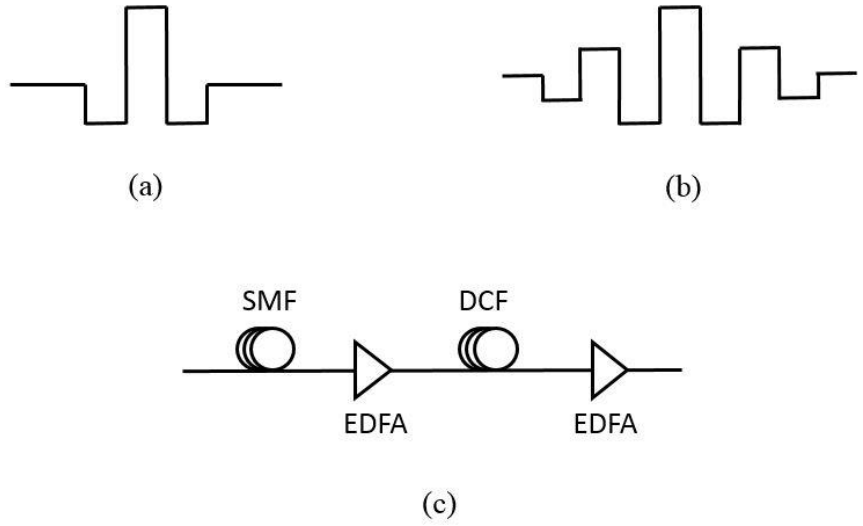

Figure 2.7: (a) index profile of a dispersion shifted fiber, (b) index profile of a dispersion-flattened fiber and (c) dispersion of a SMF compensated by a dispersion compensating fiber, placed between two EDFAs.

2.2 Nonlinear Effects in Optical Fibers

When operating in the linear regime, the medium properties of an optical fiber do not depend from the signal. However, in the nonlinear regime under the influence of an intense field, the material properties are modified by the signal. In this section, we will discuss the propagation of light in optical fibers, taking into consideration the nonlinear effects. When a dielectric material is imposed by an electric field, the induced polarization is given by the susceptibility of the medium, where the first order susceptibility is usually considered. However, when the light intensity becomes large, the response of the medium becomes nonlinear due to anharmonic motion of bound electrons, thus the higher order terms of the polarization should also be considered. The total induced polarization **P** in the material is given by

$$\mathbf{P} = \epsilon_0\left(\chi^{(1)}.\,\mathbf{E} + \chi^{(2)}\!:\mathbf{EE} + \chi^{(3)}\vdots\,\mathbf{EEE} + \cdots\right) \tag{2.15}$$

where ϵ_0 is the vacuum permittivity, $\chi^{(j)}(j = 1,2,\ldots)$ is the jth order susceptibility and it is a tensor of rank j+1. $\chi^{(1)}$ is the first order linear susceptibility. $\chi^{(2)}$ is the second order

susceptibility, and is responsible for nonlinear effects such as second-harmonic generation and sum-frequency generation [89]. However, $\chi^{(2)}$ vanishes in silica fibers due to molecular symmetry, thus, optical fibers do not exhibit second-order nonlinear effects and $\chi^{(2)}$ can be ignored. Accordingly, nonlinear effects in optical fibers are governed by the third order susceptibility $\chi^{(3)}$, where effects such as SPM, XPM and FWM can be considered.

2.2.1 Kerr Effect

In addition to the linear refractive index introduced in section 2.1.3, the refractive index depends on the intensity of the light propagating through the optical fiber as well. The effect of this intensity dependent modification coming from the third order susceptibility $\chi^{(3)}$ is called the Kerr effect. Therefore, the total refractive index of the medium can be given by

$$n(\omega, I) = n_0(\omega) + n_2 I \tag{2.16}$$

where $n_0(\omega)$ is the linear part. The refractive index is a function of ω due to the dispersive nature of the glass. The linear part is related to the complex quantity $\chi^{(1)}$ of the polarization, that includes dispersion and attenuation effects. The nonlinearity is given by the second term $n_2\, I$, where I is the optical intensity in the fiber and n_2 is the nonlinear refractive index that depends on the material. It is related to the third order susceptibility $\chi^{(3)}$ by [8]

$$n_2 = \frac{3}{8n_0}\chi^{(3)} \tag{2.17}$$

For silica glass, n_2 is approximately equal to 2.6×10^{-20} m^2/W.

2.2.2 Nonlinear Schrödinger Equation

The propagation of an optical pulse through an optical fiber along a distance z can be described by the propagation equation [8]

$$\frac{\partial A}{\partial z} + \beta_1 \frac{\partial A}{\partial t} - i\frac{\beta_2}{2}\frac{\partial^2 A}{\partial t^2} + \frac{\alpha}{2}A = i\gamma|A|^2 A \tag{2.18}$$

where A is the slowly varying envelope, α is the fiber loss, β_1 and β_2 are the IGV and the GVD, respectively. γ is the nonlinear parameter defined as

$$\gamma = \frac{n_2 \omega_0}{c A_{\text{eff}}} \tag{2.19}$$

where the parameter A_{eff} is known as the effective core area where the light is confined in the optical fiber, and it is defined as

$$A_{\text{eff}} = \frac{(\iint |F|^2 dxdy)^2}{\iint |F|^4 dxdy} \tag{2.20}$$

with $F(x, y)$ as the modal distribution of the mode propagating in the optical fiber. The effective area depends on the fiber parameters such as the size of the core and the core-cladding index difference. A typical value of A_{eff} ranges from $20 - 100\ \mu\text{m}^2$, if $n_2 \approx 2.6 \times 10^{-20}\ \text{m}^2/\text{W}$ is used for silica glass. Therefore, the corresponding value of γ ranges within $1 - 100\ \text{W}^{-1}/\text{km}^{-1}$.

Equation (2.18) describes the propagation of the pulse in the optical fiber. The first term β_1 is the inverse of the group velocity $1/v_g$, at which the pulse is moving. By defining a new time frame T, where the pulse is moving with the group velocity

$$T = t - \frac{z}{v_g} = t - \beta_1 z \tag{2.21}$$

Equation (2.18) becomes

$$\frac{\partial A}{\partial z} - i\frac{\beta_2}{2}\frac{\partial^2 A}{\partial T^2} + \frac{\alpha}{2}A = i\gamma|A|^2 A \tag{2.22}$$

Equation (2.22) is referred to as the NLSE. It governs the evolution of the envelope and describes its behavior as a function of the distance when the field distribution travels along the optical fiber.

2.2.3 Self-phase Modulation

The SPM is a process where a wave propagating through an optical fiber along a distance *L* undergoes a nonlinear phase shift, and phase modulates itself by inducing changes in the fiber refractive index. The nonlinear phase shift is given by

$$\phi_{\text{SPM}} = \gamma P L_{\text{eff}} \tag{2.23}$$

where *P* is the power of the propagating wave, and L_{eff} is the effective length defined as:

$$L_{\text{eff}} = \frac{1 - e^{-\alpha z}}{\alpha} \tag{2.24}$$

L_{eff} is often defined in order to account for fiber losses, it is smaller than the fiber length L because of fiber losses. In the absence of fiber losses, $\alpha = 0$ and $L_{\text{eff}} = L$. This case is valid when the dispersion effect is neglected. However, when considering the interaction between dispersion and SPM, it leads to the generation of optical solitons where dispersion and nonlinearities cancel out [8].

2.2.4 Cross-phase Modulation

In the previous sections, only one optical field propagating inside the optical fiber was considered. When two or more optical fields having different wavelengths propagate simultaneously inside the fiber, they interact with each other through fiber nonlinearity, which leads to the generation of new waves due to nonlinear phenomena such as FWM that will be discussed in the next section. In the case of two optical fields propagating in the fiber, the effective refractive index seen by the first field depends not only on its intensity, but also on the intensity of the second co-propagating field. Thus, the phase of the first field can be modulated by the second co-propagating field. This process is known as XPM, and is always accompanied by SPM. The induced nonlinear phase shift on the first field by the second field with a power P_2, when the two fields are co-polarized can be given by

$$\phi_{\text{XPM}} = 2\gamma P_2 L_{\text{eff}} \tag{2.25}$$

It can be realized that the nonlinear phase shift induced by XPM is twice the nonlinear phase shift induced by SPM.

Considering two pulses propagating in the fiber, they generally have different GVD, and different speeds because of the difference in their group velocities that plays an important role as it limits the XPM interaction. Furthermore, the two pulses slide through each other. Therefore, the nonlinear interaction between them occurs when they overlap, and the XPM phenomena can be observed. However, when they walk off from each other, the XPM vanishes because the two pulses are not interacting anymore. Thus, a walk-off parameter can be defined as [8]

$$d = v_g^{-1}(\lambda_1) - v_g^{-1}(\lambda_2) \tag{2.26}$$

If the group velocity difference in a given fiber between the two pulses is small, strong interaction occurs between them. As the nonlinear phase in XPM is affected by additional fields propagating in the optical fiber, it is desirable to avoid the XPM phenomena in some cases such as WDM systems, when its effect becomes important due to the number of transmitted channels. Therefore, a fiber with large group velocities should be used, thus, large dispersion in the fiber is expected. Therefore, the walk off time will be very short and the nonlinear interaction between the pulses will be very small, due to the difference between the velocities of the propagating fields. In other cases, the XPM phenomena can be useful for some applications whenever a strong interaction between the different fields is desired. In this case, dispersion-shifted or dispersion-flattened fibers can be used, so that the fields propagate with similar velocities, and the walk off time will be long enough to obtain strong interaction between the different fields.

2.2.5 Four-wave Mixing

The third order susceptibility that results in the SPM and XPM nonlinear phenomena is also responsible for another effect called FWM. Its main features can be understood by considering the third order nonlinear polarization term given by

$$\mathbf{P}_{NL} = \epsilon_0 \, \chi^{(3)} \vdots \, \boldsymbol{E_1 E_2 E_3} \tag{2.27}$$

where ϵ_0 is the vacuum permittivity, and three optical fields were considered at three different frequencies ω_1, ω_2 and ω_3. The three optical fields interact and produce a frequency ω_4 that can be given by

$$\omega_4 = \omega_1 \pm \omega_2 \pm \omega_3 \tag{2.28}$$

where the wave numbers are given by

$$k_4 = k_1 \pm k_2 \pm k_3 \tag{2.29}$$

When the three frequencies propagate inside the fiber, new frequencies can be generated due to nonlinearity. The possible combinations of the new generated frequencies can be given as

$\omega_1 + \omega_2 - \omega_3$	$2\omega_1 - \omega_2$	$2\omega_2 - \omega_3$
$\omega_1 + \omega_3 - \omega_2$	$2\omega_1 - \omega_3$	$2\omega_3 - \omega_1$
$\omega_3 + \omega_2 - \omega_1$	$2\omega_2 - \omega_1$	$2\omega_3 - \omega_2$

Therefore, two common types of FWM are known as degenerate FWM, and non-degenerate FWM. In the degenerate FWM, two of the four frequencies coincide ($\omega_1 = \omega_2$), and a single strong pump propagate in the fiber along with a signal (ω_3). Nonlinear interaction produces a new wave called idler (ω_4) due to the Kerr effect, that causes photons pairs to transfers energy from the frequency of the pump, to the frequencies of the signal and idler, as shown in Figure 2.8(a), where the generated idler's frequency is always symmetrical to the signal frequency with respect to the pump frequency. As for the non-degenerate FWM, two pumps (ω_1 and ω_2) propagate in the fiber with a signal (ω_3), and generate an idler (ω_4). In this case, the Kerr effect causes photon pairs from the pumps to transfer energy to the signal and idler frequencies, as shown in Figure 2.8(b).

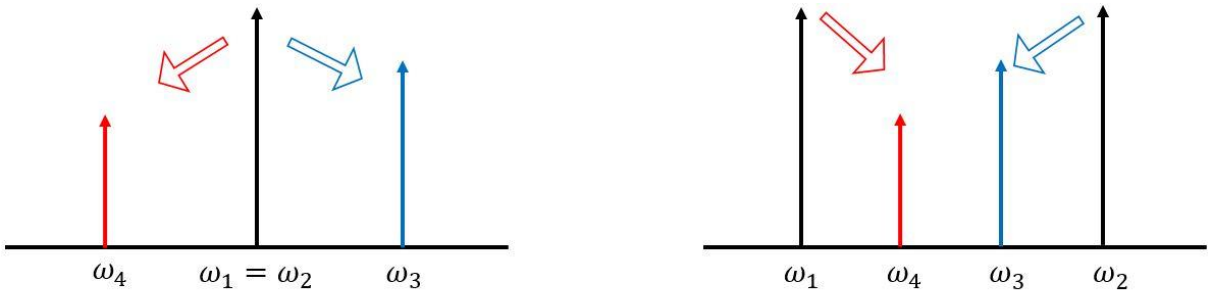

Figure 2.8: (a) Degenerate FMW and (b) non-degenerate FWM principle.

Significant FWM occurs only if the two basic FWM conditions are fulfilled: energy conservation and phase matching [90]. The first one defines the frequency spacing between the interacting waves. For the two degenerate and non-degenerate FWM processes, it can be given respectively as

$$2\omega_1 = \omega_3 + \omega_4 \tag{2.30}$$

$$\omega_1 + \omega_2 = \omega_3 + \omega_4 \tag{2.31}$$

Their corresponding phase matching conditions can be expressed from the propagation constants of the interacting waves, as

$$\Delta\beta_{deg.\ FWM} = 2\beta(\omega_1) - \beta(\omega_3) - \beta(\omega_4) = 0 \tag{2.32}$$

$$\Delta\beta_{non-deg.FWM} = \beta(\omega_1) + \beta(\omega_2) - \beta(\omega_3) - \beta(\omega_4) = 0 \tag{2.33}$$

The newly generated idler by FWM depends on the phase matching condition. A small phase matching ($\Delta\beta \approx 0$) leads to the generation of a strong idler. The phase matching depends on the dispersion parameters of the fiber. Therefore, a specific fiber design is always required in order to achieve a desired process based on FWM, as will be shown later. The FWM phenomena can be used for applications such as wavelength routed networks, where wavelength conversion is required so that the data on a given wavelength can be transmitted to another channel.

2.2.5.1 Intramodal FWM

When all the interacting waves propagate on the same mode inside the optical fiber, the FWM process can be called intramodal FWM. Its phase matching condition can be written as in Equation (2.33). By using Taylor series expansions of the propagation constants around a frequency ω_0 as defined previously in Equation (2.9), and by considering dispersion terms up to β_2 for simplicity, Equation (2.33) can be written as

$$\frac{\beta_2}{2}[(\Delta\omega_1)^2 + (\Delta\omega_2)^2 - (\Delta\omega_3)^2 - (\Delta\omega_4)^2] = 0 \tag{2.34}$$

where β_2 is the GVD taken at a reference angular frequency ω_0, and $\Delta\omega_i = \omega_i - \omega_0$, where i = 1,2,3,4. In the case of degenerate FWM ($\omega_1 = \omega_2$), Equation (2.34) becomes

$$\frac{\beta_2}{2}[2(\Delta\omega_1)^2 - (\Delta\omega_3)^2 - (\Delta\omega_4)^2] = 0 \tag{2.35}$$

It can be realized that the two equations depend only on the GVD (β_2), whereas the phase constant β_0 and the IVG (β_1) are canceled out. This means that in order to have a complete phase matching, the fiber should have small β_2.

2.2.5.2 Intermodal FWM

When all the interacting waves propagate on different modes inside the optical fiber, the FWM process can be called intermodal FWM. The interacting waves can propagate in up to four fiber modes, however, in this case, the phase matching condition is altered due to the different propagation constants of the fiber modes.

Starting with the case of two modes, and considering two fiber modes LP_{01} and LP_{11}, where ω_1 and ω_3 are propagating on the mode LP_{01}, and ω_2 on the mode LP_{11}; the idler ω_4 will be generated on the mode LP_{11}, as can be seen in Figure 2.9. Three ways exist to fulfill energy

conservation between the three waves in this case [75] where ω_4 can assume to be one of the three values

$$(Process\ 1) \qquad \omega_4 = \omega_1 + \omega_2 - \omega_3 \tag{2.36}$$

$$(Process\ 2) \qquad \omega_4 = -\omega_1 + \omega_2 + \omega_3 \tag{2.37}$$

$$(Process\ 3) \qquad \omega_4 = \omega_1 - \omega_2 + \omega_3 \tag{2.38}$$

The corresponding phase matching condition for Process 1 can be written as:

$$\Delta\beta = \beta^{01}(\omega_1) - \beta^{01}(\omega_3) + \beta^{11}(\omega_2) - \beta^{11}(\omega_4) = 0 \tag{2.39}$$

where $\beta^{(01)}$ and $\beta^{(11)}$ are the propagation constants of the modes LP_{01} and LP_{11}, respectively. By expanding each mode's propagation constant into a Taylor series around a frequency ω_0, Equation (2.39) can be written as

$$\beta_1^{01}[\Delta\omega_1 - \Delta\omega_3] + \beta_1^{11}[\Delta\omega_2 - \Delta\omega_4] = \frac{\beta_2^{01}}{2}[(\Delta\omega_3)^2 - (\Delta\omega_1)^2] + \frac{\beta_2^{11}}{2}[(\Delta\omega_4)^2 - (\Delta\omega_2)^2] \tag{2.40}$$

It can be realized that the equation depends on the GVD β_2^{01} and β_2^{11} of the two modes, as well as their IGVs $\beta_1^{01}$and β_1^{11}, unlike in the previous intramodal case. It can also be realized that the phase constants of the two modes β_0^{01} and β_0^{11} are still canceling out. Equation (2.40) shows that the phase matching of the intermodal FWM can be achieved when the IGVs evaluated at the average frequencies of the two waves present in each mode are equal [75, 77]. Therefore, strong intermodal FWM can be achieved in a fiber possessing these properties, as was shown experimentally in [75].

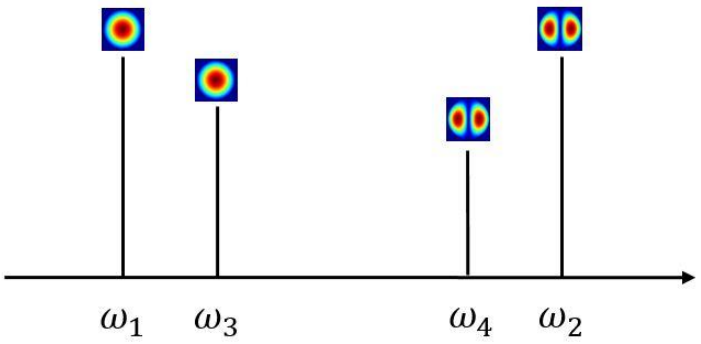

Figure 2.9: Spectral arrangement of an intermodal FWM, where two frequency components propagate on the mode LP_{01}, and two others propagate on the mode LP_{11}.

The corresponding phase matching condition for Process 2 can be written as

$$\beta_1^{01}[\Delta\omega_1 - \Delta\omega_3] + \beta_1^{11}[\Delta\omega_4 - \Delta\omega_2] = \frac{\beta_2^{01}}{2}[(\Delta\omega_3)^2 - (\Delta\omega_1)^2] + \frac{\beta_2^{11}}{2}[(\Delta\omega_2)^2 - (\Delta\omega_4)^2] \tag{2.41}$$

The same reasoning of Process 1 can be applied in this case, that was also shown experimentally in [75]. However, the corresponding phase matching condition for Process 3 can be written as:

$$2(\beta_0^{11} - \beta_0^{01}) = \beta_1^{01}[\Delta\omega_1 + \Delta\omega_3] - \beta_1^{11}[\Delta\omega_2 + \Delta\omega_4] + \frac{\beta_2^{01}}{2}[(\Delta\omega_1)^2 + (\Delta\omega_3)^2] - \frac{\beta_2^{11}}{2}[(\Delta\omega_2)^2 + (\Delta\omega_4)^2] \tag{2.42}$$

It can be realized that the phase constants β_0^{01} and β_0^{11} did not cancel out in Process 3, unlike Process 1 and Process 2. This process was not observed in [75] because the phase matching depends on $\beta_0^{11} - \beta_0^{01}$. In fact, and according to [75], the phase constants β_0 of the modes are subject to fast variations along the fiber, which makes the phase matching sensitive to fluctuations with distance of the relative β_0 between the modes, thus preventing the phase matching. Therefore, the first two processes out of the three two-mode intermodal FWM processes, were observed.

After studying the phase matching condition for the single-mode and two-mode cases, it might be interesting as well to study the phase matching condition for the case of three or four modes, since the interacting waves can propagate in up to four fiber modes. Therefore, we will consider the case of the intermodal FWM between four distinct modes, where ω_1, ω_2 and ω_3 are propagating on the modes LP_{01}, LP_{11} and LP_{21}, respectively; and ω_4 is considered to be generated on the mode LP_{02}. The phase matching condition in this case can be written as

$$\Delta\beta = \beta^{01}(\omega_1) - \beta^{21}(\omega_3) + \beta^{11}(\omega_2) - \beta^{02}(\omega_4) \tag{2.43}$$

After expanding each mode's propagation constant into Taylor series around a frequency ω_0, Equation (2.43) becomes

$$(\beta_0^{21} + \beta_0^{02}) - (\beta_0^{01} + \beta_0^{11}) = \beta_1^{01}(\Delta\omega_1) + \beta_1^{11}(\Delta\omega_2) - \beta_1^{21}(\Delta\omega_3) - \beta_1^{02}(\Delta\omega_4) + \frac{\beta_2^{01}}{2}(\Delta\omega_1)^2 + \frac{\beta_2^{11}}{2}(\Delta\omega_2)^2 - \frac{\beta_2^{21}}{2}(\Delta\omega_3)^2 - \frac{\beta_2^{02}}{2}(\Delta\omega_4)^2 \tag{2.44}$$

It can be realized that Equation (2.44) depends on the phase constants of the four modes β_0^{01}, β_0^{11}, β_0^{21} and β_0^{02}. These phase constants are subject to fast variations as described previously, thus preventing phase matching.

2.3 Multimode Nonlinear Schrödinger Equation

In section 2.2.2, we studied the NLSE that governs the propagation in SMFs. In the following, we will extend our study and investigate the NLSE in multimode fibers [91, 92, 93, 21], and describe the slowly varying envelopes of different fiber modes.

2.3.1 Generalized Nonlinear Schrodinger Equation for Multimode Fibers

The propagation of the slowly varying pulse envelope $A_p(z,T)$ propagating in mode p in an optical fiber supporting N total number of modes can be generally described as [91, 92, 93, 21]

$$\frac{\partial A_p}{\partial z} = -\frac{\alpha}{2}A_p + i(\beta_{0p} - \beta_{0r})A_p - \left(\beta_{1p} - \frac{1}{v_{gr}}\right)\frac{\partial A_p}{\partial T} - i\frac{\beta_{2p}}{2}\frac{\partial^2 A_p}{\partial T^2} + i\sum_{l=1}^{N}\sum_{m=1}^{N}\sum_{n=1}^{N}\gamma_{plmn}\,A_l A_m A_n^* \tag{2.45}$$

where α is the attenuation coefficient that can be mode-dependent, β_{0r} and v_{gr} are the references propagation constant and group velocity, respectively. $\beta_{0p} = \beta_p(\omega_0)$, $\beta_{1p} = \partial\beta_p/\partial\omega\,|_{\omega 0}$ and $\beta_{2p} = \partial^2\beta_p/\partial\omega^2\,|_{\omega 0}$ are respectively the propagation constant, IGV and GVD of the p^{th} mode. The last term in the multimode NLSE represents the nonlinear part, where γ_{plmn} is the nonlinear parameter defined previously in Equation (2.19) as

$$\gamma_{plmn} = \frac{n_2\omega_0}{cA_{eff}^{(plmn)}} \tag{2.46}$$

however, in this case the effective area is defined with the following overlap

$$A_{eff}^{plmn} = \frac{\left(\iint |F_p|^2 dxdy \iint |F_l|^2 dxdy \iint |F_m|^2 dxdy \iint |F_n|^2 dxdy\right)^{1/2}}{\iint F_p^* F_l F_m^* F_n \, dxdy} \tag{2.47}$$

with $F_{(plmn)}$ as the field distributions of the (p,l,m,n)th modes, respectively. When only one fiber mode of the multimode fiber is excited, Equation (2.45) can be written as Equation (2.18), and the effective area can be written as Equation (2.20), which will take us back to the case of the single mode pulse propagation described in section 2.2.2. Further, if only one wavelength is considered, the process can then be described by the SPM process described previously in section 2.2.3, when the phase of the signal is modulated by its own power $|A_p|^2$.

2.3.2 Simplified Nonlinear Schrödinger Equation for Multimode Fibers

If two modes p and l of the multimode fiber are excited, Equation (2.45) can be written in this case for the mode p as

$$\begin{aligned}\frac{\partial A_p}{\partial z} = &-\frac{\alpha}{2}A_p + i(\beta_{0p} - \beta_{0r})A_p - \left(\beta_{1p} - \frac{1}{v_{gr}}\right)\frac{\partial A_p}{\partial T} - i\frac{\beta_{2p}}{2}\frac{\partial^2 A_p}{\partial T^2} \\ &+ i\big(\gamma_{pppp}A_pA_pA_p^* + \gamma_{pppl}A_pA_pA_l^* + \gamma_{pplp}A_pA_lA_p^* + \gamma_{ppll}A_pA_lA_l^* \\ &+ \gamma_{plpp}A_lA_pA_p^* + \gamma_{plpl}A_lA_pA_l^* + \gamma_{pllp}A_lA_lA_p^* \\ &+ \gamma_{plll}A_lA_lA_l^*\big)\end{aligned} \tag{2.48}$$

It can be realized that the number of nonlinear coupling coefficients increases with the number of modes. However, because of the specific form of Equation (2.47), many of these coefficients are identical, more specifically the ones containing the following indices: $\gamma_{ppll} = \gamma_{pllp} = \gamma_{plpl}$. Moreover, when the number of modes propagating in a fiber is large, the number of nonlinear coefficients becomes tremendous. Many of these coefficients can be averaged to zero and vanish, owing to the symmetry of the modes. Coming back to Equation (2.48), and after simplifications it can be written as

$$\begin{aligned}\frac{\partial A_p}{\partial z} = &-\frac{\alpha}{2}A_p + i(\beta_{0p} - \beta_{0r})A_p - \left(\beta_{1p} - \frac{1}{v_{gr}}\right)\frac{\partial A_p}{\partial T} - i\frac{\beta_{2p}}{2}\frac{\partial^2 A_p}{\partial T^2} \\ &+ i\left(\gamma_{pppp}|A_p|^2 + 2\,\gamma_{ppll}|A_l|^2\right)A_p\end{aligned} \tag{2.49}$$

The process in Equation (2.49) can be described by the XPM described in section 2.2.4, where the phase of the pulse A_p propagating in mode p gets affected by the power of the pulse A_l propagating in mode l. Same process occurs as well if the two pulses were propagating in the same fiber mode. Therefore, the two processes can be distinguished as intermodal XPM and intramodal XPM, respectively. For instance, if a pump is propagating on the mode p and a signal on the mode l, a maximum broadening of the signal occurs at a wavelength difference where the group velocities of the two modes become identical, leading to intermodal XPM.

After showing the complexity of the generalized multimode NLSE and the number of nonlinear coupling coefficients that increases with the number of modes of the fiber, as well as the simplifications that help to make the equation simpler and easier such as for the case of the two-modes described above, a general equation for the simplified NLSE can now be written as

$$\frac{\partial A_p}{\partial z} = -\frac{\alpha}{2}A_p + i\left(\beta_{0p} - \beta_{0r}\right)A_p - \left(\beta_{1p} - \frac{1}{v_{gr}}\right)\frac{\partial A_p}{\partial T} - i\frac{\beta_{2p}}{2}\frac{\partial^2 A_p}{\partial T^2} + i\left(\gamma_{pppp}\left|A_p\right|^2 + 2\sum_{l\neq p}\gamma_{ppll}|A_l|^2\right)A_p \tag{2.50}$$

This equation is given when only one polarization of each mode is considered. However, when the two polarization of one mode are considered, the process is usually described by the Manakov equation [94], and it would be interesting sometimes to analyze the nonlinear influence that originates from one polarization to another, which may also lead to intermodal FWM between them, as each polarization can be considered as a mode. In short length fibers, it might be possible to perform FWM between the two polarizations of one mode, when the group velocity difference between them is still small.

2.4 Numerical Method

Equation (2.50) will be used in the simulations in the following chapters 3 and 4, and it requires numerical solutions to be solved. One way to solve it is to use the split-step Fourier method [8], by defining two operators: dispersion and nonlinearity. The dispersion is considered in the frequency domain, while the nonlinearity is considered in the time domain. Therefore, the equation is alternatively solved in frequency and time. Considering the case of a single mode

propagation, where Equation (2.22) is employed, the operator that accounts for dispersion and absorption can be defined as

$$\widehat{D} = i\frac{\beta_2}{2}\frac{\partial^2}{\partial T^2} - \frac{\alpha}{2} \tag{2.51}$$

and the nonlinear operator that governs fiber nonlinearities as

$$\widehat{N} = i\gamma|A|^2 \tag{2.52}$$

The dispersion operator is applied in the frequency domain, while the nonlinear operator is applied in the time domain, and Equation (2.22) can then be written as

$$\frac{\partial A}{\partial z} = \left(\widehat{D} + \widehat{N}\right) A \tag{2.53}$$

where the solution is given by

$$\frac{\partial A}{A} = \left(\widehat{D} + \widehat{N}\right)\partial z$$

$$\int \frac{\partial A}{A} = \int \left(\widehat{D} + \widehat{N}\right) \partial z$$

$$\ln(A) = \int \left(\frac{1}{2}\widehat{D} + \widehat{N} + \frac{1}{2}\widehat{D}\right) \partial z$$

$A(z + dz, T)$

$$= F^{-1}\left\{\exp\left(\frac{dz}{2}\widehat{D}(\omega)\right).F\left\{\exp\left(\int_z^{z+dz}\widehat{N}(z', T)dz'\right).F^{-1}\left\{\exp\left(\frac{dz}{2}\widehat{D}(\omega)\right)F\{A(z,T)\}\right\}\right\}\right\}$$

(2.54)

where F and F^{-1} are the direct and inverse Fourier transform operators, respectively. This scheme is known as symmetrized split-step Fourier method, due to the symmetrical form of the operators in Equation (2.54).

The integral given in the equation can be evaluated using the trapezoidal formula as

$$\int_z^{z+dz}\widehat{N}(z', T)dz' = \frac{dz}{2}\left(\widehat{N}(z + dz, T) + \widehat{N}(z, T)\right) \tag{2.55}$$

$\widehat{N}(z+dz,T)$ depends on $A(z+dz,T)$, therefore the correct solution should be obtained using an iterative procedure in order to determine $A(z+dz,T)$ from $A(z,T)$. Moreover, if the step size dz is small enough, the integral in Equation (2.54) can be approximated by exp (dzN), which is often the case.

Figure 2.10 shows the implementation of the split-step Fourier algorithm. A fiber length L is divided into a large number of small segments of length dz, where the split-step Fourier algorithm can be applied in each one. The output envelope $A(z=L,T)$ is calculated using Equation (2.54). The optical field $A(z,T)$ propagates first at a distance $dz/2$ in the segment of length dz, where only the dispersion is considered. Then the field is multiplied by the nonlinear term at the mid-plane $z+dz/2$. Finally, the field propagates in the remaining distance $dz/2$ where only the dispersion is considered again.

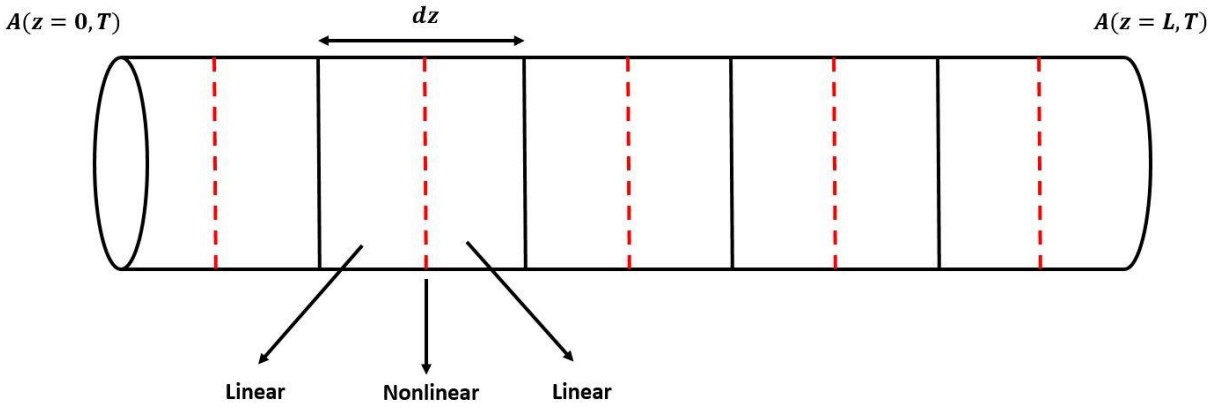

Figure 2.10: Split-step Fourier algorithm.

Same reasoning can be applied for the multimode case. Equation (2.22) is used for the single mode propagation. However, when the number of modes propagating in the fiber increases, the number of equations to be considered when applying the split-step Fourier method increases as well. For instance, if two modes p and l are propagating, the propagation equation for mode p can be written as in Equation (2.49). Thus, the dispersion operator in this case can be written as

$$\widehat{D}_P = -\frac{\alpha}{2} + i\left(\beta_{0p} - \beta_{0r}\right) - \left(\beta_{1p} - \frac{1}{v_{gr}}\right)\frac{\partial}{\partial T} - i\frac{\beta_{2p}}{2}\frac{\partial^2}{\partial T^2} \tag{2.56}$$

while the nonlinear operator as

$$\widehat{N}_P = i\left(\gamma_{pppp}\left|A_p\right|^2 + 2\,\gamma_{ppll}|A_l|^2\right) \tag{2.57}$$

Dispersion $\widehat{D}_l$, and nonlinear $\widehat{N}_l$ operators for the propagation equation for mode l can also be defined. Consequently, the split-step Fourier algorithm can be applied for each equation of the two modes simultaneously, by applying its corresponding dispersion and nonlinear operators as shown in the Appendix A. In the next sections, γ_{pppp} will be written as γ_{pp}, and γ_{ppll} as γ_{pl}, for simplification.

2.5 Conclusion

In this chapter, the properties of an optical fiber and fundamental topics such as dispersion and nonlinear refraction were recalled from the literature. When the intensity of light becomes large, different nonlinear phenomena inside an optical fiber appear. Most of the nonlinear contribution is due to the third order susceptibility. Phenomena such as SPM take place when the signal propagates in the fiber. When multiple signals propagate, a signal will get affected by the other copropagating signals, and the phase of the signal gets modified by the other copropagating signals, under the phenomena that is called the XPM. The same phenomena also create new frequencies which is called the FWM. These phenomena will prove particularly relevant in the forthcoming chapters. We also discussed in this chapter the multimode propagation in optical fibers based on the multimode NLSE, on which all simulations will be based subsequently.

3 Mode-independent Intramodal Nonlinear Processes in Mode-Division Multiplexing

3.1 Introduction

Most of telecommunication systems are based on optical fibers. However, the fully potential of an optical fiber is yet to be discovered. Due to long distances to be traveled in optical fibers, the signals must be processed regularly, for example in terms of regeneration, amplification, multiplying or copying signals. These processes are usually performed electronically. While nonlinear effects occurring in optical fibers are considered as detrimental for signal transmission, it is however believed that they can be exploited to simplify and speed up the processing of the signals, by avoiding electronic processes. This leads to all-optical networks where light controls light. Accordingly, as mentioned in the outline, this chapter will be dedicated to the intramodal goal, where mode-independent processes will be investigated in a specially designed fiber. However, the fiber in this case is a FMF, thus, mode-independent processes such as the wavelength conversion shown in Figure 3.1 will be multiplied in the fiber, according to the number of the modes of the fiber.

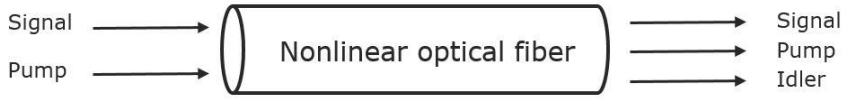

Figure 3.1: wavelength conversion by FWM in a nonlinear optical fiber.

Mode-independent processes based intramodal FWM were investigated numerically in specially designed fibers, such as dispersion shifted FMFs of two and four spatial modes with special dispersion properties to achieve few-mode parametric amplification across the C-band, with minimal crosstalk [64]. In another study related to few-mode parametric amplification, an elliptical-core dispersion shifted FMF was proposed to eliminate the mode coupling between degenerate modes, that causes gain reduction [65]. Moreover, two-mode wavelength conversion in the O-band using both intra- and intermodal FWM has been investigated in a dual-mode fiber [58], where the conversion efficiencies of all the FWMs that occur simultaneously between the two modes and affect each other in the fiber were studied individually, and a method was presented to realize mode-preserving wavelength conversion.

However, the simultaneous wavelength conversion of different signals belonging to different modes has not been demonstrated yet. Therefore, in this chapter, we present the design of a fiber that allows to perform multiple wavelength conversion processes on different modes simultaneously, using the intramodal FWM nonlinear effect known as modulation instability (MI) process. Thereafter, several mode-independent processes will be studied, such as PSFC and PSA.

The FWM configurations MI, PC and BS are introduced along with their phase matching conditions in Section 3.2. In Section 3.3, the design of the FMF and its properties are presented. Sections 3.4, 3.5, 3.6, show mode-independent processes; wavelength conversion, PSFC and PSA, applied in the fiber, respectively. Section 3.7 concludes the chapter.

3.2 Theory

Assuming two pumps (P1) and (P2) on the modes LP_{01} and LP_{11}, respectively, with a signal (S) on the mode LP_{01}, Figures 3.2(a)−(c) show the three pump(s) and signal configurations to achieve the three FWM processes, MI, PC and BS, respectively. For the degenerate MI process, two pump photons are annihilated and another two photons at the signal and idler frequencies are generated within the same mode LP_{01}. However, for the non-degenerate PC and BS processes, a photon in mode LP_{01} and another in mode LP_{11a} are annihilated, and another two photons in the same modes are created. MI and PC are amplification processes where one degenerate pump, or two separate pumps amplify the signal, and simultaneously generate the idler. BS is an energy exchange process where photons from the signal are converted to the idler. As explained in Section 2.2.5, two conditions need to be fulfilled to obtain FWM: energy conservation and phase matching. The energy conservation condition defines the frequencies of the idlers. If the angular frequencies of P1, P2 and S are ω_{P1}, ω_{P2} and ω_S, respectively, idlers (I) for the three MI, PC and BS processes, are created at the angular frequencies

$$\omega_{\mathrm{I,MI}} = 2\omega_{\mathrm{P1}} - \omega_{\mathrm{S}} \tag{3.1}$$

$$\omega_{\mathrm{I,PC}} = \omega_{\mathrm{P1}} - \omega_{\mathrm{S}} + \omega_{\mathrm{P2}} \tag{3.2}$$

and

$$\omega_{\mathrm{I,BS}} = -\omega_{\mathrm{P1}} + \omega_{\mathrm{S}} + \omega_{\mathrm{P2}} \tag{3.3}$$

The three types of idlers created through intra- and intermodal FWM interactions inside the FMF propagation can be seen in Figure 3.2(d). The corresponding phase matching condition of each of the processes can be expressed from the propagation constants of the interacting waves:

$$\Delta\beta_{\mathrm{MI}} = 2\beta^{01}(\omega_{\mathrm{P1}}) - \beta^{01}(\omega_{\mathrm{S}}) - \beta^{01}(\omega_{\mathrm{I}}) = 0\,, \tag{3.4}$$

$$\Delta\beta_{\mathrm{PC}} = \beta^{01}(\omega_{\mathrm{P1}}) - \beta^{01}(\omega_{\mathrm{S}}) + \beta^{11a}(\omega_{\mathrm{P2}}) - \beta^{11a}(\omega_{\mathrm{I}}) = 0\,, \tag{3.5}$$

$$\Delta\beta_{\mathrm{BS}} = -\beta^{01}(\omega_{\mathrm{P1}}) + \beta^{01}(\omega_{\mathrm{S}}) + \beta^{11a}(\omega_{\mathrm{P2}}) - \beta^{11a}(\omega_{\mathrm{I}}) = 0 \tag{3.6}$$

where $\beta^{ij}(\omega)$ is the propagation constant of the $\mathrm{LP_{ij}}$ mode at angular frequency ω. By introducing Taylor series expansions of the propagation constants of each mode around a frequency ω_0, the phase matching condition of each of the three processes can be respectively expressed as in Equation (2.35), Equation (2.40) and Equation (2.41).

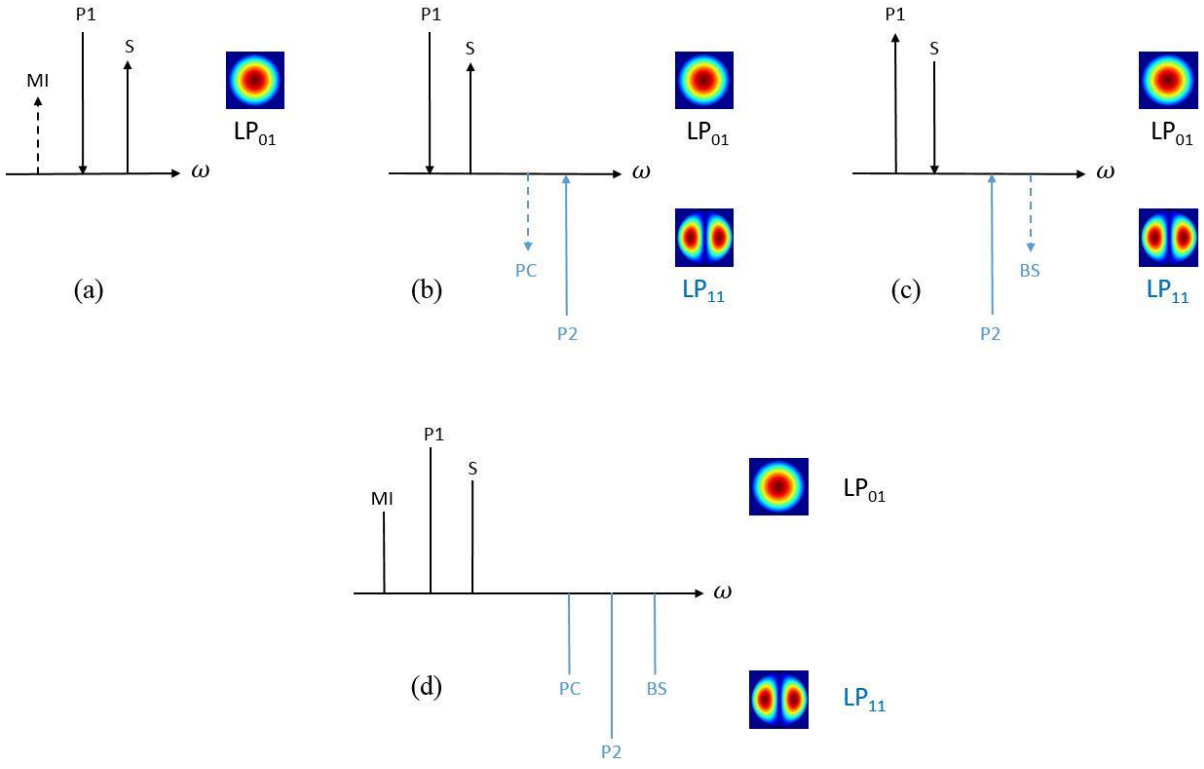

Figure 3.2: Different configurations of FWM using two pumps P1 and P2, a signal S, and idlers (a) modulation instability (MI), (b) phase conjugation (PC), (c) Bragg scattering (BS) and (d) the three idlers that can be created in the FMF propagation. The direction of an arrow towards the horizontal axis indicates losing energy, and gaining energy for a direction away from the axis.

By following the notations of Equations (3.4)−(3.6), the phase matching conditions of the three processes can be written as

$$\frac{\beta_2^{01}}{2}[2(\Delta\omega_{\mathrm{P1}})^2-(\Delta\omega_{\mathrm{S}})^2-(\Delta\omega_{\mathrm{I}})^2]=0, \tag{3.7}$$

$$\beta_1^{01}[\Delta\omega_{\mathrm{P1}}-\Delta\omega_{\mathrm{S}}]+\beta_1^{11a}[\Delta\omega_{\mathrm{P2}}-\Delta\omega_{\mathrm{I}}] = \frac{\beta_2^{01}}{2}[(\Delta\omega_{\mathrm{S}})^2-(\Delta\omega_{\mathrm{P1}})^2]+\frac{\beta_2^{11a}}{2}[(\Delta\omega_{\mathrm{I}})^2-(\Delta\omega_{\mathrm{P2}})^2], \tag{3.8}$$

$$\beta_1^{01}[\Delta\omega_{\mathrm{S}}-\Delta\omega_{\mathrm{P1}}]+\beta_1^{11a}[\Delta\omega_{\mathrm{P2}}-\Delta\omega_{\mathrm{I}}] = \frac{\beta_2^{01}}{2}[(\Delta\omega_{\mathrm{P1}})^2-(\Delta\omega_{\mathrm{S}})^2]+\frac{\beta_2^{11a}}{2}[(\Delta\omega_{\mathrm{I}})^2-(\Delta\omega_{\mathrm{P2}})^2], \tag{3.9}$$

where $\beta_1^{(ij)}$ is the IGV of mode $\mathrm{LP_{ij}}$, and $\beta_2^{(ij)}$ is its GVD, both taken at the reference angular frequency ω_0, and $\Delta\omega_i=\omega_i-\omega_0$, where i = P1, P2, S or I. Contributions from higher-order terms such as third-order (β_3) and fourth-order (β_4) dispersion are not taken into account, but will be considered later in the calculations. Equation (3.7) that refers to the phase matching condition of the MI process depends only on the GVD of the mode. This means that in order to have a phase matched MI processes, the fiber should have a near-zero GVD for the mode involved. Note that we only consider here the linear contribution to the phase mismatch. As for Equation (3.8) and Equation (3.9) that refer to the intermodal PC and BS processes, respectively, the phase matching conditions depend on the GVD of the modes, as well as on their IGVs. The three types of parametric processes can be optimized by controlling the values of the relevant parameters in these three equations. In this chapter, we will focus on the intramodal MI process, and we will come back to the two intermodal PC and BS cases in Chapter 4.

Several graded or step index FMFs were designed to achieve mode-independent processes based on intramodal MI process, such as parametric amplification [63, 64, 65], since MDM systems require multimode optical amplifiers so that all data channels carried over different spatial modes can be amplified simultaneously. The fibers were designed in a way to achieve a good phase matching over a large bandwidth according to Equation (3.7). This was done by tailoring the refractive index of the fiber in a way to have close ZDWs for all the modes, and a high IGV differences between the modes to prevent all intermodal processes whose efficiency is governed by Equation (3.8) and (3.9). In the following, we will show a similar fiber design

to [64]. However, the core will be taken as elliptical which breaks the degeneracy between the modes $LP_{11a,b}$. The fiber allows to simultaneously wavelength convert signals present on the two modes, in addition to the fundamental mode. Mode-independent PSFC and PSA will also be investigated.

3.3 Fiber Design

To perform simultaneous few-mode intramodal MI processes in MDM, the MI process for all the participating modes should be phase matched ($\Delta\beta_{\mathrm{MI}} \rightarrow 0$). According to Equation (3.7), this can be achieved if the fiber has small GVD for all the modes involved. Another condition to ensure MDM performance and efficient MI processes, is to minimize undesired intermodal PC and BS processes ($\Delta\beta_{\mathrm{PC}} \gg 0$ & $\Delta\beta_{\mathrm{BS}} \gg 0$). In fact, MDM that is based on different optical modes as independent channels to transmit the data, suffers from intermodal crosstalk. When these intermodal interactions occur simultaneously with the MI processes, they will cause the data in any mode to be affected by the data in other modes, which leads to crosstalk. For instance, if two signals in modes LP_{01} and LP_{11} are launched into the fiber at the same wavelength ω_S, an idler in mode LP_{11} will be generated through $P^{01} + P^{11} \rightarrow S^{01} + I^{11}$, when PC occurs. The idler will also take part in the MI process $2P^{11} \rightarrow S^{11} + I^{11}$. As a result, a signal in mode LP_{11} is generated at ω_S, and will interfere with the signal which was originally launched into the fiber in the same mode LP_{11}, and cause crosstalk. The same interference can happen as well when considering MI and BS. Therefore, in order to perform AOSP in the same fiber for all the modes simultaneously and independently, high efficiency intramodal FWM, and low efficiency intermodal FWM is required. This requires a specific fiber design, where the intramodal phase matching condition should be satisfied, unlike the intermodal one. The key to achieve these two conditions, is to manipulate the phase matching condition that depends on the dispersion properties of the fiber, in a way to have a large difference between the IGVs of the modes ($\Delta\beta_1 = \beta_1^{01} - \beta_1^{11}$), and to minimize the dispersion between them ($\Delta\beta_2 = \beta_2^{01} - \beta_2^{11}$).

In order to design the proposed FMF, the starting point was to redesign the graded-index core double-clad fiber given in [64], in order to validate the model. Then the circular core was converted into an elliptical one to break the degeneracy between the linearly polarized degenerate modes LP_{11a} and LP_{11b}, along with some other parameters of the fiber that were

modified as will be shown later. The fiber core is doped with germanium with an alpha-law index profile, and a low index trench in the cladding. The refractive index profile as a function of the distance r from the center of the core is shown in Figure 3.3 along the major and minor axes, and is given by

$$n(r) = \begin{cases} n_1 \left[1 - 2\Delta n_{co} \rho \left(\frac{r}{a}\right)^{\alpha}\right]^{1/2} & 0 \le r \le a \\ \frac{n_{cl}}{(1-2\Delta n_{tr})^{1/2}} & a < r \le b \\ n_1 (1 - 2\Delta n_{co})^{1/2} = n_{cl} & r > b \end{cases} \quad (3.10)$$

where a is the core radius and b is the inner cladding radius. The refractive index at the center of the core is n_1, and n_{cl} is the index of the outer cladding. Δn_{co} is the refractive index difference between the center of the core and the outer cladding, and Δn_{tr} is the one between the inner cladding (trench) and the outer cladding. α is the profile exponent that describes the shape of the core. When $\alpha = 1$, the core index profile is triangular, while $\alpha = \pm\infty$ leads to a uniform index profile. ρ is the grading parameter that controls how graded the refractive index is between the core center and the core edge. When $\rho = 1$, the refractive index at the core edge is equal to that of the outer cladding $n(a) = n_{cl}$, and when $\rho < 1$, it leads to a refractive index at the core edge higher than that of the outer cladding $n(a) > n_{cl}$.

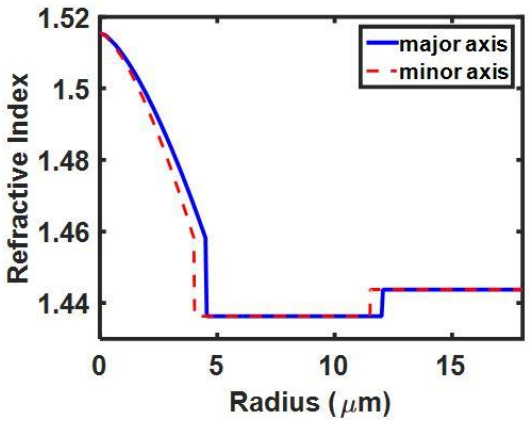

Figure 3.3: Refractive index profile of the proposed fiber along the major and minor axes.

The fiber profile is elliptical, therefore, the radius of the elliptical core is taken as $a_1 = 4.5$ µm along the major axis, and $a_2 = 4$ µm along the minor axis. The modal analysis of the fiber parameters is performed using a finite-element mode-solver (COMSOL), where a default physics-controlled mesh was used. It is a simple unstructured tetrahedral mesh, and is automatically created and adapted for the fiber model, as shown in Figure 3.4. The intensity distribution of the resulting three modes LP_{01}, LP_{11a} and LP_{11b} supported by the fiber are shown

in Figure 3.5. The resulting data are integrated into Matlab, and the dispersion properties are calculated. Figure 3.6(a) shows the IGVs of the three modes, and Figure 3.6(b) shows their GVDs, taking material dispersion properties into account, given by Sellmeier equations [95]. The refractive index is then described as a function of the wavelength using the Sellmeier equation, in which the Sellmeier coefficients depend on the germanium doping concentration in the core taken as 49 mol.%, and the relationship to represent the refractive index of GeO_2-SiO_2 composition can be given by [95]

$$n^2 - 1 = \sum_{i=1}^{3} \frac{[SA_i + X(GA_i - SA_i)]\lambda^2}{\lambda^2 - [Sl_i + X(Gl_i - Sl_i)]^2} \tag{3.11}$$

where SA, Sl, GA, Gl are the Sellmeier corfficients for the SiO_2 and GeO_2 glasses given in Table 3.1, respectively, and X is the mole fraction of GeO_2. Fabrication of fibers with a germanium concentration of up to 97 mol.% has been reported [96], therefore, fabricating this fiber might be possible.

SiO_2	SA_1	Sl_1	SA_2	Sl_2	SA_3	Sl_3
	0.6961663	0.0684043	0.4079426	0.1162414	0.8974794	9.896161
GeO_2	GA_1	Gl_1	GA_2	Gl_2	GA_3	Gl_3
	0.80686642	0.068972606	0.71815848	0.15396605	0.85416831	11.841931

Table 3.1: Sellmeier coefficients for SiO_2 and GeO_2.

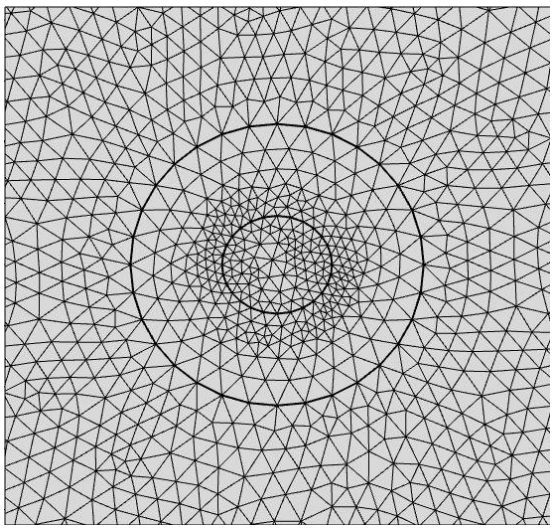

Figure 3.4: Physics-controlled mesh

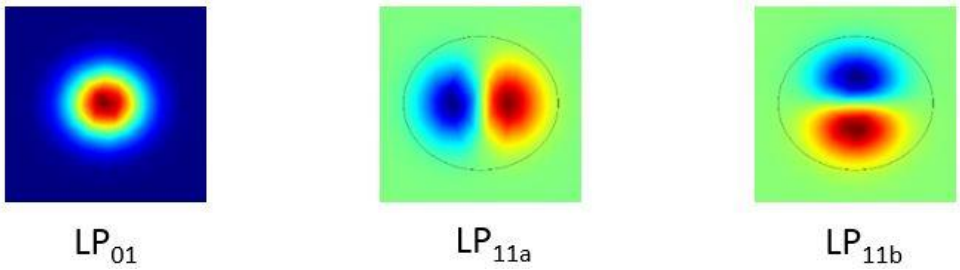

Figure 3.5: Intensity distribution of the resulting three modes LP_{01}, LP_{11a} and LP_{11b} supported by the fiber.

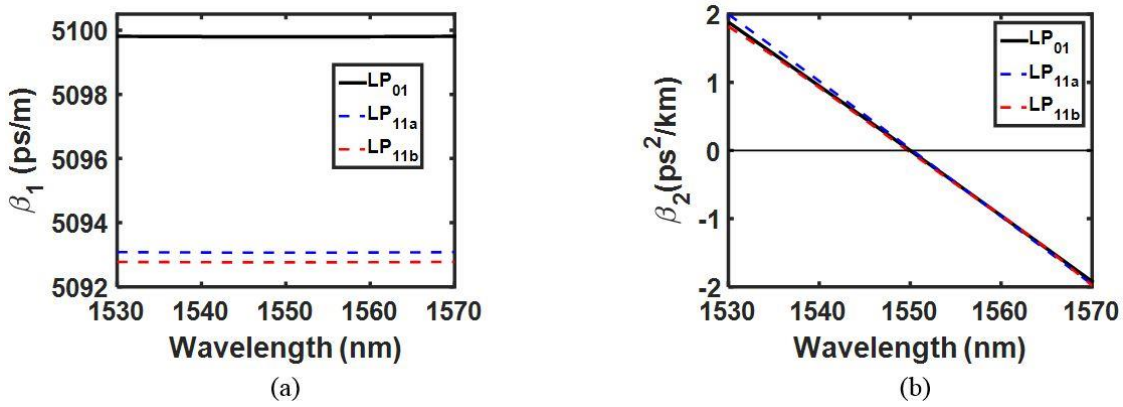

Figure 3.6: (a) Inverse group velocity of the three modes and (b) group velocity dispersion of the three modes.

The fiber parameters are optimized in a way that the ZDW of the three modes are minimized and shifted around 1.55 μm in the C-band. However, the difference between their IGVs $\Delta\beta_1$ is large. In fact, α is the parameter that affects $\Delta\beta_1$ the most. For a parabolic index profile ($\alpha = 2$), the modes have similar IGVs. In our case, α will be taken as 1.45 to prevent all intermodal processes among the modes. In order to bring closer the ZDWs of the three modes, and match them around 1.55 μm, ρ is chosen as 0.73. These parameters will finally make it possible to simultaneously satisfy the phase matching condition for three intramodal MI processes on the three fiber modes. It should be pointed that the fiber supports an additional mode (LP_{02}), that will be ignored. It can however be assumed that there will not be any significant linear coupling, because of the large difference in the propagation constants of the modes, as shown in Figure 3.7(a). And, if the mode was to be excited, its group velocity is such that there will not be any nonlinear intermodal interaction with the other modes due to the large IGV difference, as shown in Figure 3.7(b). Therefore, it will not cause any modal crosstalk and will not affect the MI processes.

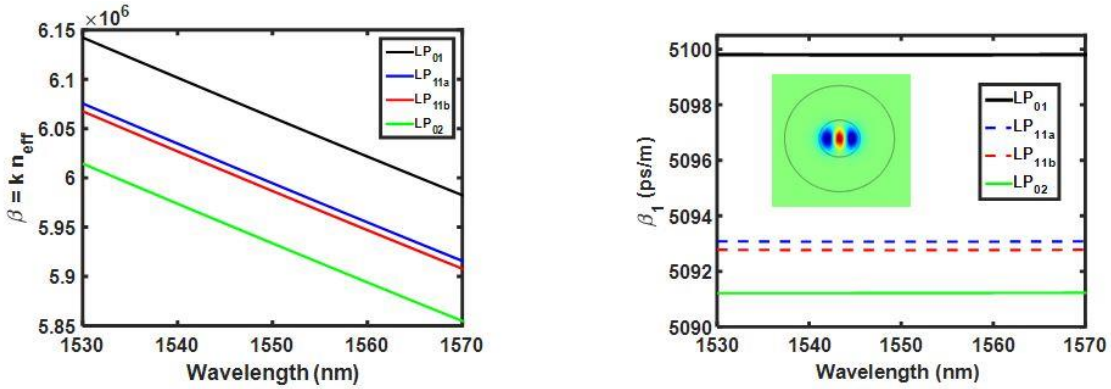

Figure 3.7: (a) Propagation constants of the modes and (b) inverse group velocities of the modes with the distribution profile of the mode LP_{02}.

3.4 Mode Independent Wavelength Conversion

Considering a pump and a signal propagating on the three modes LP_{01}, LP_{11a} and LP_{11b} denoted as $P^{01/11a/11b}$ and $S^{01/11a/11b}$, an idler $I^{01/11a/11b}$ can be created on the three modes as well through several intra and intermodal FWM processes listed in Table 3.2 among one or two pump modes (P^{01} and P^{11a}, P^{01} and P^{11b}, P^{11a} and P^{11b}), and one of the signal modes (S^{01}, S^{11a}, S^{11b}) as shown in Figure 3.8.

FWM 1-3 are MI intramodal processes, where the pump, signal and idler are all propagating on the same mode. The rest of the FWM processes are intermodal processes with two modes involved, where FWM 4-7 represent the PC processes. Therefore, the created idlers from FWM 1-6-7-9-11 are in the LP_{01} mode, and the idlers generated by FWM 1-9-11 carry the data initially modulated on the LP_{01} signal mode. However, FWM 6-7 carry the data initially modulated on the LP_{11a} and LP_{11b} signal modes, respectively. Similarly, for the idlers created on the LP_{11a} and LP_{11b} modes. All the FWM processes can be divided into degenerate and nondegenerate FWMs according to the number of the participant pump modes.

	FWM Process
FWM 1	$2P^{01} \longrightarrow S^{01} + I^{01}$
FWM 2	$2P^{11a} \longrightarrow S^{11a} + I^{11a}$
FWM 3	$2P^{11b} \longrightarrow S^{11b} + I^{11b}$
FWM 4	$P^{01} + P^{11a} \longrightarrow S^{01} + I^{11a}$
FWM 5	$P^{01} + P^{11b} \longrightarrow S^{01} + I^{11b}$
FWM 6	$P^{01} + P^{11a} \longrightarrow S^{11a} + I^{01}$
FWM 7	$P^{01} + P^{11b} \longrightarrow S^{11b} + I^{01}$
FWM 8	$2P^{01} \longrightarrow S^{11a} + I^{11a}$
FWM 9	$2P^{11a} \longrightarrow S^{01} + I^{01}$
FWM 10	$2P^{01} \longrightarrow S^{11b} + I^{11b}$
FWM 11	$2P^{11b} \longrightarrow S^{01} + I^{01}$
FWM 12	$2P^{11a} \longrightarrow S^{11b} + I^{11b}$
FWM 13	$2P^{11b} \longrightarrow S^{11a} + I^{11a}$

Table 3.2: FWM processes in a three-mode fiber.

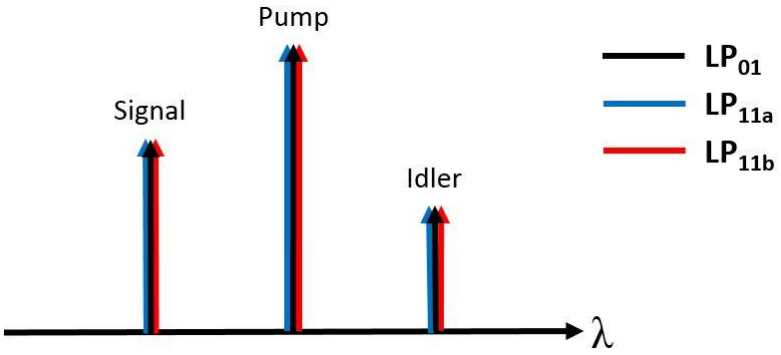

Figure 3.8: Schematic description of the FWM processes.

The phase mismatches for the different FWM processes are calculated according to Equations (2.35) and (2.40) and shown in Figure 3.9(a), when the wavelength of the three pumps on the three modes ($P^{01/11a/11b}$) are fixed at the ZDW 1550 nm, while varying the wavelength of the signal. It can be realized that the intramodal processes given by FWM 1-3 are well matched, which can be confirmed by the expansion of their phase mismatch in Figure 3.9(b), given that their phase matching conditions are only related to the second derivative of the propagation constant. The phase mismatches of the intermodal PC processes given by FWM 4-7 are large and far from being matched. However, it is normal to obtain phase

matching when the wavelength of the signal approaches and coincides with the wavelength of the pump. Once getting away from the wavelength of the pump, the phase matching is immediately lost and the conversion bandwidth in this case will be narrow. In fact, as described earlier, the fiber was designed in a way that the IGV differences between the three modes are large enough to prevent all intermodal processes. Similar reasoning applies to the BS processes, and their phase mismatches will be very close and similar to the PC processes, and thus are not included in our discussion. The intermodal FWM 8-13 contain a large phase mismatch term $(\beta_0^{01} - \beta_0^{11a})$, and the phase matching in this case cannot be met regardless of the wavelength arrangement. β_0 is larger than the higher order terms β_1 and β_2, and it depends on the propagation mode. Therefore, β_0^{01} is different than β_0^{11a}. As a result, FWM 8-13 can be ignored because the power of the idler is much smaller than the other FWM processes due to their large phase mismatches. Subsequently, only intramodal FWMs take place in the fiber, and the process can then be called mode-independent wavelength conversion.

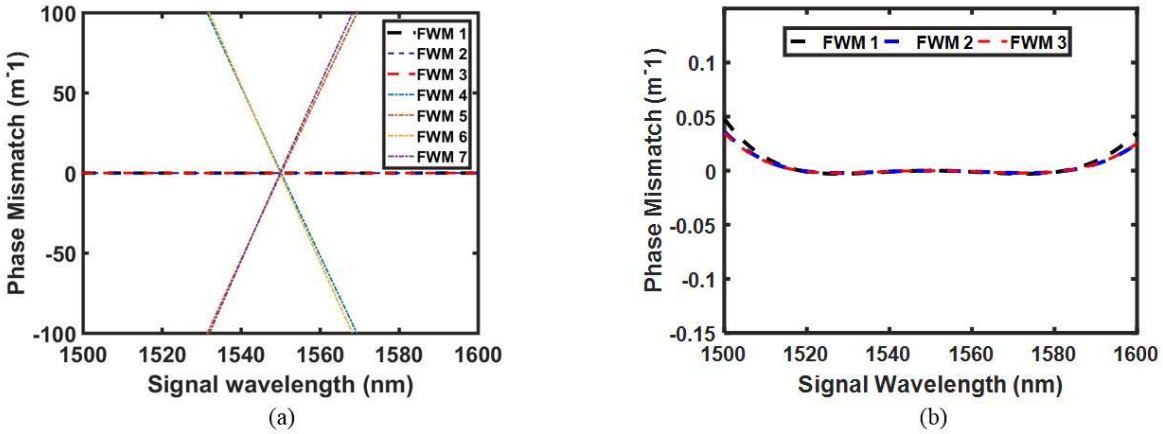

Figure 3.9: (a) Phase mismatches of the different FWM processes and (b) phase mismatch expansion of the MI intramodal FWM processes given by FWM 1-3.

In the following, we will study the conversion efficiencies corresponding to the phase matching conditions in Figure 3.9(a). The propagation is simulated using the set of coupled nonlinear propagation equations given by Equation (2.50), using the split-step Fourier method. The step-size was chosen as 1 m, according to comparison and validation of the numerical simulations with other references. The nonlinear coefficient between two modes is given by Equation (2.46). Given that no longitudinal component in modes profile, Equation (2.47) is used to calculate the effective area A_{eff}. The mode fields distribution obtained by COMSOL are used to calculate the effective area A_{eff}, using the Simpson method, where the fields distributions are defined on a rectangular grid with equal spacings. Therefore, the calculated effective areas are

$A_{eff}^{01,01} = 14.8\,\mu m^2$, $A_{eff}^{11a,11a} = 21.6\,\mu m^2$, $A_{eff}^{11b,11b} = 21.9\,\mu m^2$, $A_{eff}^{01,11a} = 31.4\,\mu m^2$, $A_{eff}^{01,11b} = 32.6\,\mu m^2$ and $A_{eff}^{11a,11b} = 64.7\,\mu m^2$, which leads to the following nonlinear coefficients $\gamma_{01,01} = 7.1\,(W.km)^{-1}$, $\gamma_{11a,11a} = 4.9\,(W.km)^{-1}$, $\gamma_{11b,11b} = 4.8\,(W.km)^{-1}$, $\gamma_{01,11a} = 3.3\,(W.km)^{-1}$, $\gamma_{01,11b} = 3.2\,(W.km)^{-1}$ and $\gamma_{11a,11b} = 1.6\,(W.km)^{-1}$. The fiber length is taken as 1 km, and the losses are considered as 0.22 dB/km for all the modes. The power of each of the three pumps on the three modes are taken as 63.1 mW, and the power of the varying signals on the three modes as 3.9 mW. Figure 3.10(a) shows the conversion efficiencies of the FWM processes, that is defined as the ratio between the output idler power and the input signal power. According to the phase mismatches in Figure 3.9(a), large intramodal and low intermodal FWM effects are expected, which can be confirmed in Figure 3.10(a) with the higher efficiency of the intramodal FWM 1-3 compared to the other intermodal FWMs. Moreover, an expansion of FWM 1-3 is shown in Figure 3.10(b). The conversion bandwidths are also different for the considered FWM processes. For instance, the intramodal FWM processes have large conversion bandwidths that exceed 65 nm, while the conversion bandwidths of the intermodal processes are extremely narrower due to their large phase mismatches, that also lead to a very low conversion efficiency. Therefore, supposing the FWM 1-6-7 that create idlers on the LP_{01} mode, while originating from different signals on the LP_{01}, LP_{11a} and LP_{11b} modes, the crosstalk resulting from these simultaneous processes in this case will be negligible, due to the low efficiency of intermodal FWM 6-7 processes that will not affect the high efficiency of the intramodal FWM 1 process. The same reasoning applies for the other FWM processes where idlers are created on the modes LP_{11a} and LP_{11b}. Therefore, all the FWM processes occur simultaneously in the fiber, and do not affect each other. FWM 1-3 have slightly different efficiencies under the same pump power condition because of the difference between their nonlinear coefficients. However, their efficiencies can be tuned by setting the pump powers to obtain the same conversion and peak efficiency -7.2 dB. Consequently, simultaneous wavelength conversion can be achieved in the fiber on the three modes independently, with high conversion efficiencies, when sweeping the signals over a broad wavelength range. Figure 3.11 shows the conversion efficiency for the three MI intramodal FWM 1-3 processes, calculated while increasing the power of the pumps. As can be seen, it is expected that the conversion efficiency for the three processes on the three modes, increases with the power of the pumps. It should however be noted that, no specific restrictions were imposed on the chosen values of the pumps−signals powers, or fiber length. Reasonable power values were chosen, in case of any limitations in practice, such as fiber melting. It should

also be noted that for shorter fiber lengths, larger conversion bandwidths can be obtained, while decreased conversion efficiencies in Figure 3.10. Therefore, all the parameters were chosen according to a compromise, in order to obtain sufficient large conversion bandwidths, and high conversion efficiencies, as the main purpose was to demonstrate simultaneous wavelength conversion processes on different modes.

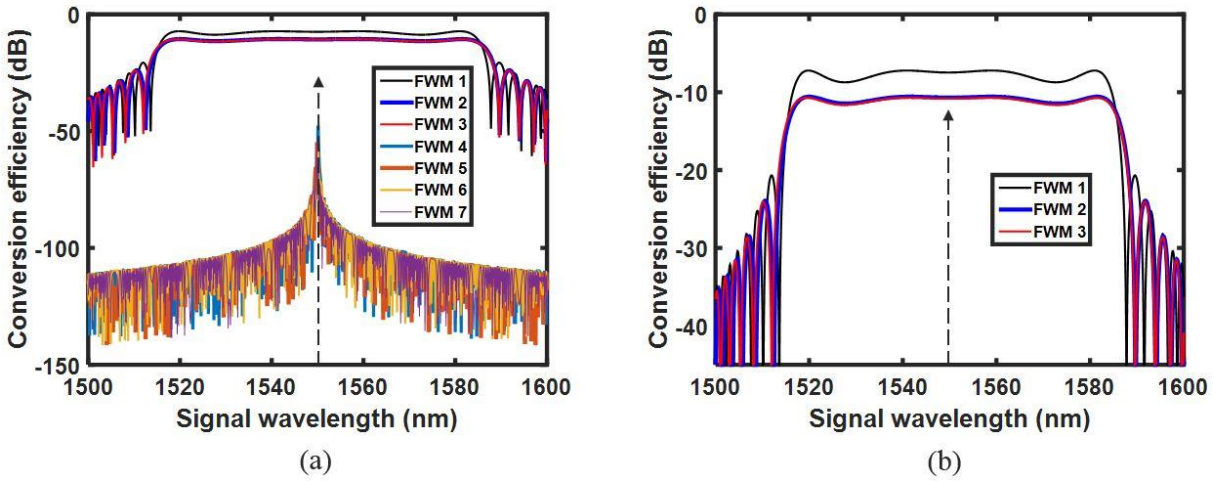

Figure 3.10: (a) Conversion efficiencies of the intra and intermodal FWMs and (b) expansion of the conversion efficiencies of the intramodal FWM 1-3. The arrow indicates the wavelength of the pumps.

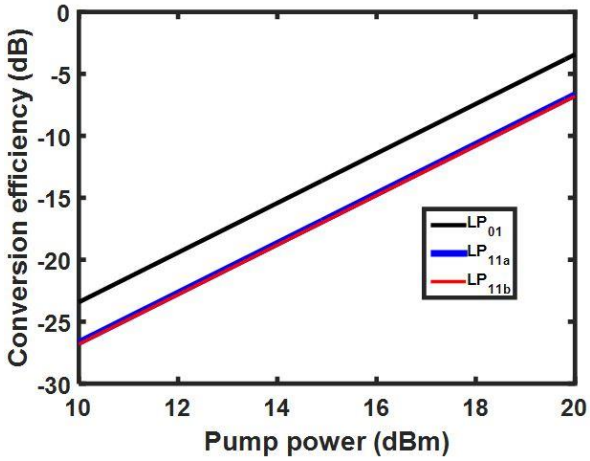

Figure 3.11: Conversion efficiency of the three intramodal processes, while increasing the power of the pumps.

Figure 3.12 shows how the conversion efficiency is affected when moving the wavelength of the pumps that was originally set at the ZDW of the fiber 1550 nm. In this case, it will be shifted 2 nm from the ZDW. As can be seen in Figure 3.12 (a), it can also be expected that, the further

the wavelength of the pumps from the ZDW, the less the phase matching is matched. This means that the conversion bandwidth will get narrower, as can be seen in Figure 3.12 (b).

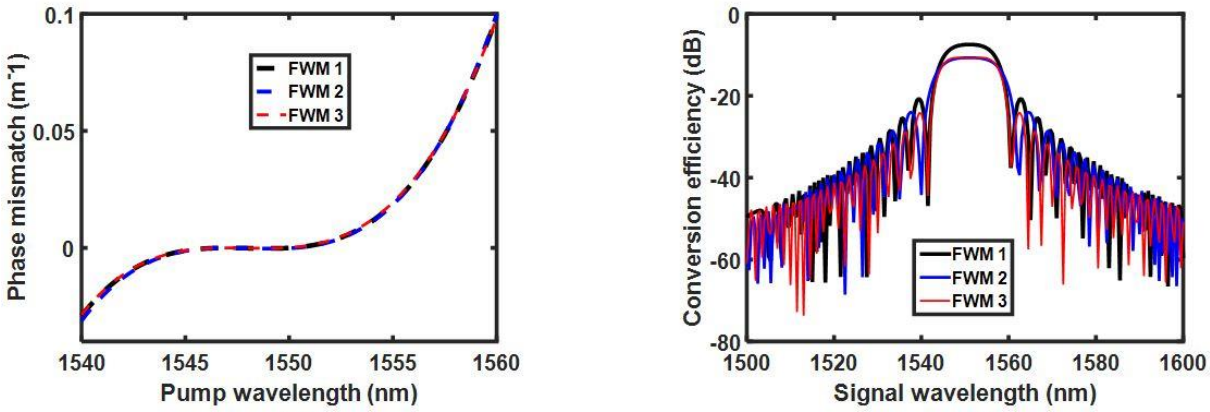

Figure 3.12: (a) Phase mismatch of the three intramodal FWM 1-3 processes when the wavelength of the pumps is shifted 2 nm from the ZDW and (b) corresponding conversion efficiencies.

3.5 Mode Independent Phase-Sensitive Frequency Conversion

PSFC AOSP has received a significant interest in recent years, and has been studied in single mode nonlinear fibers. It is based on FWM and allows the conversion of two quadrature components of a signal to two different frequencies. R. P. Webb *et al*, have demonstrated phase discrimination and frequency conversion by using four pumps together with a signal, to all-optically separate two complex quadratures of the signal by converting them to different wavelengths in a semiconductor optical amplifier as a nonlinear media, using phase-sensitive FWM [97]. Among other nonlinear media, highly nonlinear optical fibers are another option. F. Da Ros *et al*. demonstrated the conversion of the two complex quadratures of a quadrature phase-shift keying signal to two binary phase-shift keying signals in a highly-nonlinear fiber [98], and in a periodically-poled lithium niobate waveguide [99]. Besides the use of the four pumps, their power levels and phases had to be carefully adjusted. M. Baillot *et al*, demonstrated more recently the PSFC mechanism in nonlinear optical fibers by using three pumps instead of four as originally proposed. The theoretical study of the mechanism was proposed and simple relations to determine the initial values of the power levels and phases of the pumps were provided [100], where the process was experimentally demonstrated. It was

also shown that the PSFC requires careful adjustment of only two parameters (two pump phases).

The operation principle of the PSFC scheme is depicted in Figure 3.13(a). Three continuous waves (CWs) pumps P1, P2 and P3, are launched in a fiber. A signal S is injected in the fiber, located between P2 and P3. Depending on the phase of the signal ϕ_s, an idler I1 or I2 can be generated by FWM, provided that the pumps and signal are coherent. For instance, the idler I1 can be generated when $\phi_s = 0$, and I2 can be generated when $\phi_s = \pi/2$, as can be seen in Figure 3.13(a). The evolution of the powers of the two idlers can also be shown in Figure 3.13(b) as a function of the signal phase. The setup enables the simultaneous conversion of the two orthogonal quadratures of S to different wavelengths. In order to ensure that the idlers I1 and I2 correspond to the quadratures of the S, the power levels and phases of the pumps have to be carefully adjusted together with the signal power.

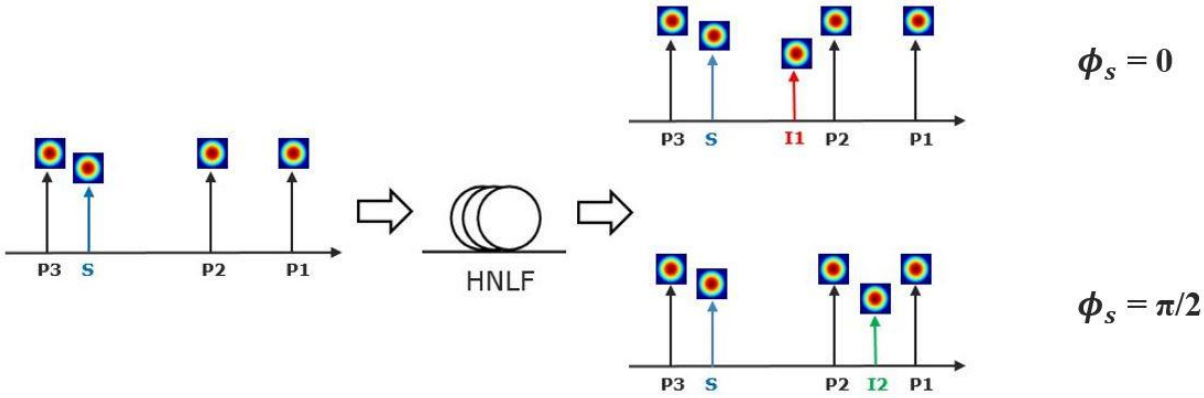

(a)

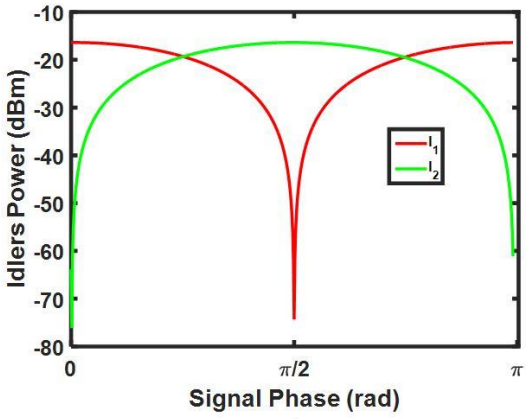

(b)

Figure 3.13: (a) Operation principle of phase-sensitive FWM frequency conversion and (b) evolution of the powers of the two idlers I1 and I2.

A theoretical study conducted in [100], to determine analytic expressions for the pump power levels and phases, led to two conditions that must be satisfied to meet the requirements of the PSFC process. The first condition related to the power, requires that the pump powers levels must be equal. The second condition concerns the phase of the interacting waves, where Table 3.3 provides examples of possible values for the phases of the different waves, to satisfy the PSFC process.

ϕ_{P1}	ϕ_{P2}	ϕ_S	ϕ_{P2}
0	π	0	0
π	0	0	π
π	π	π/2	0
0	0	π/2	π

Table 3.3: Possible values for the phases of the different waves to satisfy the PSFC process.

Coming back to our designed fiber in Section 3.3 that allows the propagation of three modes, the PSFC process will be studied in this fiber. The PSFC process will then be extended to the number of the modes of the fiber, trying to achieve three independent PSFC in the same fiber, as depicted in Figure 3.14. Therefore, three pumps and a signal propagate on the three modes simultaneously in the fiber. At a signal phase 0, the first idler I1 will be generated on the three modes simultaneously. Similarly, by changing the phase of the signal, I2 will be generated on the three modes as well.

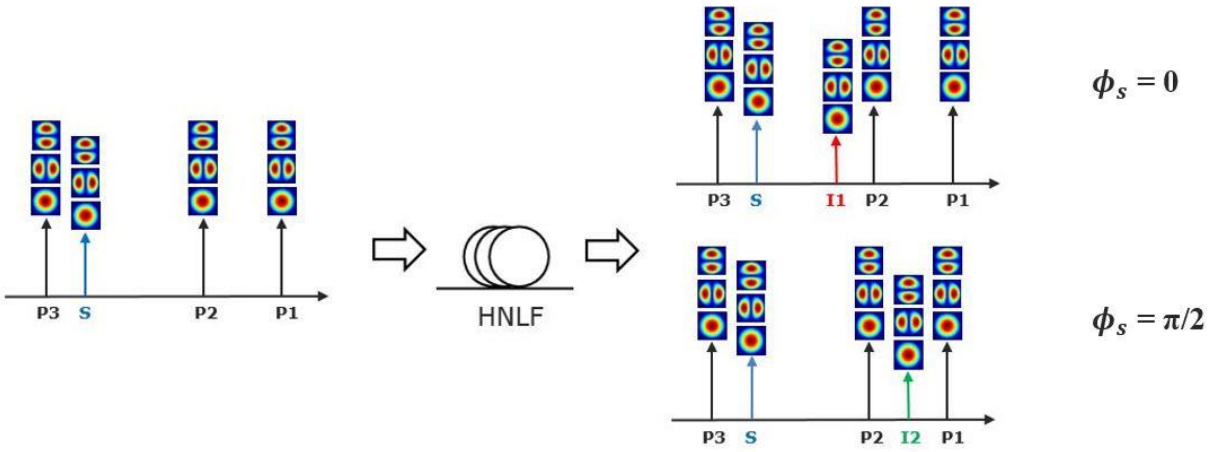

Figure 3.14: PSFC process extended to the three modes of the fiber, achieving three independent PSFC processes in the same fiber.

The propagation in the fiber is simulated using the set of coupled nonlinear propagation equations given by Equation (2.50), using the split-step Fourier method. The nonlinear coefficients and the fiber parameters are the same as in Section 3.4. Three pumps (P1, P2, P3) and a signal (S), with wavelengths of 1550.4 nm, 1550 nm, 1549.2 nm and 1549.4 nm, respectively, simultaneously propagate in the fiber on the three modes LP_{01}, LP_{11a} and LP_{11b}. Their power levels are set to the same value of 3.1 mW. No specific condition is required on the pump powers, provided that they are equal. No condition is neither required for the signal power. Their phases are chosen according to the conditions given in Table 3.3, with a phase of 0 for P1 and P3, π for P2, while the phase of the signal varies from 0 to π. Note that the phase of the signal given in Table 3.3 is when I1 is generated. Figure 3.15(a) represents the optical spectrum at the output of the fiber for a signal phase $\phi_S = 0$, where the first idler I1 is generated at 1549.8 nm on the three modes. Figure 3.15(b) represents the optical spectrum at the output of the fiber for a different signal phase $\phi_S = \pi/2$, where I1 vanishes, and the second idler I2 is generated at a different wavelength 1550.2 nm on the three modes as well. We can also notice that additional idlers are generated due to extra FWM processes. Figure 3.16 shows the evolution of the power of the six generated idlers by the three intramodal independent PSFC processes on the three modes as a function of the signal phase ϕ_S. The scheme that was originally studied with four, and three pumps, to convert the two quadrature components of a signal to different idlers, is simultaneously achieved in the designed fiber on its three modes LP_{01}, LP_{11a} and LP_{11b}.

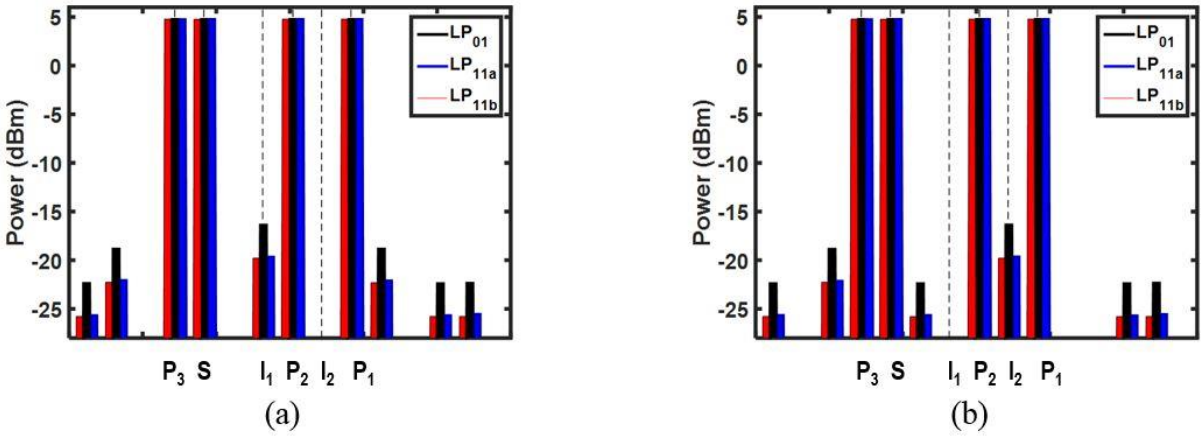

Figure 3.15: (a) Optical spectra at the output of the fiber for $\phi_S = 0$ and (b) $\phi_S = \pi/2$.

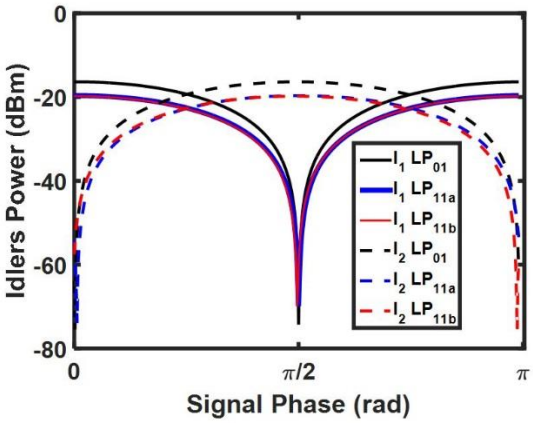

Figure 3.16: Evolution of the power of I1 and I2 as a function of the signal phase on the three modes.

As a reminder, the fiber was designed in such a way that the IGV differences between the three modes are large enough to prevent all intermodal processes between the interacting waves in the fiber. Therefore, only intramodal interactions are considered through the PSFCs. In fact, 22 intramodal FWM processes occur between the interacting waves on each of the three modes, where their phase mismatches are summarized in Table 3.4, with I3 as the idler generated at the wavelength 1549.8 nm due to extra FWM. For the results obtained in Figures 3.15 and 3.16, the wavelength separation between the interacting waves was chosen as 0.2 nm. The phase mismatch for the 22 intramodal FWM processes were calculated for a wavelength separation ranging from 0.1 to 0.5 nm and shown in Figure 3.17(a) for the intramodal PSFC process occurring on the mode LP_{01}, Figure 3.17(b) on the mode LP_{11a} and Figure 3.17(c) on the mode LP_{11b}. It can be realized that, the larger the wavelength separation between the interacting waves, the larger is the phase mismatch, which means that the PSFC process will be lost.

Intramodal FWM Processes	Phase mismatches
1	$\Delta\beta = 2\beta_{I1} - \beta_{P2} - \beta_{I3}$
2	$\Delta\beta = 2\beta_{I3} - \beta_{I1} - \beta_{S}$
3	$\Delta\beta = 2\beta_{P2} - \beta_{I2} - \beta_{I1}$
4	$\Delta\beta = 2\beta_{S} - \beta_{I3} - \beta_{P3}$
5	$\Delta\beta = 2\beta_{I2} - \beta_{P1} - \beta_{P2}$
6	$\Delta\beta = \beta_{P2} + \beta_{s} - \beta_{I1} - \beta_{I3}$
7	$\Delta\beta = \beta_{P2} + \beta_{I1} - \beta_{I3} - \beta_{I2}$
8	$\Delta\beta = \beta_{P3} + \beta_{I1} - \beta_{I3} - \beta_{S}$
9	$\Delta\beta = \beta_{P1} + \beta_{I1} - \beta_{P2} - \beta_{I2}$
10	$\Delta\beta = \beta_{I2} + \beta_{s} - \beta_{I3} - \beta_{P2}$
11	$\Delta\beta = \beta_{P3} + \beta_{P2} - \beta_{I1} - \beta_{S}$
12	$\Delta\beta = \beta_{I3} + \beta_{P1} - \beta_{I2} - \beta_{I1}$
13	$\Delta\beta = 2\beta_{I1} - \beta_{S} - \beta_{I2}$
14	$\Delta\beta = \beta_{P2} + \beta_{S} - \beta_{P3} - \beta_{I2}$
15	$\Delta\beta = \beta_{P1} + \beta_{S} - \beta_{I3} - \beta_{I2}$
16	$\Delta\beta = 2\beta_{I3} - \beta_{P3} - \beta_{P2}$
17	$\Delta\beta = 2\beta_{P2} - \beta_{I3} - \beta_{P1}$
18	$\Delta\beta = \beta_{P1} + \beta_{P3} - \beta_{I2} - \beta_{S}$
19	$\Delta\beta = \beta_{P3} + \beta_{I2} - \beta_{I1} - \beta_{I3}$
20	$\Delta\beta = \beta_{S} + \beta_{P1} - \beta_{P2} - \beta_{I1}$
21	$\Delta\beta = \beta_{P3} + \beta_{P1} - \beta_{I3} - \beta_{P2}$
22	$\Delta\beta = 2\beta_{I1} - \beta_{P1} - \beta_{P3}$

Table 3.4: The 22 intramodal FWM processes that occur between the interacting waves on each of the three modes.

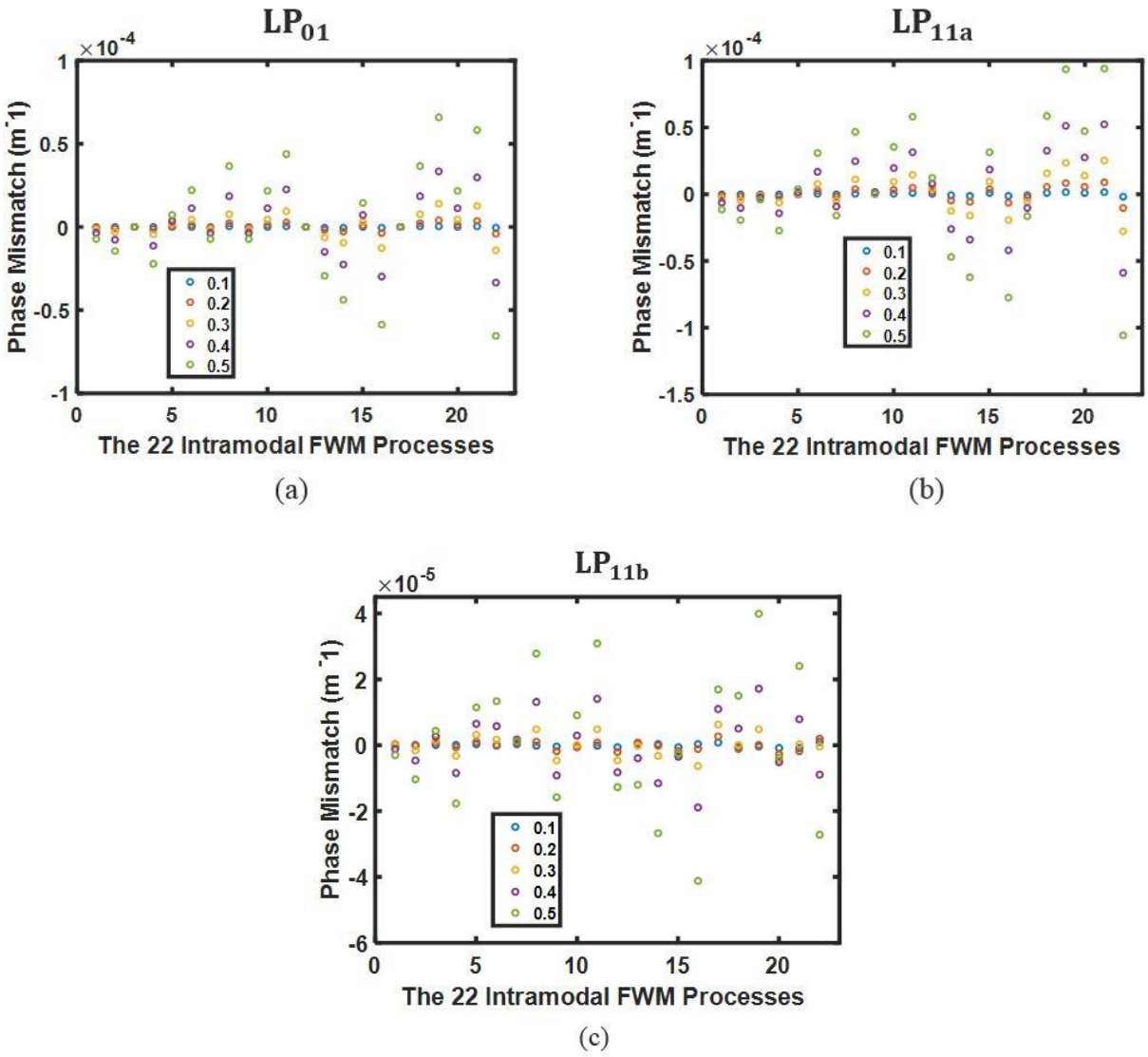

Figure 3.17: Phase mismatches for the 22 intramodal FWM processes listed in Table 3.4, calculated for wavelength separation ranging from 0.1 to 0.5 nm, on the modes (a) LP_{01}, (b) LP_{11a} and (c) LP_{11b}. The legend corresponds to the wavelength separation.

3.6 Mode Independent Phase-Sensitive Amplification

In this section, we show another AOSP application that can be performed in the designed fiber on its three modes, simultaneously and independently. Long-haul communication systems require optical amplifiers to compensate fiber loss. Amplifiers such as EDFA are used in current systems, and are phase-insensitive amplifiers, where the signal gain is independent of the signal phase. Considerable interest in PSA has arisen as well due to their potential for optical signal processing. Their potential advantages include parametric phase noise suppression [101],

all-optical regeneration [44, 102, 103], low-noise amplification [104, 105, 106] and dispersion compensation [107]. PSA can be realized in $\chi^{(2)}$ and $\chi^{(3)}$ media such as periodically-poled lithium niobate waveguide [108, 109], and highly nonlinear fiber [110, 102, 103]. The process can be performed using FWM. PSA based on intermodal FWM has been investigated when the signal and idler are frequency degenerate, and mode nondegenerate [111]. However, this chapter is based on intramodal FWM, as the main purpose is to investigate different AOSP applications on different modes of the fiber simultaneously and independently. Therefore, we will consider in the following the PSA process using intramodal FWM where the pumps and signal are all carried on the same mode. Similarly to the previous sections, the FWM effect will be extended to the number of modes supported by the fiber, thus three PSA schemes will be implemented simultaneously on the three modes. In this case, two pumps P1 and P2 with frequencies ω_1 and ω_2 respectively, along with a signal ω_3, propagate on each of the three modes of the fiber LP_{01} and $LP_{11a,b}$. The propagation causes the generation of an idler ω_4, where the signal and idler in this case are frequency degenerate ($\omega_3 = \omega_4$), as shown in Figure 3.18.

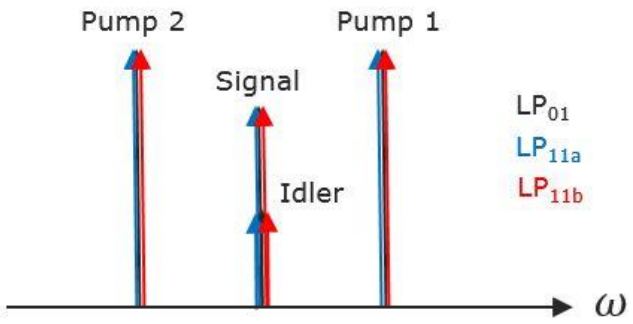

Figure 3.18: Multiple intramodal FWM on the three modes of the fiber LP_{01} and $LP_{11a,b}$, where the signal and idler are frequency degenerate.

According to the fiber design, it is also expected to obtain strong intramodal PSAs, and weak intermodal PSAs among different modes. Table 3.5 shows the intramodal and intermodal FWMs that may occur in the fiber, by representing their phase mismatches. Figures 3.19(a)-(b) represent the calculated phase mismatches, when the wavelength of the signals is fixed at 1550.1 nm, and the wavelength of P2 at 1550.3 nm, while sweeping the wavelength of P1. The wavelength of P1 should indeed be fixed at 1549.9 nm. However, we calculate the phase mismatch by sweeping P1 just to verify the absence of intermodal FWM. Therefore, it can be realized from Figure 3.19(a) the low phase mismatch for the intramodal processes, while the

large phase mismatch for the intermodal processes in Figure 3.19(b), ensuring then the absence of cross-mode PSA.

	Phase mismatches
FWM 1	$\Delta\beta = \beta_{P1}^{01} + \beta_{P2}^{01} - \beta_{S}^{01} - \beta_{I}^{01}$
FWM 2	$\Delta\beta = \beta_{P1}^{11a} + \beta_{P2}^{11a} - \beta_{S}^{11a} - \beta_{I}^{11a}$
FWM 3	$\Delta\beta = \beta_{P1}^{11b} + \beta_{P2}^{11b} - \beta_{S}^{11b} - \beta_{I}^{11b}$
FWM 4	$\Delta\beta = \beta_{P1}^{01} + \beta_{P2}^{01} - \beta_{S}^{11a} - \beta_{I}^{11a}$
FWM 5	$\Delta\beta = \beta_{P1}^{11a} + \beta_{P2}^{11a} - \beta_{S}^{01} - \beta_{I}^{01}$
FWM 6	$\Delta\beta = \beta_{P1}^{01} + \beta_{P2}^{01} - \beta_{S}^{11b} - \beta_{I}^{11b}$
FWM 7	$\Delta\beta = \beta_{P1}^{11b} + \beta_{P2}^{11b} - \beta_{S}^{01} - \beta_{I}^{01}$
FWM 8	$\Delta\beta = \beta_{P1}^{11a} + \beta_{P2}^{11a} - \beta_{S}^{11b} - \beta_{I}^{11b}$
FWM 9	$\Delta\beta = \beta_{P1}^{11b} + \beta_{P2}^{11b} - \beta_{S}^{11a} - \beta_{I}^{11a}$

Table 3.5: Phase mismatches of the intra and intermodal FWMs that occur in the fiber.

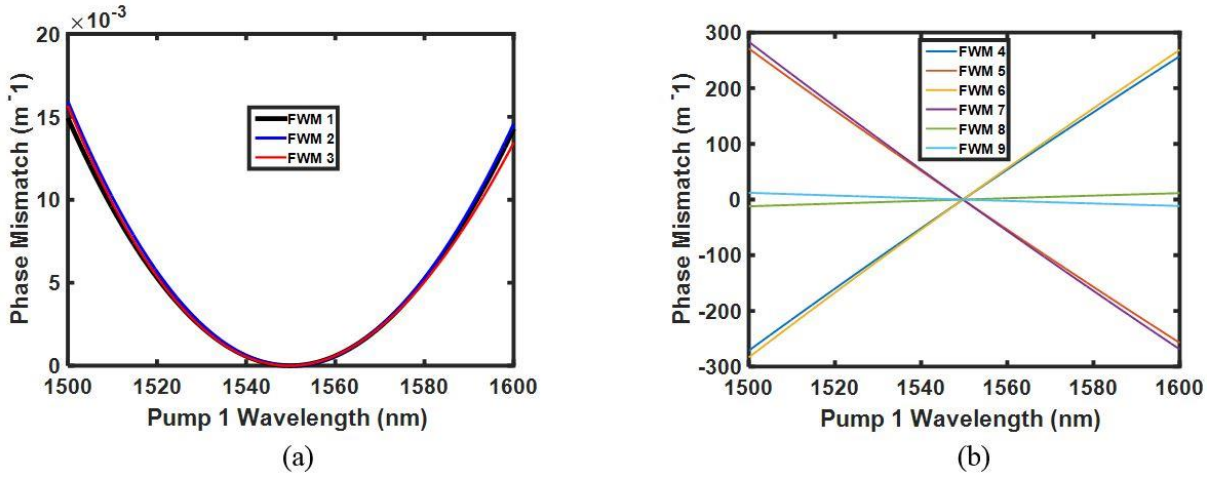

Figure 3.19: Phase mismatch of the (a) three intramodal FWMs and (b) intermodal FWMs.

In the following, we will study the PSA gain, by fixing the wavelength of P1 at 1549.9 nm. The fiber parameters are the same as in previous sections, with a 1 km fiber length. The coupled equations [8] are used to perform the calculations, where the coupled equation describing the slowly varying envelope of the signal given in a mode *x* can be written as

$$\frac{dA_{sx}}{dz} = i\left(\gamma_{xx}|A_{sx}|^2 A_{sx} + 2\sum_{n=x,y,z}\sum_{m}\gamma_{xn}|A_{mn}|^2 A_{sx} + 2\sum_{n=sx,ix}\gamma_{xx}A_{p1x}A_{p2x}A_n^* e^{-i\Delta\beta n}\right.$$

$$\left. + 2\sum_{n=sy,iy}\gamma_{xy}\,A_{p1y}A_{p2y}A_n^* e^{-i\Delta\beta n} + 2\sum_{n=sz,iz}\gamma_{xz}\,A_{p1z}A_{p2z}A_n^* e^{-i\Delta\beta n}\right) \tag{3.12}$$

Figure 3.20 shows the signal gain defined as the ratio between the signal output and input power, as a function of the signal phase ϕ for various pump power values of 25 mW, 39 mW, 63 mW and 100 mW, when the signal's power is fixed at 1 mW. The sinusoidal gain curves with a period of π on the three modes can be observed.

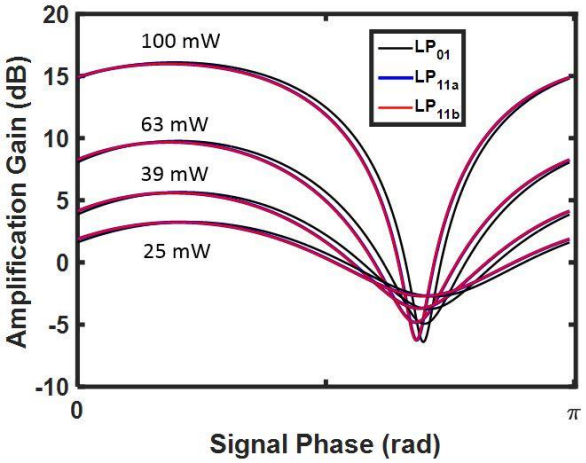

Figure 3.20: PSA gain as a function of the signal phase for various pumps power.

The gain extinction ratio (GER) is defined as the difference between the maximum and minimum signal PSA gain. The GERs for the three modes are approximately similar, and are given approximately as 22.5 dB, 14.7 dB, 9.4 dB and 5.9 dB, for the pumps power 100 mW, 63 mW, 39 mW and 25 mW, respectively, and shown in Figure 3.21. According to Figures 3.20 and 3.21, the PSA scheme can be implemented on each mode of the three modes of the fiber, simultaneously and independently, where the GERs increase with the power of the pumps.

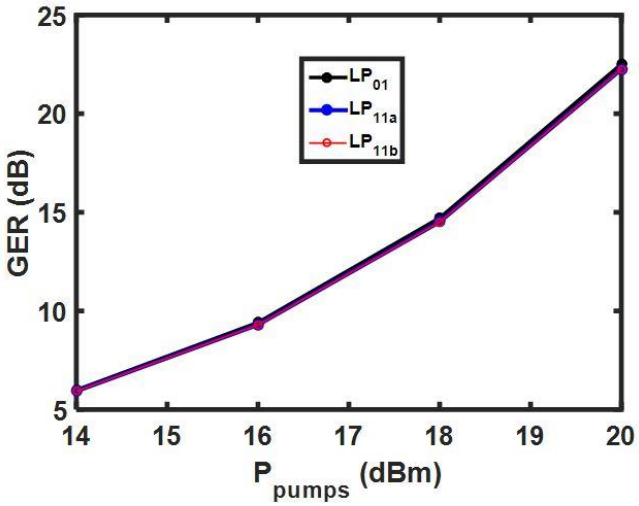

Figure 3.21: Calculated GER for the three modes, as a function of the pumps power.

3.7 Conclusion

In this chapter, we presented the design of a dispersion-shifted elliptical-core few-mode fiber that breaks the degeneracy between the LP_{11a} and LP_{11b} modes. The fiber allows to process the modes simultaneously and independently, using the intramodal FWM nonlinear effect. Therefore, multiple mode-independent nonlinear effects for AOSP in MDM systems were investigated, such as wavelength conversion, PSFC and PSA.

4 Intermodal Nonlinear Processes in Mode-Division Multiplexing

4.1 Introduction

This chapter will be dedicated to the intermodal goal, where nonlinear intermodal interactions between different modes will be studied in a specially designed FMF. Stolen et al. showed intermodal FWM for the first time in short cm-length optical fibers by achieving phase matching between different guided higher order spatial modes [67]. The efficiency of the FWM process was suppressed for longer fiber length, which was attributed to fiber non-uniformity. However, intermodal FWM was experimentally shown today in km-long FMF [75], which opens the curiosity to investigate what novelty intermodal FWM can provide in addition to intramodal FWM in signal processing for MDM, and if it can be considered as a potential mean to enhance AOSP applications. In addition to wavelength conversion, intermodal FWM can provide mode conversion [112], as well as multimode amplification, where the operating frequencies can be tuned over a broader spectrum than in conventional multimode Raman amplifiers and multimode EDFAs. It can also be tuned to operate far away from the spectral bandwidth of the main noise sources, spontaneous Raman scattering [113, 114] and amplified spontaneous emission [115]. In SMFs, operating near the ZDW of the fiber was required to achieve phase matching. This same condition was also required in FMFs, when processing the modes of the fiber independently using intramodal FWM as was shown in Chapter 3. However, operating near the ZDW when performing intermodal FWM is not required, as phase matching was shown to be realized for large wavelength separations [75, 76, 77]. Thus, intermodal FWM can be fully phase matched in the presence of large dispersion in each spatial mode. The main intermodal FWM processes are known as PC and BS. In the PC, the pumps amplify the signal and generate an idler, while BS is an energy exchange process between the signal and idler photons. Several studies were performed to investigate the nonlinear PC and BS FWM processes, by characterizing their phase matching properties in terms of efficiency and bandwidth in different fibers [76, 75, 77]. It was always found that they critically depend on the frequency separation of the two pumps, and that a larger signal bandwidth of phase matching was achievable for the BS than for the PC process, or vice versa. Thus, the two processes had different bandwidths, due to their different phase matching properties that had to be

manipulated in different ways using different fibers, as will be shown in section 4.2. Therefore, designing an FMF that allows large intermodal FWM bandwidths for both PC and BS processes seems to be more complicated than the case of MI process, when dealing with intramodal FWM. As the main condition of realizing intermodal FWM (PC or BS) was always critically based on the frequency separation of the two pumps, we report in this chapter the design of an elliptical-core graded-index dispersion shifted FMF, that allows in first place to break this condition and reduce the constraint of limited frequency separation between the interacting waves carried by different modes in order to obtain the intermodal PC and BS processes. Thereafter, the fiber breaks the degeneracy between the modes LP_{11a} and LP_{11b}, and shows low GVD and low DMD between its modes LP_{01}, LP_{11a} and LP_{11b}, and allows the sweeping relaxation of the pumps to bandwidths that can reach up to 23 nm, while maintaining an intermodal conversion efficiency that can reach up to 4.5 nm for both PC and BS processes, simultaneously. Note that in previous reported work on intermodal FWM, bandwidths of 4 nm [76, 77], or higher [78, 79], were obtained for PC or BS processes individually using different fibers, and once again, this was realized for a single critical frequency separation between the pumps.

In the following, Section 4.2 shows the approaches that have been followed in order to manipulate the phase matching properties of the intermodal processes. In Section 4.3, the design of the FMF and its properties are presented. Section 4.4 presents the results of numerical simulations of intermodal FWM processes based on the multimode NLSE. The sensitivity of the structural parameters of the fiber due to fabrication imperfections is analyzed in Section 4.5. Finally, Section 4.6 concludes the chapter.

4.2 Theory

According to Equations (3.8) and (3.9) that refer to the phase matching conditions of the intermodal PC and BS processes, respectively, it can be realized that they depend on the GVD of the modes, as well as on their IGVs. Therefore, achieving a large signal bandwidth of phase matching in this case is challenging, giving that the two terms β_1 and β_2 are involved, unlike the intramodal case that is only β_2 depended. Different fibers were designed for this purpose, for instance, a step-index MMF was designed for bandwidth enhancement for the PC process [78] that was depicted in Figure 3.2(b). In this case, when tuning the signal wavelength, the PC idler wavelength (Figure 3.2(b)) will move in the opposite direction due to energy

conservation. The fiber was then designed so that the IGVs of the two modes exhibit a mirror symmetry as shown in Figure 4.1(a). Consequently, for a given frequency separation, the modes (in this case LP_{01} and LP_{02}) will have similar IGVs, while having opposite GVDs, in order to satisfy the phase matching in Equation (3.8). Similarly, a graded-index MMF was designed for bandwidth enhancement for the BS process [79]. In this case, however, when tuning the signal wavelength, the BS idler wavelength moves in the same direction as the signal (Figure 3.2(c)). The fiber was therefore designed so that the IGVs versus wavelength curves of the two modes (in this case LP_{01} and LP_{11}) are parallel as shown in Figure 4.1(b), while their GVD values are similar. While the conditions followed for the two processes are different, as well as being limited by the frequency separation between the interacting waves carried by different modes in order to obtain similar IGVs and maintain the phase matching, we will follow another approach to satisfy the phase matching of the two processes. According to Equations (3.8) and (3.9), the fiber should have small IGV and GVD differences between the modes so that both terms on both sides of the two equations can be canceled. With the correct fiber design, the IGV can compensate the GVD. Therefore, following our approach, the impact of an effect can be compensated by another. We will show in the following section a more flexible fiber design that allows to cancel the main condition that imposes the limited frequency separation, and broadens the detuning range between the interacting waves, by minimizing the phase mismatch for the two processes PC and BS, simultaneously.

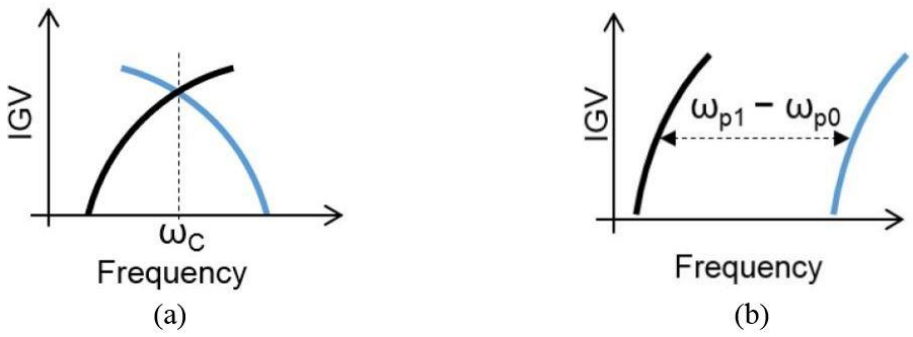

Figure 4.1: (a) Condition for broadband PC operation: the two IGVs of the two modes (black and blue) exhibit a mirror symmetry centered at $\omega_c = (\omega_{p0} + \omega_{p1})/2$ and (b) condition for broadband BS operation; the IGVs of the two modes are shifted copies of each other. (From Ref. [78]).

4.3 Fiber Design

The proposed FMF is an elliptical graded-index core double-clad fiber. The fiber core is doped with germanium with an alpha-law index profile, and a low index trench in the cladding. The refractive index distribution is given by Equation (3.10). The fiber profile is elliptical, therefore, the radius of the elliptical core is taken as a_1 = 13.5 µm along the major axis, and a_2 = 12.13 µm along the minor axis. Figure 4.2 shows the refractive index profiles of the proposed fiber along the major and minor axes.

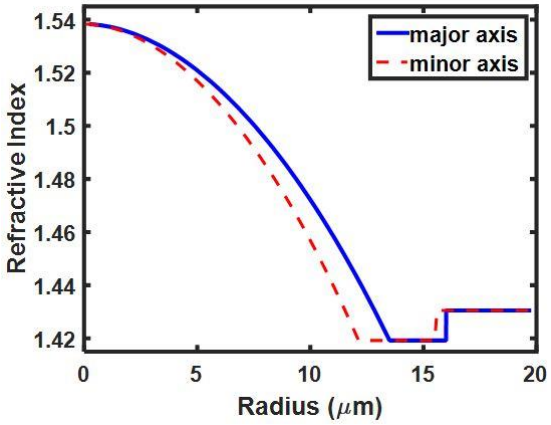

Figure 4.2: Refractive index profiles of the proposed fiber along the major and minor axes.

To obtain a good intermodal phase matching for both PC and BS processes, both terms on both sides in Equations (3.8) and (3.9) must be canceled out. Designing a fiber that has the same GVDs and IGVs for its modes to cancel out both sides of Equations (3.8) and (3.9), may not be possible. Another way to obtain a good intermodal phase matching agreement in this case is to design a fiber that has a small difference between the GVDs of its modes, and a small difference between their IGVs, in a way that both sides of Equation (3.8) or Equation (3.9) cancel each other. Figure 4.3(a) shows the GVD of the three modes calculated using a finite-element mode-solver (COMSOL), taking material dispersion properties into account. Figure 4.3(b) shows the DMD of the modes LP_{11a} and LP_{11b} with respect to LP_{01}, resulting from the small difference between the IGVs of the modes. Note that the present design does not require special conditions on the IGVs versus wavelength dependence of the modes, such as being parallel or exhibiting a mirror symmetry, unlike in the previously reported designs [78, 79]. The only condition that matters is to have a small difference between the IGVs of the modes in order to compensate the small difference between their GVDs.

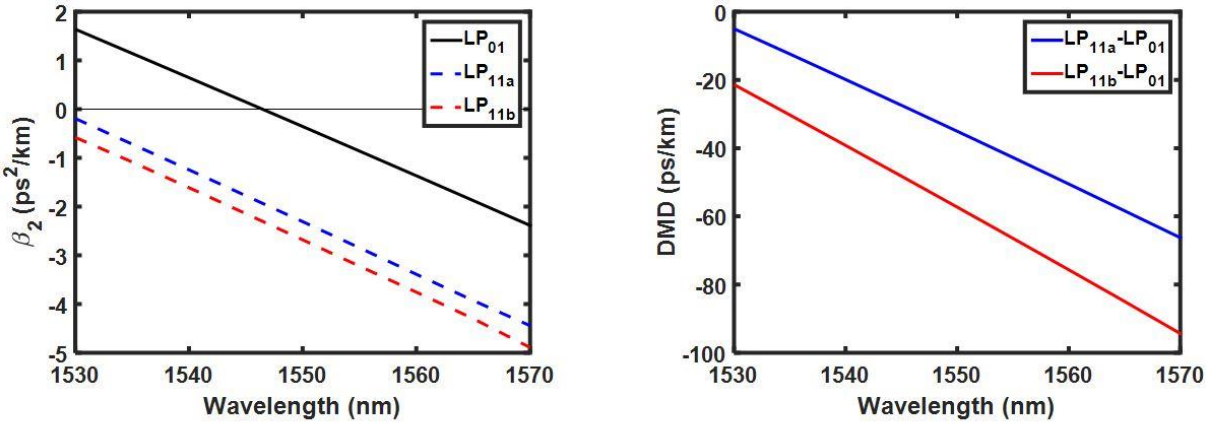

Figure 4.3: (a) Group velocity dispersion of the three modes as a function of wavelength and (b) differential mode delay as a function of wavelength of the modes LP_{11a} and LP_{11b} with respect to LP_{01}.

The main parameter that affects the IGVs of the modes is α. In order to have a small difference between the IGVs of the modes ($\Delta\beta_1$), α should be set equal to 2, that leads to the well-known parabolic index profile. In our case, α will be set to 1.9. This value provides the DMD between the modes shown in Figure 4.3(b) that is sufficient to compensate the GVD difference between the modes shown in Figure 4.3(a). On the other way, in order to keep a small difference between the GVD of the modes, the grading parameter ρ will be set to 1.1. The fiber is then designed in a way to have a small difference between the GVD of the modes. As can be clearly seen from Figure 4.3(a), the mode LP_{01} has a ZDW in the C-band, while the GVDs of the two modes LP_{11a} and LP_{11b} are anomalous, achieving then a small difference between the GVDs of the modes LP_{01}-LP_{11a} and LP_{01}-LP_{11b}. Similarly, the small DMD of the modes LP_{11a} and LP_{11b} with respect to LP_{01} can be visualized in Figure 4.3(b). These small differences of the GVD and the DMD between the modes, will help achieving a good intermodal phase matching according to Equations (3.8) and (3.9), and as a result, relaxes the detuning range of the pumps, while maintaining a good intermodal conversion efficiency, as will be shown in the next section.

4.4 Intermodal FWM Bandwidth

In this section, we will study the bandwidths related to the detuning range of the pumps belonging to different modes, while considering the intermodal conversion efficiency, according to the two intermodal FWM processes between the two modes LP_{01}-LP_{11a} and LP_{01}-LP_{11b}.

4.4.1 Intermodal FWM ($LP_{01}-LP_{11a}$)

A pump P1 and a signal S propagate on the mode LP_{01}, with another pump P2 propagating on the mode LP_{11a}. By fixing the wavelengths of P1 and S and sweeping the wavelength of P2 across the C-L bands, the tolerance to the pump frequency separation detuning for the two intermodal FWM processes PC and BS will be first studied. Figures 4.4 (a-b) show the phase mismatches for the PC and BS processes, respectively, calculated using Equations (3.8) and (3.9), respectively, for different signal to pump 1 wavelength detunings ($\Delta\lambda_{P1\text{-}S} = \lambda_S - \lambda_{P1}$) ranging from 0.1 nm to 0.5 nm, when λ_{P1} is fixed at 1540 nm, while sweeping P2. The phase matching is completely satisfied when λ_{P2} is 1565.19 nm for PC, and 1564.67 nm for the BS process. Moreover, the closer λ_S is to λ_{P1}, the smaller is the phase mismatch.

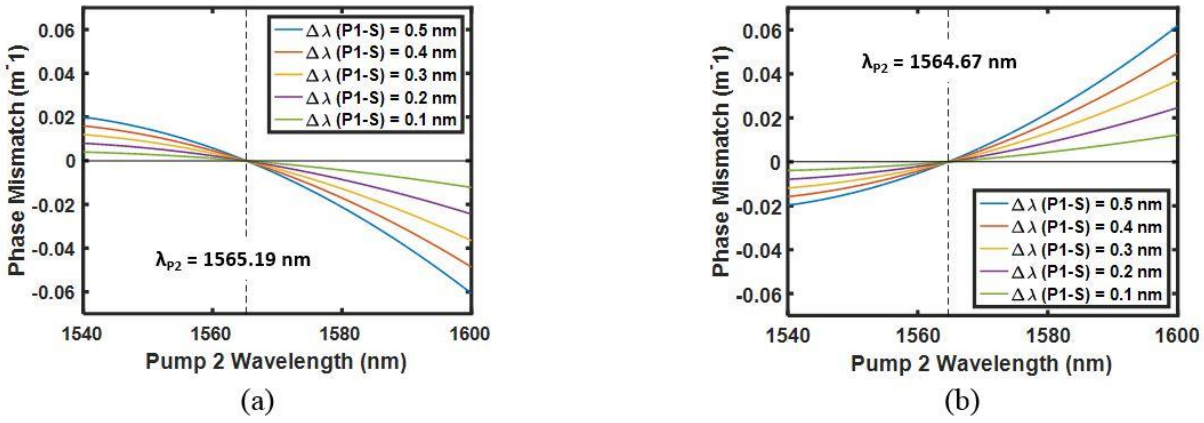

Figure 4.4: Phase mismatches for (a) the PC process, (b) for BS process as a function of the wavelength of P2 for different values of $\Delta\lambda_{P1\text{-}S}$ ranging from 0.1 nm to 0.5 nm.

By fixing λ_{P2} at 1565 nm, and assuming CWs, the optical spectrum at the output of the fiber is shown in Figure 4.5, for $\Delta\lambda_{P1\text{-}S}$ = 0.5 nm, where the propagation was calculated using Equation (2.49), with a power of 100 mW for the pumps P1 and P2, and 3.9 mW assumed for S, using a fiber length of 1 km with 0.22 dB/km losses considered for all modes. Similarly

to Section 3.4, no specific restrictions are imposed on the chosen values. The calculated effective areas are $A_{eff}^{01,01} = 32\ \mu m^2$, $A_{eff}^{11a,11a} = 42.9\ \mu m^2$ and $A_{eff}^{01,11a} = 64.3\ \mu m^2$, leading to the following nonlinear coefficients $\gamma_{01,01} = 3.3\ (W.km)^{-1}$, $\gamma_{11a,11a} = 2.5\ (W.km)^{-1}$ and $\gamma_{01,11a} = 1.63\ (W.km)^{-1}$.

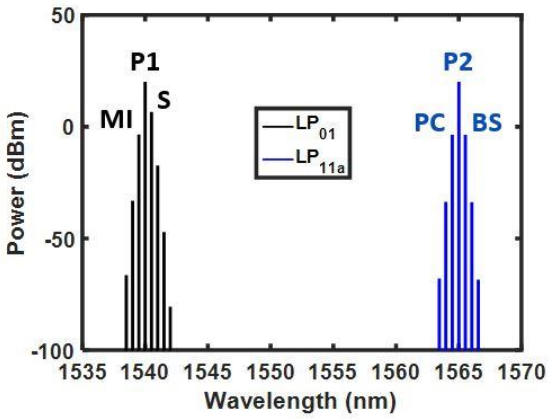

Figure 4.5: Optical spectra at the output of the fiber on each LP_{01} and LP_{11a} mode for $\Delta\lambda_{P1\text{-}S}$ = 0.5 nm and λ_{P2} = 1565 nm.

The generation of MI idler on the mode LP_{01} as a result of intramodal FWM between P1 and S can also be noticed in Figure 4.5. Additional idlers are generated as well due to extra cascaded FWM processes on both modes. The conversion efficiency is defined as the ratio between the output idler power and the input signal power, and it usually depends on the detuning of the S with respect to P1. However, we will study in this case the corresponding conversion efficiencies related to phase mismatches in Figures 4.4(a-b), that can be represented in Figures 4.6(a-b), respectively, in order to calculate the bandwidths on which intermodal PC and BS processes can be held when sweeping P2. Therefore, the conversion efficiency in this case depends on the detuning of P2 with respect to S. It can be realized how the full-width at half maximum (FWHM) conversion bandwidth decreases with $\Delta\lambda_{P1\text{-}S}$. This can also be verified by plotting the extracted FWHM for both PC and BS processes, as a function of $\Delta\lambda_{P1\text{-}S}$ in Figure 4.7. For instance, the FWHM bandwidth reaches 5 nm for PC and BS when $\Delta\lambda_{P1\text{-}S}$ = 0.5 nm, and 23 nm when $\Delta\lambda_{P1\text{-}S}$ = 0.1 nm. While in previous work, the separation between P2 and S had to be fixed in order to obtain similar IGVs for the two modes and achieve phase matching, it can be realized in our case that λ_{P2} can now be shifted between 5 nm and 23 nm according to $\Delta\lambda_{P1\text{-}S}$, while maintaining a good phase matching. In order to observe more clearly the behavior of the bandwidths of the two processes, we present in Figures 4.8(a)-(b)

the conversion efficiency for both PC and BS processes, respectively, as a function of λ_{P2} and $\Delta\lambda_{P1\text{-}S}$. It can clearly be seen how the conversion bandwidth shrinks from 23 nm at $\Delta\lambda_{P1\text{-}S}$ = 0.1 nm, to 2 nm at $\Delta\lambda_{P1\text{-}S}$ = 1.5 nm.

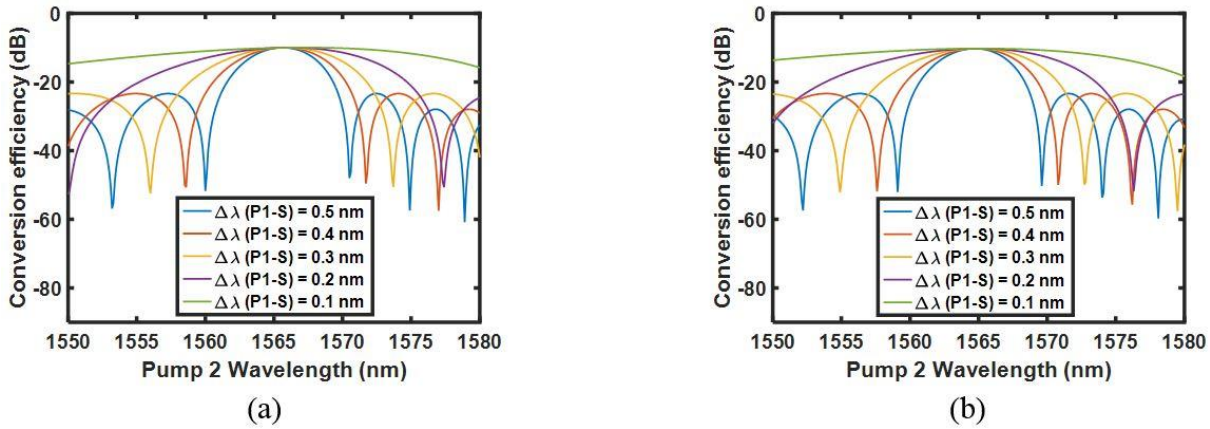

Figure 4.6: Conversion efficiencies as a function of the wavelength of P2 for (a) the PC process and (b) the BS process for different values of $\Delta\lambda_{P1\text{-}S}$ ranging from 0.1 nm to 0.5 nm.

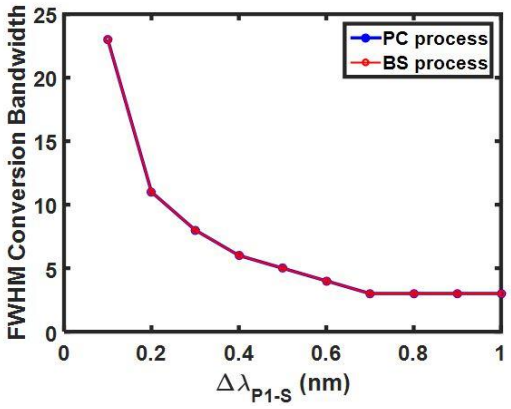

Figure 4.7: FWHM bandwidth of the two processes as a function of $\Delta\lambda_{P1\text{-}S}$.

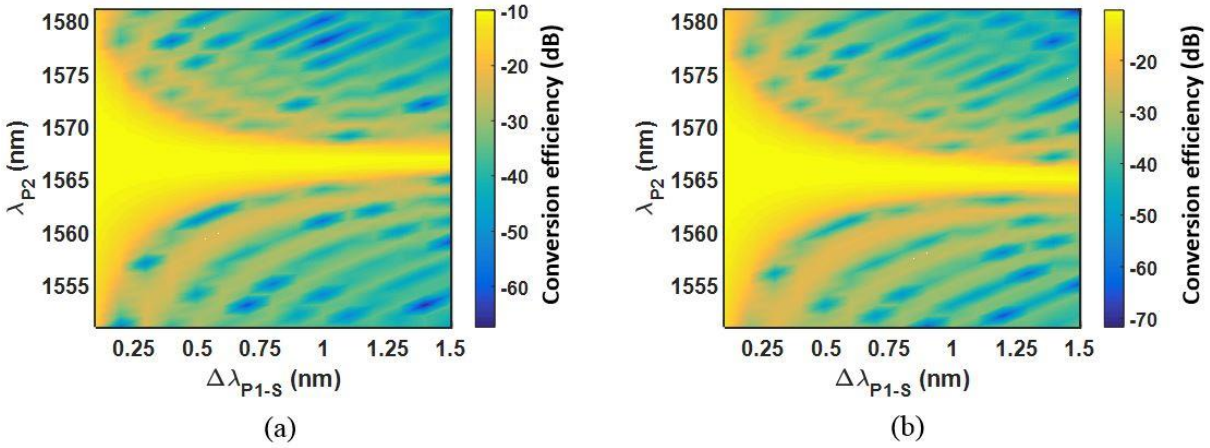

Figure 4.8: Conversion efficiency for (a) the PC process and (b) the BS process as a function of λ_{P2} and $\Delta\lambda_{P1\text{-}S}$.

Previously reported fibers were designed to achieve large conversion bandwidths for $\Delta\lambda_{P1\text{-}S}$, by following specific operation principles [78, 79]. However, they were always limited by challenges, where the main condition was to maintain the frequency separation between the interacting waves carried by different modes, due to non-identical dispersion parameters mainly in the IGVs. We have broken this condition, and using the parameters of the designed fiber, we showed intermodal phase matching can be maintained when sweeping λ_{P2} on a large bandwidth, that depends on $\Delta\lambda_{P1\text{-}S}$, as shown in Figure 4.8. We will show in a second stage that intermodal phase matching can also be maintained on a large bandwidth by fixing λ_{P2}, while sweeping λ_{P1}, and by always considering the $\Delta\lambda_{P1\text{-}S}$. In the following, we will start by studying this case for the PC process, by fixing λ_{P2} at 1566 nm, while sweeping λ_{P1}, and for each value of λ_{P1}, the conversion efficiency related to $\Delta\lambda_{P1\text{-}S}$ will be calculated. This can be represented in Figure 4.9(a) that shows the conversion efficiency of the PC process, for varying λ_{P1} as a function of λ_S, and a constant λ_{P2}. It can be realized that, for each value of λ_{P1}, $\Delta\lambda_{P1\text{-}S}$ is phase matched on a specific region, where high conversion efficiencies are achieved. For clarity, we will consider a cross section of Figure 4.9(a). For example, for a λ_{P1} of 1544 nm, a conversion bandwidth of 4.13 nm is calculated and shown in Figure 4.9(b). Figure 4.10 shows all the calculated conversion bandwidths of the conversion efficiencies in Figure 4.9(a). It can be realized that a minimum bandwidth of 4 nm can be obtained for a λ_{P1} range of 6 nm.

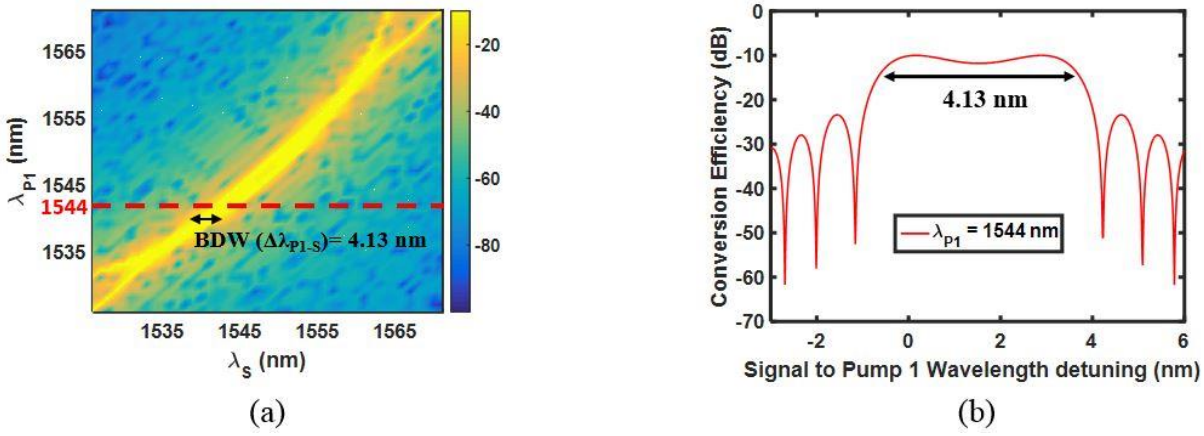

Figure 4.9: (a) Conversion efficiency for the PC process as a function of λ_{P1} and λ_S for λ_{P2} = 1566 nm and (b) conversion efficiency as a function of the signal to pump 1 wavelength detuning when λ_{P1} = 1544 nm.

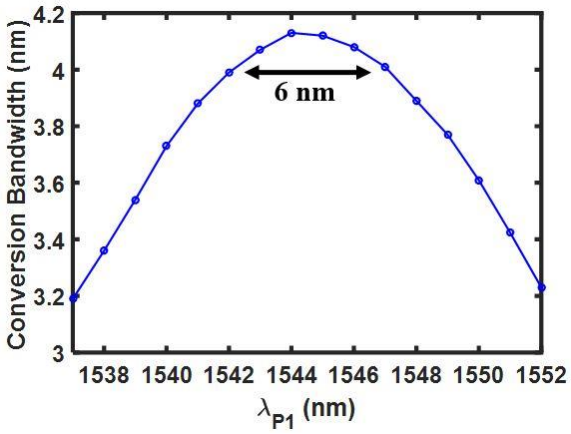

Figure 4.10: Calculated FWHM conversion bandwidths of the signal to pump 1 detuning as a function of λ_{P1}.

The results in Figures 4.9 and 4.10 were obtained for a fixed λ_{P2} of 1566 nm. However, they are subject to variations when λ_{P2} changes, which is the object of the next study. For instance, λ_{P2} is fixed at 1563 nm. Figure 4.11(a) shows the conversion efficiency in this case as a function of λ_{P1} and λ_S. In fact, the impact of shifting λ_{P2}, is that the ‘‘parabolic’’ curve in Figure 4.9(a) will also be shifted. In this case, it is shifted towards shorter signal wavelengths, and the region where high conversion efficiencies are achieved has a different shape than the one in Figure 4.9(a), as it appears in Figure 4.11(a). Figure 4.11(b) shows all the conversion bandwidths extracted from Figure 4.11(a). Two maximum bandwidths, equal to 4.54 nm when λ_{P1} is around 1543 nm and 4.13 nm when λ_{P1} is around 1552 nm are obtained. In between them, a region with a minimum bandwidth of 4 nm is obtained for a λ_{P1} range of 10 nm.

It can be realized that the calculated conversion bandwidths in Figure 4.11(b) are non-symmetrical, due to the non-symmetry of the conversion efficiencies that can be observed in Figure 4.11(a), while the conversion efficiencies in Figure 4.9(a) appear to be symmetrical. In fact, since the impact of shifting λ_{P2}, is that the conversion efficiency ‘‘parabolic’’ curve in Figure 4.9(a) and Figure 4.11(a) will also be shifted, the non-symmetry can also be realized on the lower left and the upper right of Figure 4.9(a).

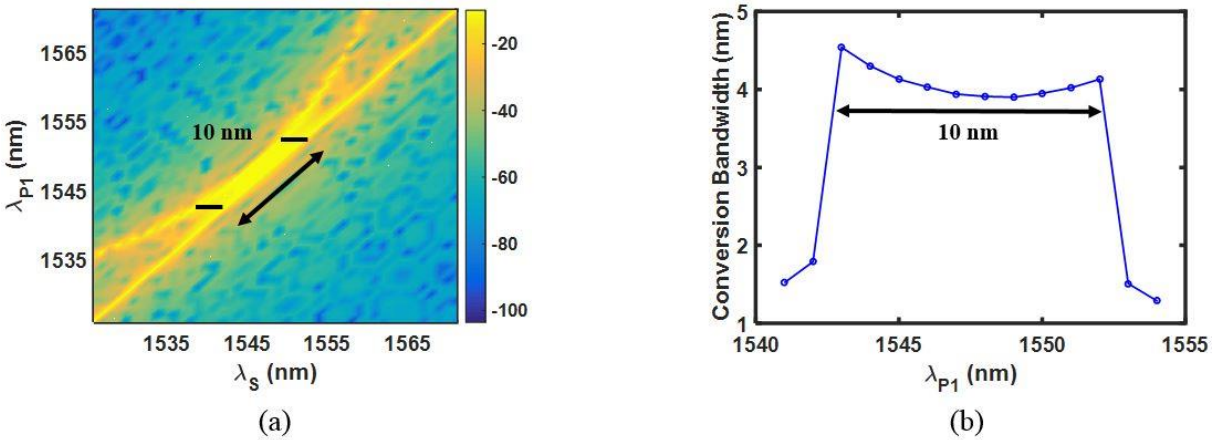

Figure 4.11: (a) Conversion efficiency for the PC process as a function of λ_{P1} and λ_S, at a constant λ_{P2} = 1563 nm and (b) calculated bandwidths as a function of λ_{P1}.

The same study is conducted for the BS process. Figure 4.12(a) shows the conversion efficiency as a function of λ_{P1} and λ_S, when λ_{P2} is fixed to 1563.3 nm. High conversion efficiencies are calculated around the phase-matched signal and pump 1 wavelengths. However, the ‘‘parabolic’’ curve in this case is reversed compared to the previously investigated case of PC. Figure 4.12(b) shows all the calculated conversion bandwidths for two cases, when λ_{P2} is fixed at 1563.3 nm and 1564 nm. In the first case, two maxima are observed when λ_{P1} is around 1541 nm and 1551 nm, with corresponding conversion bandwidths of 3.3 nm and 3.9 nm, respectively. In between, a region with a minimum bandwidth of 3 nm is obtained for a λ_{P1} range of 11 nm. In the second case, the two maxima are shifted to 1537 nm and 1554 nm (separation of 17 nm), with bandwidths of 3.1 nm and 3.7 nm. However, the bandwidth is reduced to a minimum of 2 nm across this range. The conversion bandwidths can then be controlled by moving λ_{P2}, through the same shifting mechanism of the ‘‘parabolic’’ curve, as explained previously for the PC process. In fact, when the ‘‘parabolic’’ curve intersects with the diagonal one in Figure 4.12(a), the maximum bandwidths of the conversion efficiencies are obtained at the boundaries of the intersection between the two curves. Note that for wavelengths longer than 1565 nm, the shape of the areas of high conversion efficiencies in the λ_{P1}-λ_S plane, and their corresponding calculated bandwidths will be similar to the PC process in Figure 4.9.

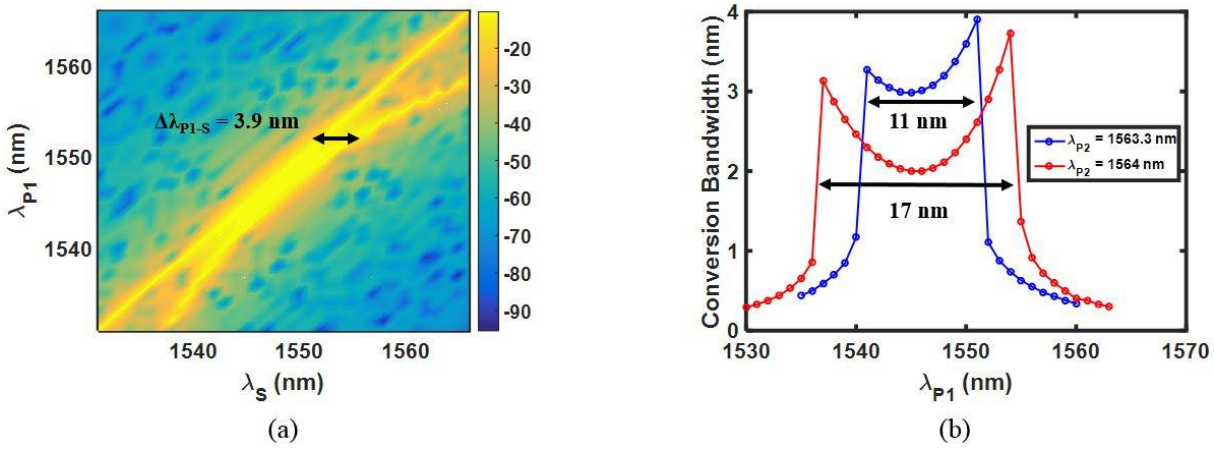

Figure 4.12: (a) Conversion efficiency for the BS process as a function of λ_{P1} and λ_S, at a constant λ_{P2} = 1563.3 nm and (b) calculated conversion bandwidths as a function of λ_{P1} when λ_{P2} = 1563.3 nm and λ_{P2} = 1564 nm.

4.4.2 Intermodal FWM ($LP_{01}-LP_{11b}$)

The same study can be applied for the intermodal FWM processes between the modes LP_{01}-LP_{11b}. Similarly to the previous case, we will first show the results when the wavelengths of P1 and S are fixed, while sweeping the wavelength of the pump on the mode LP_{11b} that will be denoted P3 in this case, and we will compare the calculated bandwidths to the previous case (LP_{01} – LP_{11a}). The phase mismatches as a function of the wavelength of P3 for the PC and BS processes can be visualized in Figures 4.13(a)-(b), respectively, where phase matching in this case is completely satisfied when λ_{P3} is around 1570 nm. By fixing λ_{P3} at 1570 nm, the optical spectrum at the output of the fiber is shown in Figure 4.14 for $\Delta\lambda_{P1\text{-}S}$ = 0.5 nm. The considered calculated effective areas in this case are $A_{eff}^{01,01} = 32\ \mu m^2$, $A_{eff}^{11b,11b} = 43.2\ \mu m^2$ and $A_{eff}^{01,11b} = 64.8\ \mu m^2$, leading to the following nonlinear coefficients $\gamma_{01,01} = 3.3\ (W.km)^{-1}$, $\gamma_{11b,11b} = 2.4\ (W.km)^{-1}$ and $\gamma_{01,11b} = 1.62\ (W.km)^{-1}$.

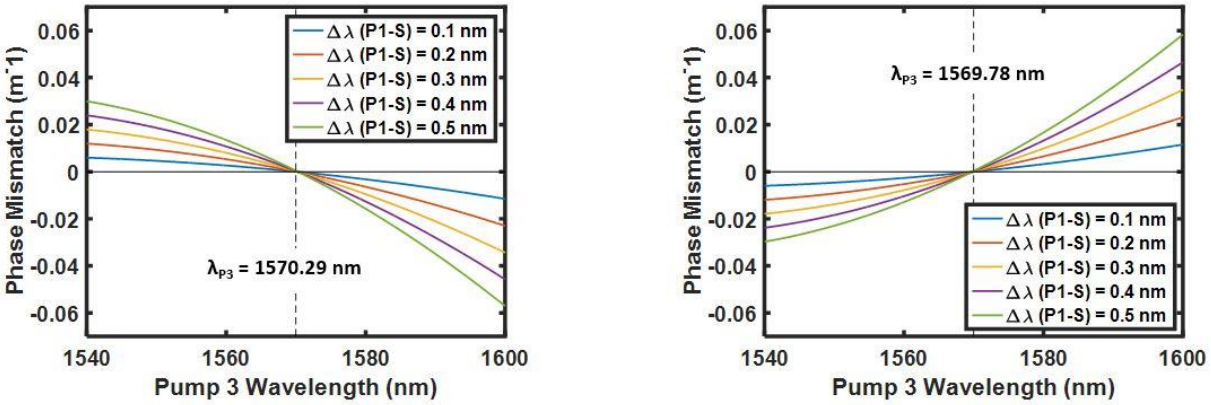

Figure 4.13: Phase mismatch as a function of the wavelength of P3 for different values of $\Delta\lambda_{P1\text{-}S}$ for (a) the PC process and (b) the BS process.

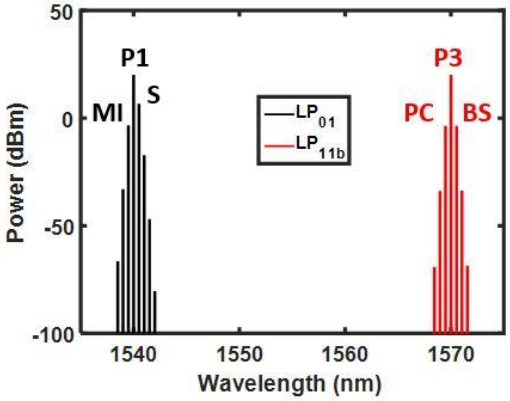

Figure 4.14: Optical spectra at the output of the fiber.

The conversion efficiencies are shown in Figure 4.15(a) for the PC and BS processes, where it can be seen that the FWHM bandwidth reaches 4 nm for both processes when $\Delta\lambda_{P1\text{-}S}$ = 0.5 nm. The small shift between the conversion efficiencies of the two processes originates from the phase mismatch in Figures 4.13(a-b). In fact, the phase matching for the PC process is completely matched at λ_{P3} = 1570.29 nm, while a λ_{P3} = 1569.78 nm for BS process as depicted in Figures 4.13(a-b), resulting then in this small shift between the two conversion efficiencies. While the maximum bandwidth reached 23 nm in the case of the LP_{01}-LP_{11a} process, it now reaches 18 nm as shown in Figure 4.15(b), that represents the calculated FWHM conversion bandwidth for PC and BS processes as a function of $\Delta\lambda_{P1\text{-}S}$.

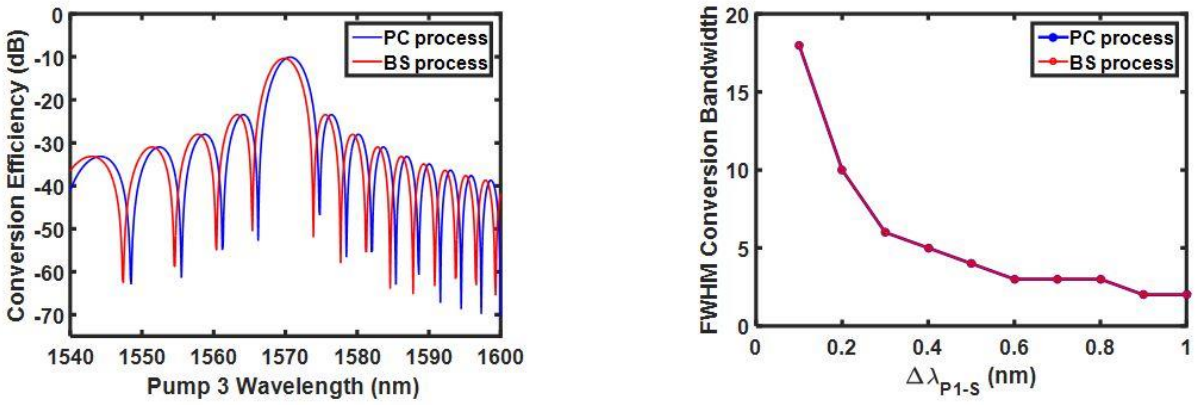

Figure 4.15: (a) conversion efficiencies for PC and BS processes for $\Delta\lambda_{P1\text{-}S}$ = 0.5 nm and (b) FWHM bandwidths of the two processes as a function of $\Delta\lambda_{P1\text{-}S}$.

The bandwidths in the case of intermodal FWM between the modes LP_{01}-LP_{11a} are a bit larger than in the LP_{01}-LP_{11b} case. This is due to the dispersion parameters of the fiber. The DMD between the modes LP_{01}-LP_{11a} shown in Figure 4.3(b), resulting from their IGV difference, is smaller than the one between LP_{01}-LP_{11b}, which results in a broader bandwidth. Therefore, the smaller difference between the GVDs and IGVs of the modes LP_{01}-LP_{11a}, allows both terms on both sides of the phase matching conditions in Equations (3.8) and (3.9) to be balanced over a larger bandwidth than the one between the modes LP_{01}-LP_{11b}.

We will now study the reversed case, when λ_{P3} is fixed and sweeping λ_{P1} and λ_S. Starting with the PC process, λ_{P3} is fixed at 1571.1 nm. Figure 4.16(a) shows the conversion efficiency for varying λ_{P1} and λ_S, and a constant λ_{P3}. $\Delta\lambda_{P1\text{-}S}$ is phase matched at the high conversion efficiencies region, where a maximum bandwidth of 3.3 nm can be achieved at a λ_{P1} = 1545 nm. Figure 4.16(b) shows all the calculated conversion bandwidths of the conversion efficiencies in Figure 4.16(a), where a minimum bandwidth of 3 nm can be obtained for a λ_{P1} range of 9 nm.

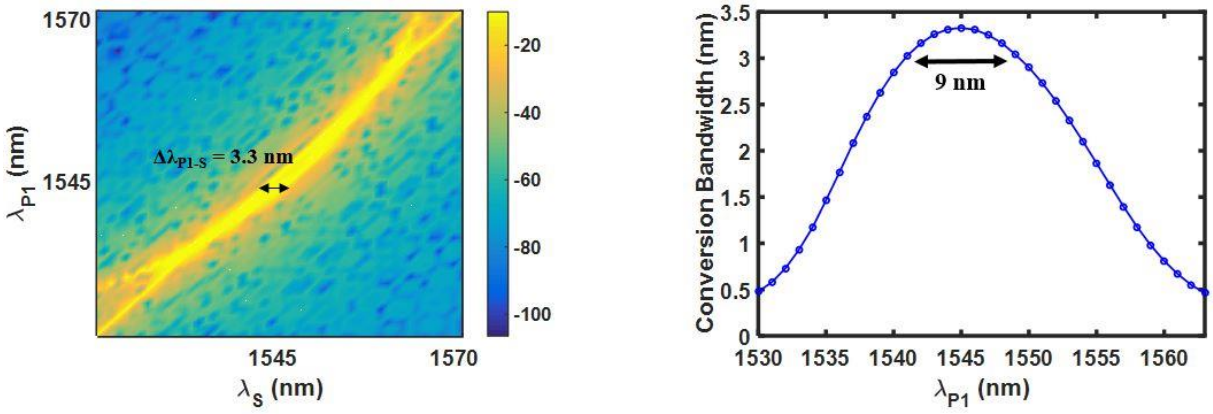

Figure 4.16: Conversion efficiency for the PC process as a function of λ_{P1} and λ_S for λ_{P3} = 1571.1 nm and (b) calculated FWHM conversion bandwidths of the signal to pump 1 detuning as a function of λ_{P1}.

As for the BS process, Figure 4.17(a) shows the conversion efficiency for varying λ_{P1} and λ_S, and a constant λ_{P3} fixed at 1568.3 nm. A maximum bandwidth of 3.3 nm can be achieved at a λ_{P1} = 1548 nm in the high conversion efficiencies region. Figure 4.17(b) shows all the calculated conversion bandwidths extracted from Figure 4.17(a).

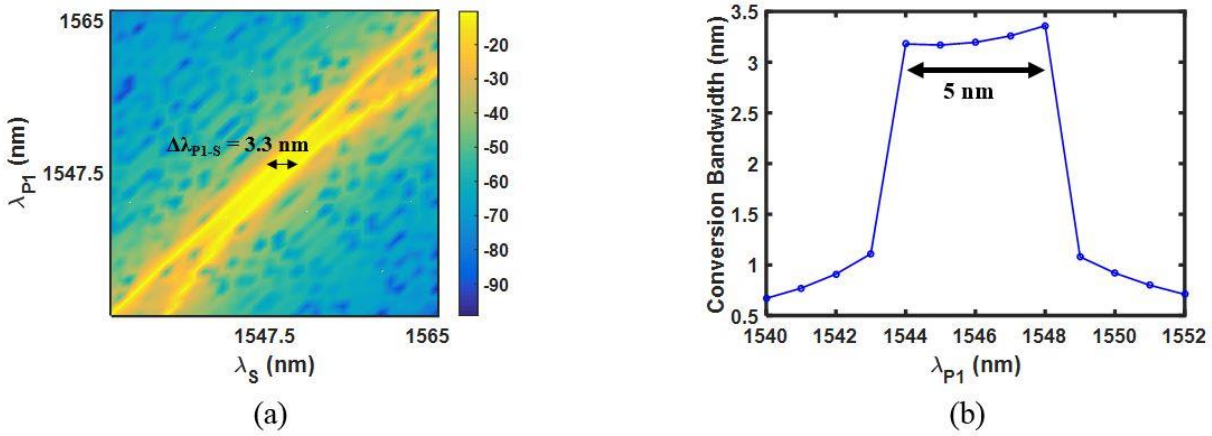

Figure 4.17: Conversion efficiency for the PC process as a function of λ_{P1} and λ_S for λ_{P3} = 1568.3 nm and (b) calculated FWHM conversion bandwidths of the signal to pump 1 detuning as a function of λ_{P1}.

Two maximum bandwidths equal to 3.1 nm and 3.3 nm are obtained, when λ_{P1} is around 1544 nm and 1548 nm, respectively. In between them, a region with a minimum bandwidth of 3 nm is obtained for a λ_{P1} range of 5 nm. Same reasoning can be applied here as the previous case of the LP_{01}-LP_{11a} intermodal FWM process, that is the range of λ_{P1} on which $\Delta\lambda_{P1\text{-}S}$ is

phase matched can be controlled by moving λ_{P3}. However, this will be at the expense of the conversion bandwidth of $\Delta\lambda_{P1\text{-}S}$, that is going to decrease. The smaller conversion bandwidths obtained compared to the previous case LP_{01}-LP_{11a}, comes back to the DMD between the modes, as explained earlier.

4.5 Sensitivity Analysis

In this section, we analyze the sensitivity of intermodal phase matching towards the structural parameters of the fiber that may be due to fabrication process imperfection. We will only study the case of the phase mismatch of the LP_{01}-LP_{11a} FWM process, considering the PC idler. Similar analysis can be applied to the LP_{01}-LP_{11b} FWM process, as well as to the BS idler. Some physical parameters of the fiber will be modified from the values used in the previous studies reported earlier in previous sections. Starting with the core ellipticity that can be defined as [116]

$$e = \frac{a_1 - a_2}{(a_1 + a_2)/2} \tag{4.1}$$

that was initially 10%, Figure 4.18(a) shows the calculated phase mismatches for core ellipticity values of 3%, 10% and 14%, where the wavelengths of P1 and S are fixed with a $\Delta\lambda_{P1\text{-}S}$ = 0.5 nm, and the wavelength of P2 is swept across the C-L bands. In the case of 10% ellipticity, the phase matching is completely satisfied for λ_{P2} = 1565 nm, as shown earlier in Figure 4.4(a). The wavelength λ_{P2} resulting in phase matching depends on the ellipticity. Its value is 1562 nm at 3% ellipticity and 1569 nm at 14% ellipticity. This will result in a shift of the conversion efficiency curves as shown in Figure 4.18(b), and possibly, a small modification of their FWHM.

Figure 4.19(a) investigates the impact of the grading parameter ρ on the phase mismatch curves, and compares the phase mismatch obtained with the initially chosen value of 1.1 to two other cases, ρ=1 and ρ=1.2. The impact of the value of ρ is also to shift the phase mismatch curves, hence the conversion efficiency curves. As for the parameter α chosen initially as 1.9, we realize from Figure 4.19(b) that phase matching is hard to achieve when going away from this value. Since α is the main parameter that affects the IGVs of the modes, changing its value leads to the loss of balance between the two terms on both sides of the phase matching equations (Equation (3.8) and Equation (3.9)). Therefore, both terms in the equations cannot cancel each other anymore. However, changing the ellipticity or the grading parameter does not heavily

affect the IGVs and the GVDs of the modes, and both terms in the phase matching equation remain balanced. Hence, they do not have a big impact as was shown in Figures 4.18(a) and Figure 4.19(a).

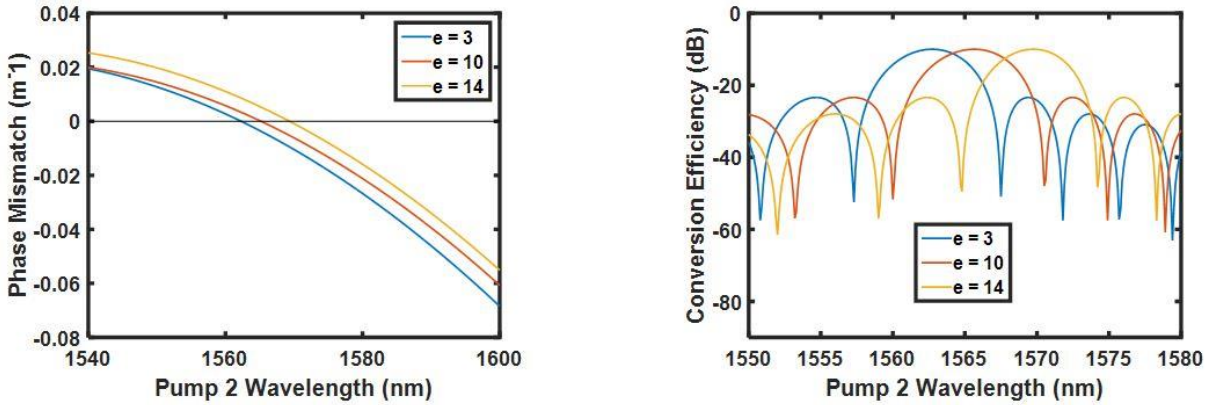

(a) (b)

Figure 4.18: (a) Phase mismatch for an ellipticity of 3%, 10% and 14%, (b) conversion efficiency for an ellipticity of 3%, 10% and 14%.

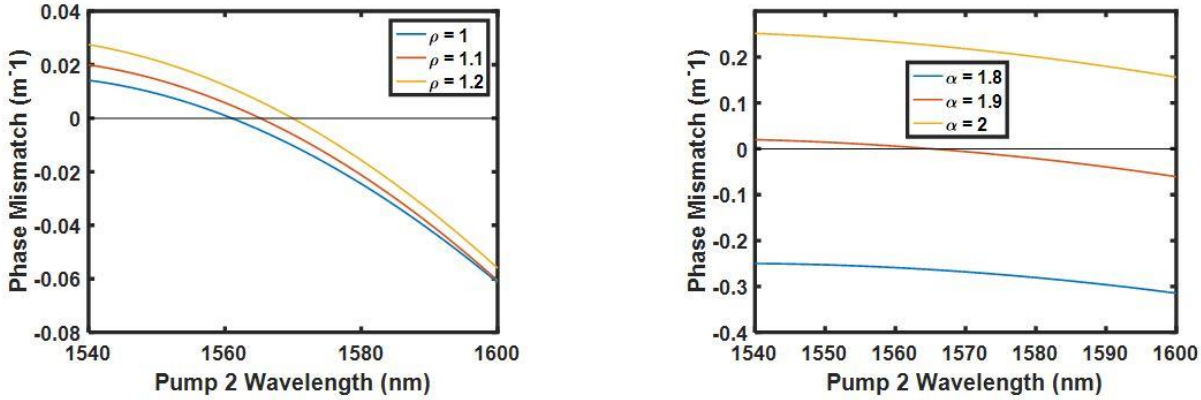

(a) (b)

Figure 4.19: (a) Phase mismatch for a grading parameter of 1, 1.1, 1.2, (b) phase mismatch for α = 1.8, 1.9, 2.

4.6 Conclusion

In this chapter, we have shown the design of a three-mode nonlinear dispersion-shifted elliptical-core FMF that breaks the degeneracy between the LP_{11a} and LP_{11b} modes. The fiber presents low GVD and low DMD between its modes LP_{01}, LP_{11a} and LP_{11b}, and allows to reduce the constraint of limited frequency separation, thus relaxing the detuning range between the interacting waves carries by different modes, for both intermodal PC and BS processes simultaneously. We have also evaluated the sensitivity of the fiber parameters to fabrication imperfections. The results showed that the most sensitive parameter is the profile exponent that describes the shape of the core.

Summary and outlook

While the main advantage of optical communications is to enable transmission of ultra-high capacities by multiplexing dozens of wavelength channels operating at high bit rates, the processing of the data, for instance in view of its regeneration or routing, needs to be performed in the electrical domain, thus requiring OEO conversions. Some processing functionalities could be performed more efficiently directly in the optical domain, which is known as AOSP. Functionalities such as wavelength conversion, all-optical regeneration and all-optical switching have typically been studied in the context of optical communications systems employing SMF. However, a strong interest in MMFs is expected to grow in the future, as new techniques exploiting the spatial dimension in MMFs have been proposed in order to further increase the transmitted capacity. Therefore, a better understanding of nonlinear effects associated with multimode interactions is desirable. This thesis aimed to explore paths for AOSP in MDM. In particular, the target was to demonstrate how nonlinear effects in MMFs could be used to manipulate the properties of optical signals, either in a mode independent way, or mode dependent way. Two types of FMFs were designed. The first one allows to perform some AOSP functionalities for all the modes of the fiber individually and simultaneously, by using the intramodal FWM nonlinear effect. Applications such as wavelength conversion, PSFC and PSA were numerically investigated. The second fiber was designed in a way to perform AOSP between different modes of the fiber, using intermodal FWM.

The main future work that follows, is to fabricate and test the proposed designed fibers. This in turns can lead the way to explore other applications. The designed fibers are FMFs, and the numerical simulations are performed for a low number of spatial modes, thus showing the fundamental effects that arise in MDM. For a practical and commercial success of MDM, the fiber capacity should be largely increased. Therefore, similar fibers with many more spatial modes need to be designed. Moreover, the use of integrated multimode waveguides is also very interesting in this context, as phase regeneration for two modal channels has been numerically analyzed [117]. Therefore, it would always be desirable to enhance the design that relies on the dispersion engineering, and explore all potential applications in multimode components.

Appendix A

Split-step Fourier method

Considering three modes propagating in the fiber LP_{01}, LP_{11a} and LP_{11b}, the equations describing the propagation on each mode can be written as

$$\frac{\partial A_{01}}{\partial z} = -\frac{\alpha}{2}A_{01} + i(\beta_0^{01} - \beta_{0r})A_{01} - \left(\beta_1^{01} - \frac{1}{v_{gr}}\right)\frac{\partial A_{01}}{\partial T} - i\frac{\beta_2^{01}}{2}\frac{\partial^2 A_{01}}{\partial T^2} + i\left(\gamma_{01,01}|A_{01}|^2 + 2\,\gamma_{01,11a}|A_{11a}|^2 + 2\gamma_{01,11b}|A_{11b}|^2\right)A_{01} \quad (A.1)$$

$$\frac{\partial A_{11a}}{\partial z} = -\frac{\alpha}{2}A_{11a} + i(\beta_0^{11a} - \beta_{0r})A_{11a} - \left(\beta_1^{11a} - \frac{1}{v_{gr}}\right)\frac{\partial A_{11a}}{\partial T} - i\frac{\beta_2^{11a}}{2}\frac{\partial^2 A_{11a}}{\partial T^2} + i\left(\gamma_{11a,11a}|A_{11a}|^2 + 2\,\gamma_{01,11a}|A_{01}|^2 + 2\gamma_{11a,11b}|A_{11b}|^2\right)A_{11a} \quad (A.2)$$

$$\frac{\partial A_{11b}}{\partial z} = -\frac{\alpha}{2}A_{11b} + i\left(\beta_0^{11b} - \beta_{0r}\right)A_{11b} - \left(\beta_1^{11b} - \frac{1}{v_{gr}}\right)\frac{\partial A_{11b}}{\partial T} - i\frac{\beta_2^{11b}}{2}\frac{\partial^2 A_{11b}}{\partial T^2} + i\left(\gamma_{11b,11b}|A_{11b}|^2 + 2\,\gamma_{01,11b}|A_{01}|^2 + 2\gamma_{11a,11b}|A_{11a}|^2\right)A_{11b} \quad (A.3)$$

When we apply the split-step, we have three dispersion operators to apply, as well as three nonlinear operators. The dispersion operators can be written as

$$\widehat{D^{01}} = -\frac{\alpha}{2} + i(\beta_0^{01} - \beta_{0r}) - \left(\beta_1^{01} - \frac{1}{v_{gr}}\right)\frac{\partial}{\partial T} - i\frac{\beta_2^{01}}{2}\frac{\partial^2}{\partial T^2} + \frac{\beta_3^{01}}{6}\frac{\partial^3}{\partial T^3} + i\frac{\beta_4^{01}}{24}\frac{\partial^4}{\partial T^4} \quad (A.4)$$

$$\widehat{D^{11a}} = -\frac{\alpha}{2} + i(\beta_0^{11a} - \beta_{0r}) - \left(\beta_1^{11a} - \frac{1}{v_{gr}}\right)\frac{\partial}{\partial T} - i\frac{\beta_2^{11a}}{2}\frac{\partial^2}{\partial T^2} + \frac{\beta_3^{11a}}{6}\frac{\partial^3}{\partial T^3} + i\frac{\beta_4^{11a}}{24}\frac{\partial^4}{\partial T^4} \quad (A.5)$$

$$\widehat{D^{11b}} = -\frac{\alpha}{2} + i\left(\beta_0^{11b} - \beta_{0r}\right) - \left(\beta_1^{11b} - \frac{1}{v_{gr}}\right)\frac{\partial}{\partial T} - i\frac{\beta_2^{11b}}{2}\frac{\partial^2}{\partial T^2} + \frac{\beta_3^{11b}}{6}\frac{\partial^3}{\partial T^3} + i\frac{\beta_4^{11b}}{24}\frac{\partial^4}{\partial T^4} \quad (A.6)$$

where the higher-order dispersion terms β_3 and β_4 are also considered, and the nonlinear operators can be written as

$$\widehat{N^{01}} = i\left(\gamma_{01,01}|A_{01}|^2 + 2\,\gamma_{01,11a}|A_{11a}|^2 + 2\gamma_{01,11b}|A_{11b}|^2\right) \quad (A.7)$$

$$\widehat{N^{11a}} = i\left(\gamma_{11a,11a}|A_{11a}|^2 + 2\,\gamma_{01,11a}|A_{01}|^2 + 2\gamma_{11a,11b}|A_{11b}|^2\right) \quad (A.8)$$

$$\widehat{N^{11b}} = i\left(\gamma_{11b,11b}|A_{11b}|^2 + 2\,\gamma_{01,11b}|A_{01}|^2 + 2\gamma_{11a,11b}|A_{11a}|^2\right) \quad (A.9)$$

In order to implement the split-step, and considering the propagation on the mode LP_{01} as given in equation A.1, the optical field propagates first at half the distance of the first segment of length dz, where the Fourier transform operator is applied, followed by the dispersion operator $\widehat{D^{01}}$, as shown in Figure A.1. Then the inverse Fourier transform operator is applied at mid-plane, followed by the nonlinear operator $\widehat{N^{01}}$. Then the optical field propagates in the other half of the segment where the Fourier transform operator is applied again, followed the by the dispersion operator $\widehat{D^{01}}$, and finally the inverse Fourier transform operator can be applied, as given in Equation (2.54). The dispersion and nonlinear operators ($\widehat{D^{11a}}$, $\widehat{D^{11b}}$ and $\widehat{N^{11a}}$ and $\widehat{N^{11b}}$) should also be applied for the two other modes LP11a and LP11b simultaneously, when applying this process for the mode LP01.

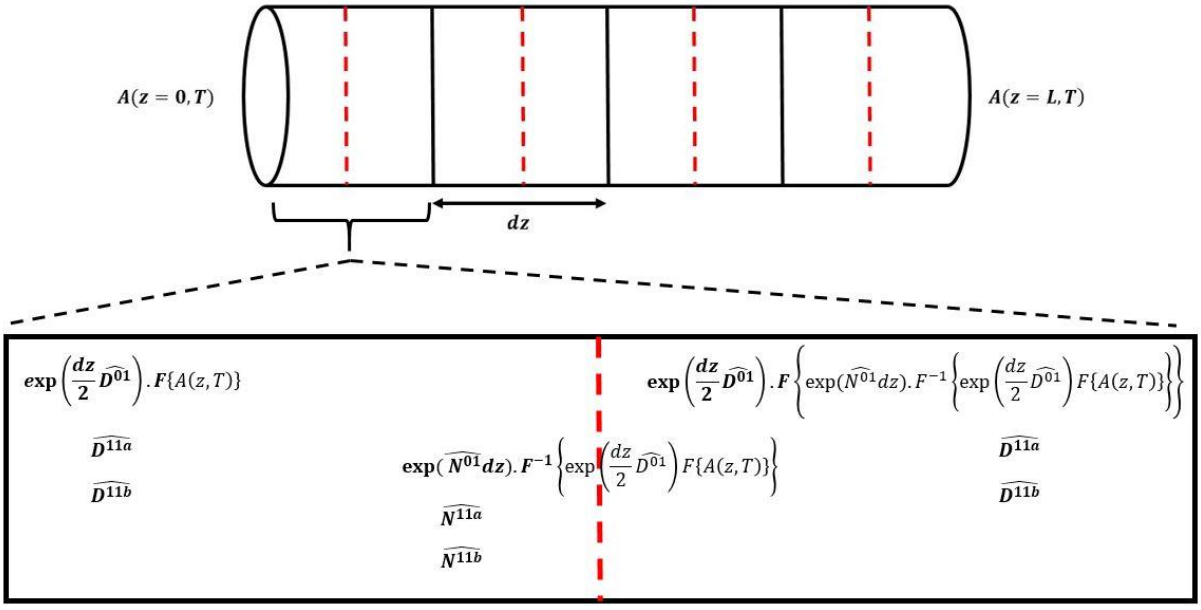

Figure A.1: Implementation of the split-step when three modes are propagating.

Bibliography

[1] N. S. Kapany, Fiber Optics: Principles and Applications, New York: Academic, 1967.

[2] Cisco, "The Zettabyte Era: Trends and Analysis," *Cisco Public White Paper, San Jose, CA, USA,* 2015.

[3] Cisco, "Cisco Global Cloud Index: Forecast and Methodology, 2012-2017," *Cisco Public White Paper, San Jose, CA, USA,* 2013.

[4] Cisco, "Cisco Visual Networking Index: Global Mobile Data Traffic Forecast Update, 2014-2019," *Cisco Public White Paper, San Jose, CA, USA,* 2015.

[5] A. Chraplyvy, "The coming capacity crunch," *ECOC Plenary talk,* 2009.

[6] C. E. Shannon, "A Mathematical Theory of Communication," *Bell System Technical Journal,* vol. 27(3), pp. 379-423, 1948.

[7] J. Proakis, Digital Communications, Mcgraw-Hill Publ.Comp., 2001.

[8] G. Agrawal, Nonlinear Fiber Optics, Academic Press, 2001.

[9] R.-J. Essiambre, G. Kramer, P. J.Winzer, G. J. Foschini and B. Goebel, "Capacity limits of optical fiber networks," *J. Lightw. Technol.,* vol. 28 (4), pp. 662-701, 2010.

[10] R.-J. Essiambre, "Impact of fiber parameters on nonlinear fiber capacity," *Proc. Opt. Fiber Commun. Conf. Expo./Nat. Fiber Opt. Eng. Conf., OTuJ1,* 2011.

[11] P. Mitra and J. Stark, "Nonlinear limits to the information capacity of optical fibre communications," *Nature 411,* p. 1027–1030, 2001.

[12] T. Morioka, Y. Awaji, R. Ryf, P. Winzer, D. Richardson and F. Poletti, "Enhancing Optical Communications with Brand New Fibers," *IEEE Commun. Magazine,* vol. 50 (2), pp. S31-S42, 2012.

[13] D. J. Richardson, J. M. Fini and L. E. Nelson, "Space-division multiplexing in optical fibres," *Nature Photon.,* vol. 7, pp. 354-362, 2013.

[14] P. J. Winzer, "Making spatial multiplexing a reality," *Nature Photon.,* vol. 8, pp. 345-348, 2014.

[15] B. J. Puttnam, R. S. Luis, W. Klaus, J.Sakaguchi, J.-M. D. Mendinueta, Y. Awaji, N. Wada, Y. Tamura, T. Hayashi, M. Hirano and J. Marciante, "2.15 Pb/s transmission using a 22 core homogeneous single-mode multi-core fiber and wideband optical comb," *ECOC, PDP 3.1,* 2015.

[16] R. G. H. v. Uden, R. A. Correa, E. A. Lopez, F. M. Huijskens, C. Xia, G. Li, A. Schülzgen, H. d. Waardt, A. M. J. Koonen and C. M. Okonkwo, "Ultra-high-density spatial division multiplexing with a few-mode multicore fibre," *Nature Photon,* vol. 8, pp. 865-870, 2014.

[17] S. R. R. Ryf, A. H. Gnauck, C. Bolle, A. Sierra, S. Mumtaz, M. Esmaeelpour, E. C. Burrows, R. J. Essiambre, P. J. Winzer, D. W. Peckham, A. H. McCurdy and R. Lingle, "Mode-division multiplexing over 96 Km of few-mode fiber using coherent 6 × 6 MIMO processing," *J. Lightw. Technol.,* vol. 30, pp. 521-531, 2012.

[18] C. Koebele, M. Salsi, L. Milord, R. Ryf, C. Bolle, P. Sillard, S. Bigo and G. Charlet, "40 km Transmission of five mode division multiplexed data streams at 100 Gb/S with lowMIMO-DSP complexity," *ECOC, Th.13.C.3,* 2011.

[19] K. Saitoh, M. Koshiba, K. Takenaga and S. Matsuo, "Homogeneous and heterogeneous multi-core fibers," *IEEE Summer Topical,* pp. 210-211, 2012.

[20] A. Shah, R. Hsu, A. Tarighat, A. H. Sayed and B. Jalali, "Coherent optical mimo (COMIMO)," *Journal of Lightwave Technology,* vol. 23(8), p. 2410–2419, 2005.

[21] S. Mumtaz, R. Essiambre and G. Agrawal, "Nonlinear Propagation in Multimode and Multicore Fibers: Generalization of the Manakov Equations," *Journal of Lightwave Technology,* vol. 31(3), pp. 398-406, 2013.

[22] C. Koebele, M. Salsi, L. Milord, R. Ryf, C. Bolle, P. Sillard, S. Bigo and G. Charlet, "B40 km transmission of five modedivision multiplexed data streams at 100 Gb/s with low MIMO DSP complexity," *European Conference on Optical Communication,* p. Th.13.C.3, 2011.

[23] W. Klaus, J. Sakaguchi, B. J. Puttnam, Y. Awaji, N. Wada, T. Kobayashi and M. Watanabe, "Free-Space Coupling Optics for Multicore Fibers," *IEEE Photonics Technology Letters,* vol. 24(21), pp. 1902-1905, 2012.

[24] S. Randel, R. Ryf, A. Sierra, P. Winzer, A. Gnauck, C. Bolle, D. Peckham, A. Mccurdy and R. Lingle, "Transmission over 33-km Few-Mode Fiber Enabled by 6 X 6 MIMO Equalization," *Optics Express,* vol. 19(17), p. 16697–16707, 2011.

[25] A. Koonen, H. Chen, H. P., A. v. d. Boom and O. Raz, "Silicon Photonic Integrated Mode Multiplexer and Demultiplexer," *IEEE Photonics Technology Letters,* vol. 24(21), pp. 1961-1964, 2012.

[26] B. Wohlfeil, C. Stamatiadis, L. Zimmermann and K. Petermann, "Compact Fiber Grating Coupler on SOI for Coupling of Higher Order Fiber Modes," *Optical Fiber Communication Conference,* p. OTh1B–2, 2013.

[27] R. Ryf, N. Fontaine and R. Essiambre, "Spot-Based Mode Couplers for Mode-Multiplexed Transmission in Few-Mode Fiber," *IEEE Photonics Technology Letters,* vol. 24(21), p. 1973–1976, 2012.

[28] N. Fontaine, R. Ryf, J. Bland-Hawthorn and S. Leon-Saval, "Geometric Requirements for Photonic Lanterns in Space Division Multiplexing," *Optics Express,* vol. 20(24), pp. 27123-27132, 2012.

[29] H. Takahashi, T. Tsuritani, E. L. T. d. Gabory, T. Ito, W. R. Peng, K. Igarashi, K. Takeshima, Y. Kawaguchi, I. Morita, Y. Tsuchida, Y. Mimura, K. Maeda, T. Saito, K. Watanabe, K. Imamura and R. Sugizaki, "First demonstration of MC EDFA repeatered SDM transmission of 40 x 128

Gbit/s PDM QPSK signals per core over 6160 km 7 core MCF," *European Conference on Optical Communication,* p. Th.3.C.3, 2012.

[30] K. S. Abedin, T. F. Taunay, M. Fishteyn, D. J. DiGiovanni, V. R. Supradeepa, J. M. Fini, M. F. Yan, B. Zhu, E. M. Monberg and F. V. Dimarcello, "Cladding-pumped erbium-doped multicore fiber amplifier," *Optics Express,* vol. 20(18), pp. 20191-20200, 2012.

[31] Y. Jung, S. Alam, Z. Li, A. Dhar, D. Giles, I. P. Giles, J. K. Sahu, F. Poletti, L. Gruner-Nielsen and D. J. Richardson, "First demonstration of multimode amplifier for spatial division multiplexed transmission systems," *European Conference on Optical Communication,* p. Th.13.K.4, 2011.

[32] J. M. Rivas-Moscoso, B. Shariati, A. Mastropaolo, D. Klonidis and I. Tomkos, "Cost Benefit Quantification of SDM Network Implementations based on Spatially Integrated Network Elements," *European Conference on Optical Communications,* 2016.

[33] M. J. F. Digonnet, Rare-Earth Doped Fiber Lasers and Amplifiers, New York: Dekker, 1993.

[34] E. P. Ippen and R. H. Stolen, "Stimulated Brillouin scattering in optical fibers," *Appl. Phys. Lett.,* vol. 21, p. 539, 1972.

[35] R. H. Stolen, E. P. Ippen and A. R. Tynes, "Raman oscillation in glass optical waveguide," *Appl. Phys. Lett.,* vol. 20, p. 62, 1972.

[36] R. H. Stolen and A. Askin, "Optical Kerr effect in glass waveguide," *Appl. Phys. Lett.,* vol. 22, p. 294, 1973.

[37] A. Willner, S. Khaleghi, M. R. Chitgarha and O. F. Yilmaz, "All-Optical Signal Processing," *J. Lightw. Technol.,* vol. 32(4), pp. 660-680, 2014.

[38] J. Leuthold, L. Moller, J. Jaques, S. Cabot, L. Zhang, P. Bernasconi, M. Cappuzzo, L. Gomez, E. Laskowski, E. Chen, A. Wong-Foy and A. Griffin, "160 Gbit/s SOA all-optical wavelength converter and assessment of its regenerative properties," *IEEE Electron. Lett.,* vol. 40(9), pp. 554-555, 2004.

[39] S. Radic, "Parametric Signal Processing," *IEEE J. Sel. Topics Quantum Electron.,* vol. 18(2), pp. 670-680, 2012.

[40] J. Leuthold, C. Koos and W. Freude, "Nonlinear silicon photonics," *Nature Photon.,* vol. 4(8), pp. 535-544, 2010.

[41] K. Uchiyama, T. Morioka, M. Saruwatari, M. Asobe and T. Ohara, "Error free all-optical demultiplexing using a chalcogenide glass fiber based nonlinear optical loop mirror," *IEEE Electron. Lett.,* vol. 32(17), pp. 1601-1602, 1996.

[42] C. Langrock, S. Kumar, J. E. McGeehan, A. E.Willner and M. M. Fejer, "All-optical signal processing using χ2 nonlinearities in guided-wave devices," *J. Lightw. Technol.,* vol. 24(7), pp. 2579-2592, 2006.

[43] J. C. Knight and D. V. Skryabin, "Nonlinear waveguide optics and photonic crystal fibers," *Opt. Exp.,* vol. 15, pp. 15365-15376, 2007.

[44] K. Croussore, I. Kim, Y. Han, C. Kim, G. Li and S. Radic, "Demonstration of phase-regeneration of DPSK signals based on phase-sensitive amplification," *Optics Exoress,* vol. 13(11), pp. 3945-3950, 2005.

[45] R. Slavík, F. Parmigiani, J. Kakande, C. Lundström, M. Sjödin, P. A. Andrekson, R. Weerasuriya, S. Sygletos, A. D. Ellis, L. Grüner-Nielsen, D. Jakobsen, S. Herstrøm, R. Phelan, J. O'Gorman and A. Bogris, "All-optical phase and amplitude regenerator for next-generation telecommunications systems," *Nature Photonics,* vol. 4, p. 690–695, 2010.

[46] R. Jopson, A. Gnauck and R. Derosier, "Compensation of fibre chromatic dispersion by spectral inversion," *Electron. Lett.,* vol. 29(7), pp. 576-578, 1993.

[47] B. P.-P. Kuo, E. Myslivets, V. Ataie, E. G. Temprana, N. Alic and S. Radic, "Wideband Parametric Frequency Comb as Coherent Optical Carrier," *J. Lightwave Technol.,* vol. 31(21), pp. 3414-3419, 2013.

[48] P. Andrekson, N. Olsson, J. Simpson, T. Tanbun-Ek, R. Logan and M. Haner, "16 Gbit/s all-optical demultiplexing using four-wave mixing," *Electron. Lett.,* vol. 27(11), pp. 922-924, 1991.

[49] P. A. Andrekson, "Picosecond optical sampling usinf gour-wave mixing in fibre," *Electron. Lett. ,* vol. 27(16), pp. 1440-1441, 1991.

[50] W. Imajuku, A. Takada and Y. Yamabayashi, "Low-noise amplification under the 3 dB noise figure in high-gain phase-sensitive fibre amplifier," *Electron. Lett. ,* vol. 35(22), pp. 1954-1955, 1999.

[51] B. Ramamurthy and B. Mukherjee, "Wavelength conversion in WDM networking," *Journal on Selected Areas in Communications,* vol. 16(7), pp. 1061-1073, 1998.

[52] T. A. Birks, I. Gris-Sánchez, S. Yerolatsitis, S. G. Leon-Saval and R. R. Thomson, "The photonic lantern," *Advances in Optics and Photonics,* vol. 7(2), pp. 107-167, 2015.

[53] R. Stolen, "The early years of fiber nonlinear optics," *J. Lightwave Technol.,* vol. 26(9), pp. 1021-1031, 2008.

[54] R. Ryf, A. Sierra, R.-J. Essiambre, S. Randel, A. H. Gnauck, C. Bolle, M. Esmaeelpour, P. J. Winzer, R. Delbue, P. Pupalaikise, A. Sureka, D. W. Peckham, A. McCurdy and R. Lingle, "Mode-equalized distributed Raman amplification in 137-km few-mode fiber," *ECOC, Th.13.K.5,* 2011.

[55] E. Nazemosadat and A. Mafi, "Nonlinear multimodal interference and saturable absorption using a short graded-index multimode optical fiber," *J. Opt. Soc. Amer. B.,* vol. 30(5), pp. 1357-1367, 2013.

[56] G. Lopez-Galmiche, Z. S. Eznaveh, M. A. Eftekhar, J. A. Lopez, L. G. Wright, F. Wise, D. Christodoulides and R. A. Correa, "Visible supercontinuum generation in a graded index multimode fiber pumped at 1064 nm," *Opt. Lett.,* vol. 41(11), pp. 2553-2556, 2016.

[57] M. A. Eftekhar, L. G. Wright, M. S. Mills, M. Kolesik, R. A. Correa, F. W. Wise and D. N. Christodoulides, "Versatile supercontinuum generation in parabolic multimode optical fibers," *Opt. Express,* vol. 25(8), pp. 9078-9087, 2017.

[58] W. Pan, Q. Jin, X. Li and S. Gao, "All-optical wavelength conversion for mode-division multiplexing signals using four-wave mixing in a dual-mode fiber," *J. Opt. Soc. Amer. B,* vol. 32(12), pp. 2417-2424, 2015.

[59] M. Guasoni, "Generalized modulational instability in multimode fibers: Wideband multimode parametric amplification," *Phys. Rev. A.,* vol. 92, p. 033849, 2015.

[60] C. J. McKinstrie, S. Radic and A. R. Chraplyvy, "Parametric amplifiers driven by two pump waves," *EEE J. Sel. Top. Quantum Electron.,* vol. 8, pp. 538-547, 2002.

[61] J. Hansryd, P. A. Andrekson, M. Westlund, J. Li and P.-O. Hedekvist, "Fiber-Based Optical Parametric Amplifiers and Their Applications," *IEEE J. Sel. Top. Quantum Electron.,* vol. 8, pp. 506-520, 2002.

[62] T. Tanemura, C. S. Goh, K. Kikuchi and S. Y. Set, "Highly efficient arbitrary wavelength conversion within entire C-band based on nondegenerate fiber four-wave mixing," *IEEE Photonics Technol. Lett.,* vol. 16, pp. 551-553, 2004.

[63] N. Zhao, B. Huang, R. Amezcua-Correa, X. Li and G. Li, "Few-mode fiber optical parametric amplifier," *OFC, OTu2D.5,* 2013.

[64] E. Nazemosadat, A. Lorences-Riesgo, M. Karlsson and P. A. Anderkson, "Design of highly nonlinear few-mode fiber for C-band optical parametric amplification," *J. Lightw. Technol.,* vol. 35(14), pp. 2810-2817, 2017.

[65] C. Guo, Z. Zhang, N. Zhao, L. Cui, X. Li, J. Zhao and G. Li, "Design of elliptical few-mode fibers for mode-coupling-free parametric amplification," *J. Opt. Soc. Amer. B,* vol. 35(3), pp. 545-551, 2018.

[66] J. Gong, J. Xu, M. Luo, X. Li, Y. Qiu, Q. Yang, X. Zhang and S. Yu, "All-optical wavelength conversion for mode division multiplexed superchannels," *Opt. Express,* vol. 24(8), pp. 8926-8939, 2016.

[67] R. H. Stolen, J. E. Bjorkholm and A. Ashkin, "Phase-matched three-wave mixing in silica fiber optical waveguides," *Appl. Phys. Lett. 24,* pp. 308-310, 1974.

[68] Y. Xiao, R.-J. Essiambre, M. Desgroseilliers, A. M. Tulino, R. Ryf, S. Mumtaz and G. P. Agrawal, "Theory of intermodal four-wave mixing with random linear mode coupling in few-mode fibers," *Opt. Express,* vol. 22, pp. 32039-32059, 2014.

[69] H. Pourbeyram, E. Nazemosadat and A. Mafi, "Detailed investigation of intermodal four-wave mixing in SMF-28: blue-red generation from green," *Opt. Express,* vol. 23, pp. 14487-14500, 2015.

[70] E. Nazemosadat, H. Pourbeyram and A. Mafi, "Phase matching for spontaneous frequency conversion via four-wave mixing in graded-index multimode optical fibers," *J. Opt. Soc. Am. B,* vol. 33, pp. 144-150, 2016.

[71] R. Dupiol, A. Bendahmane, K. Krupa, A. Tonello, M. Fabert, B. Kibler, T. Sylvestre, A. Barthelemy, V. Couderc, S. Wabnitz and G. Millot, "Far-detuned cascaded intermodal four-wave mixing in a multimode fiber," *Opt. Lett.,* vol. 42, pp. 1293-1296, 2017.

[72] J. Demas, P. Steinvurzel, B. Tai, L. Rishøj, Y. Chen and S. Ramachandran, "Intermodal nonlinear mixing with Bessel beams in optical fiber," *Optica,* vol. 2, pp. 14-17, 2015.

[73] H. Zhang, M. Bigot-Astruc, L. Bigot, P. Sillard and J. Fatome, "Multiple modal and wavelength conversion process of a 10-Gbit/s signal in a 6-LP-mode fiber," *Opt. Express,* vol. 27(11), pp. 15413-15425, 2019.

[74] H. Zhang, M. Bigot-Astruc, P. Sillard, G. Millot, B. Kibler and J. Fatome, "Multiple spatial and wavelength conversion operations based on a frequency-degenerated intermodal four-wave mixing process in a graded-index 6-LP few-mode fiber," *Appl. Opt.,* vol. 59(18), pp. 5497-5505, 2020.

[75] R.-J. Essiambre, M. A. Mestre, R. Ryf, A. H. Gnauck, R. W. Tkach, A. R. Chraplyvy, Y. Sun, X. Jiang and R. L. Jr., "Experimental investigation of inter-modal four-wave mixing in few-mode fibers," *IEEE Photon. Technol. Lett.,* vol. 25, pp. 539-542, 2013.

[76] S. M. M. Friis, I. Begleris, Y. Jung, K. Rottwitt, P. Petropoulos, D. J. Richardson, P. Horak and F. Parmigiani, "Inter-modal four-wave mixing study in a two-mode fiber," *Opt. Express,* vol. 24, pp. 30338-30349, 2016.

[77] F. Parmigiani, P. Horak, Y. Jung, L. Grüner-Nielsen, T. Geisler, P. Petropoulos and D. J. Richardson, "All-optical mode and wavelength converter based on parametric processes in a three-mode fiber," *Opt. Expre,* vol. 25, pp. 33602-33609, 2017.

[78] M.Guasoni, F.Parmigiani, P.Horak and D.J.Richardson, "Novel Fiber Design for Wideband Conversion and Amplification in Multimode Fibers," *ECOC, P1.SC1.12,* 2017.

[79] O. F. Anjum, P. Horak, Y. Jung, M. Suzuki, Y. Yamamoto, T. Hasegawa, P. Petropoulos, D. J. Richardson and F. Parmigiani, "Bandwidth enhancement of inter-modal four wave mixing Bragg scattering by means of dispersion engineering," *APL Photonics,* vol. 4, p. 022902, 2019.

[80] G. P. Agrawal, Fiber Optic Communication Systems, New York: Wiley, 2002.

[81] M. J. Adams, An Introduction to Optical Waveguides, New York: John Wiley & Sons, Inc., 1981.

[82] W. Hermann and D.Wiechert, "Refractive index of doped and undoped PCVD," *Materials Research Bulletin,* vol. 24 (9), pp. 1083-1097, 1989.

[83] L. G. Cohen, C. Lin and W. G. French, "Tailoring zero chromatic dispersion into the 1.5 -1.6mm low-loss spectral region of single-mode fibers," *Electron. Lett.,* vol. 15 (12), pp. 334-335, 1979.

[84] K. I. White and B. P. Nelson, "Zero total dispersion in step-index monomode fibers at 1.30 and 1.55 mm," *Electron. Lett.,* vol. 15 (13), pp. 396-397, 1979.

[85] M. Saifi, S. J. Jang, L. G. Cohen and a. J. Stone, "Triangular profile single-mode fiber," *Optics Letters,* vol. 7 (1), pp. 43-45, 1982.

[86] S. Kawakami and N.Nishida, "Characteristics of a doubly-clad optical fibers with a low index inner cladding," *IEEE J. Quantum Electron.,* vol. 10 (12), pp. 879-887, 1974.

[87] C. D. Poole, J. M. Wiesenfeld, D. J. DiGiovanni and A. M. Vengsarkar, "Optical fiber-based dispersion compensation using higher order modes near cutoff," *J. Lightwave Technology,* vol. 12 (10), pp. 1746-1758, 1994.

[88] A. J. Antas and D. K. Smith, "Design and characterization of dispersion compensating fiber based on LP01 mode," *J. Lightwave Technology,* vol. 12 (10), pp. 1739-1745, 1994.

[89] Y. R. Shen, Principles of Nonlinear Optics, New York: Wiley, 1984.

[90] R. H. Stolen, J. E. Bjorkholm and A. Ashkin, "Phase-matched three-wave mixing in silica fiber optical waveguides," *Appl. Phys. Lett.,* vol. 24 (7), pp. 308-310, 1974.

[91] F. Poletti and P. Horak, "Description of Ultrashort Pulse Propagation in Multimode Optical Fibers," *Journal of the Optical Society of America B,* vol. 25 (10), pp. 1645-1654, 2008.

[92] F. Poletti and P. Horak, "Dynamics of Femtosecond Supercontinuum Generation in Multimode Fibers," *Optics Express,* vol. 17 (8), pp. 11301-11312, 2009.

[93] A. Mecozzi, C. Antonelli and M. Shtaif, "Nonlinear propagation in multi-mode fibers in the strong coupling regime," *Opt. Express,* vol. 20(11), pp. 11673-11678, 2012.

[94] D. Marcuse, C. Menyuk and P. Wai, "Application of the Manakov-PMD Equation to Studies of Signal Propagation in Optical Fibers with Randomly Varying Birefringence," *Journal of Lightwave Technology,* vol. 15(9), pp. 1735-1746, 1997.

[95] J. W. Fleming, "Dispersion in GeO2-SiO2 glasses," *Appl. Opt.,* vol. 23, pp. 4486-4493, 1984.

[96] V. M. Mashinsky, V. B. Neustruev, V. V. Dvoyrin, S. A. Vasiliev, O. I. Medvedkov, I. A. Bufetov, A. V. Shubin, E. M. Dianov, A. N. Guryanov, V. F. Khopin and M. Y. Salgansky, "Germania-glass-core silica-glass-cladding modified chemical-vapor deposition optical fibers: Optical losses, photorefractivity, and Raman amplification," *Opt. Lett.,* vol. 29(22), p. 2596–2598, 2004.

[97] R. Webb, J. Dailey, R. Manning and A. Ellis, "Phase discrimination and simultaneous frequency conversion of the orthogonal components of an optical signal by four-wave mixing in an SOA," *Opt. Express,* vol. 19, pp. 20015-20022, 2011.

[98] F. D. Ros, K. Dalgaard, L. Lei, J. Xu and C. Peucheret, "QPSK-to-2xBPSK wavelength and modulation format conversion through phase-sensitive four-wave mixing in a highly nonlinear optical fiber," *Opt. Express,* vol. 21, p. 28743–28750, 2013.

[99] F. D. Ros, K. Dalgaard, Y. Fukuchi, J. Xu, M. Galili and C. Peucheret, "Simultaneous QPSK-to-2xBPSK wavelength and modulation format conversion in PPLN," *IEEE Photon. Technol. Lett.,* vol. 26, pp. 1207-1210, 2014.

[100] M. Baillot, M. Gay, C. Peucheret, M. Joindot and T. Chartier, "Phase quadrature discrimination based on three-pump four-wave mixing in nonlinear optical fibers," *Opt Express,* vol. 24, pp. 26930-26941, 2016.

[101] Y. Mu and C. M. Savage, "Parametric amplifiers in phase-noise-limited optical communications," *J. Opt. Soc. Am. B,* vol. 9(1), pp. 65-70, 1992.

[102] R. Slavik, F. Parmigiani, J. Kakande, C. Lundstrom, M. Sjodin, P. A. Andrekson, R. Weerasuriya, S. Sygletos, A. D. Ellis, L. Gruner-Nielsen, D. Jakobsen, S.Herstrøm, R. Phelan, J.O'Gorman, A. Bogris, D. Syvridis, S. Dasgupta, P. Petropoulos and D. J. Richard, "All-optical phase and amplitude regenerator for next-generation telecommunications systems," *Nat. Photon.,* vol. 4, pp. 690-695, 2010.

[103] F. Parmigiani, G. D. Hesketh, R. Slavık, P. Horak, P. Petropoulos and D. J. Richardson, "Optical phase quantizer based on phase sensitive four wave mixing at low nonlinear phase shifts," *IEEE Photon. Technol. Lett.,* vol. 26(21), pp. 2146-2149, 2014.

[104] Z. Tong, C. Lundstrom, P. A. Andrekson, C. J. McKinstrie and M. Karlsson, "Towards ultrasensitive optical links enabled by low-noise phase-sensitive amplifiers," *Nat. Photon.,* vol. 5, pp. 430-436, 2011.

[105] Z. Tong, C. Lundstrom, M. Karlsson, M. Vasilyev and P. A. A. Andrekson, "Noise performance of a frequency nondegenerate phase-sensitive amplifier with unequalized inputs," *Opt. Lett.,,* vol. 36(5), pp. 722-724, 2011.

[106] Z. Tong, A. Bogris, C. Lundstrom, C. J. McKinstrie, M. Vasilyev, M. Karlsson and P. A. Andrekson, "Modeling and measurement of the noise figure of a cascaded non degenerate phase-sensitive parametric amplifier," *Opt. Exp.,,* vol. 18(14), pp. 14820-14835, 2010.

[107] L. Ruo-Ding, P. Kumar and W. L. Kath, "Dispersion Compensation with Phase-sensitive Optical Amplifiers," *IEEE J. Lightwave Technol.,* vol. 12(3), pp. 541-549, 1994.

[108] D. Mazroa, "BPSK phase regeneration based on second-order nonlinearities in periodically poled lithium niobate," *J. Lightw. Technol.,* vol. 31(15), pp. 2501-2507, 2013.

[109] B. J. Puttnam, D. Mazroa, S. Shinada and N. Wada, "Phase-squeezing properties of non-degenerate PSAs using PPLN waveguides," *Opt. Exp.,* vol. 19(26), pp. B131-B139, 2011.

[110] K. Croussore and G. Li, "Phase regeneration of NRZ-DPSK signals based on symmetric-pump phase-sensitive amplification," *IEEE Photon. Technol. Lett.,* vol. 19(11), pp. 864-866, 2007.

[111] A. Trichili, M. Zghal, L. Palmieri and M. Santagiustina, "Phase-Sensitive Mode Conversion and Equalization in a Few Mode Fiber Through Parametric Interactions," *IEEE Photonics Journal,* vol. 9(1), p. 7800710, 2017.

[112] M. Schnack, T. Hellwig, M. Brinkmann and C. Fallnich, "Ultrafast two-color all-optical transverse mode conversion in a graded-index fiber," *Opt. Lett.,* vol. 40, pp. 4675-4678, 2015.

[113] Z. Tong, A. Bogris, M. Karlsson and P. A. Andrekson, "Raman-induced asymmetric pump noise transfer in fiber-optical parametric amplifiers," *IEEE Photon. Technol. Lett.,* vol. 22, pp. 386-388, 2010.

[114] S. M. M. Friis, K. Rottwitt and C. J. McKinstrie, "Raman and loss induced quantum noise in depleted fiber optical parametric amplifiers," *Opt. Express,* vol. 21, pp. 29320-29331, 2013.

[115] Z. Tong, A. Bogris, M. Karlsson and P. A. Andrekson, "Full characterization of the signal and idler noise figure spectra in single-pumped fiber optical parametric amplifiers," *Opt. Express,* vol. 18, pp. 2884-2893, 2010.

[116] G. Peng and M.-J. Li, "Elliptical core multimode optical fibers," *Opto-Electronics and Communications Conference (OECC 2012), 5C2-2,* 2012.

[117] W. Yang, Y. Yu, L. Chen, G. Chen, M. Ye and X. Zhang, "Simultaneous Phase Regeneration of MDM Signals Utilizing a Multimode Silicon Waveguide," *J. Lightwave Technol.,* vol. 34(11), pp. 2702-2709, 2016.

List of publications

Joseph Slim, Mathilde Gay and Christophe Peucheret, “Mode-independent phase-sensitive frequency conversion in a few-mode elliptical-core fiber”, Nonlinear Photonics, OSA Advanced Photonics Congress, Zürich, Switzerland, paper NpTh4H.6, 5 Jul. 2018.

Joseph Slim, Mathilde Gay and Christophe Peucheret, “Design of an elliptical-core few-mode fiber for mode-independent wavelength conversion”, Pacific Rim Conference on Lasers and Electro-Optics, CLEO-PR 2018, Hong Kong, Hong Kong SAR, China, paper W4E.4, 1 Aug. 2018.

Joseph Slim, Mathilde Gay and Christophe Peucheret, “Design of a few-mode fiber for bandwidth-enlarged intermodal four-wave mixing”, OptoElectronics and Communications Conference/International Conference on Photonics in Switching and Computing, Fukuoka, Japan, paper MC1-1, 8 Jul. 2019.

Mode-Independent Phase-Sensitive Frequency Conversion in a Few-Mode Elliptical-Core Fiber

Joseph Slim, Mathilde Gay, and Christophe Peucheret
Univ Rennes, CNRS, FOTON – UMR 6082, F-22305 Lannion, France
joseph.slim@univ-rennes1.fr

Abstract: We propose an elliptical-core graded-index dispersion-shifted few-mode fiber that allows simultaneous intramodal phase-sensitive frequency conversion. The fiber breaks the degeneracy between the LP_{11a} and LP_{11b} modes and prevents intermodal processes. © 2018 The Author(s)
OCIS codes: (060.4370) Nonlinear Optics, fibers; (190.4380) Nonlinear Optics, four-wave mixing

1. Introduction

While mode-division multiplexing (MDM) is currently being investigated as a mean to scale up the capacity of optical communication systems beyond the current limits of single-mode fibers [1], the processing of the data generally needs to be performed in the electrical domain, thus potentially requiring multiple optical-to-electrical-to-optical (OEO) conversions. However, the number of optoelectronic devices scales with the number of the modes in multimode fibers, thus complicating the systems. Some processing functionalities could be performed directly in the optical domain, known as all-optical signal processing (AOSP) [2], where OEO can be avoided and signal processing can be performed in a single nonlinear medium, which is advantageous for MDM systems.

Parametric processes based on four-wave mixing (FWM) are particularly attractive for AOSP functionalities. Intermodal FWM has been investigated in a few-mode fiber (FMF) [3], and elliptical-core few-mode fiber (EC-FMF) [4]. Mode-independent processes based on intramodal FWM such as mode-independent wavelength conversion [5] and mode-independent amplification [6,7], have been investigated in a FMF and EC-FMF.

Phase-sensitive all-optical signal processing has received a great interest in recent years. Phase-sensitive frequency conversion (PSFC) based on FWM, which allows the conversion of two quadrature components of a signal to two different idlers at different frequencies [8-10] has been studied using single mode nonlinear fiber. Using three pumps and a signal, two different idlers can be generated depending on the phase of the signal.

We present here the design of a highly nonlinear dispersion-shifted EC-FMF that breaks the degeneracy between the LP_{11a} and LP_{11b} modes and allows simultaneous PSFC for the three modes, LP_{01} and $LP_{11a,b}$, in the same fiber.

2. Fiber design

The proposed FMF is an elliptical graded-index core double-clad fiber. Figure 1(a) shows the refractive index profiles of the proposed fiber along the major and minor axis. The fiber has a central core doped with germanium with an alpha-law index profile, and a low index trench in the cladding. It is designed in such a way that the inverse group velocity differences between two modes $\Delta\beta_1$ are sufficiently large to prevent all intermodal processes [6]. The material dispersion properties are given by Sellmeier equations, and the dispersion properties of the three modes are calculated using a finite element mode solver (COMSOL) and shown in Fig. 1(b).

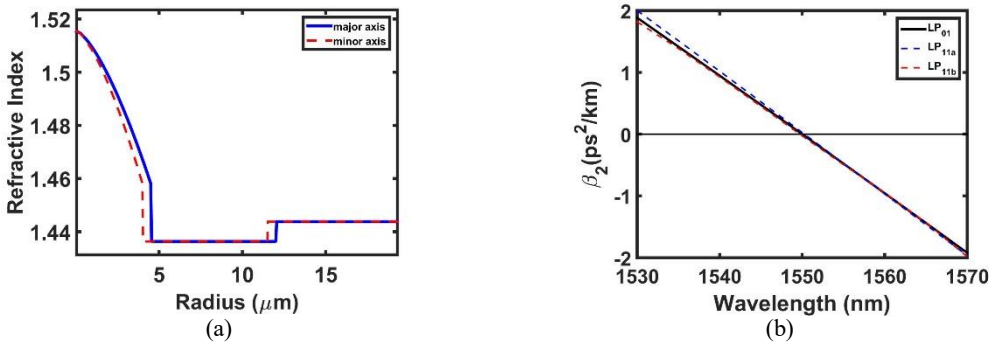

Fig. 1. (a) Refractive index profiles and (b) dispersion properties of the three modes in the C-band.

The zero-dispersion wavelengths (ZDWs) of the three modes are shifted to 1.55 µm in the C-band. Fiber fabrication imperfections affect the modes dispersions, thus shifting their ZDWs. It was however shown in [5], that it is still possible to achieve mode independent processes.

3. Phase-sensitive frequency conversion

Propagation in the proposed fiber is simulated using the multimode nonlinear Schrödinger equation [11]. The effective areas are $A_{eff}^{01,01} = 14.8\ \mu m^2$, $A_{eff}^{11a,11a} = 21.6\ \mu m^2$, $A_{eff}^{11b,11b} = 21.9\ \mu m^2$, $A_{eff}^{01,11a} = 31.4\ \mu m^2$, $A_{eff}^{01,11b} = 32.6\ \mu m^2$, $A_{eff}^{11a,11b} = 64.7\ \mu m^2$, leading to nonlinear coefficients of 7.1, 4.9, 4.8, 3.3, 3.2 and 1.6 $W^{-1}\cdot km^{-1}$, respectively. The fiber length is 1 km and its loss is 0.22 dB/km for all modes. Three pumps (P1, P2, P3) and a signal (S), with wavelengths of 1550.4 nm, 1550 nm, 1549.2 nm and 1549.4 nm, respectively, simultaneously propagate in the fiber on the three modes LP_{01} and $LP_{11a,b}$. Their power levels and phases are chosen according to the conditions described in [10], with a power of 5 dBm for the pumps and the signal, a phase of 0 for P1 and P3, and π for P2, while the phase of the signal varies from 0 to π. Figure 2(a) represents the optical spectrum at the output of the fiber for a signal phase of $\varphi_s = 0$, where an idler I_1 is generated at 1549.8 nm on the three modes. Figure 2(b) represents the optical spectrum for $\varphi_s = \pi/2$, where I_1 vanishes and I_2 is generated at 1550.2 nm. We can also notice that additional idlers are generated due to extra FWM processes. Figure 2(c) shows the evolution of the power of I_1 and I_2, for the three intramodal PSFC processes on the three modes as a function of the signal phase φ_s. The scheme that was originally studied with four, and three pumps, to convert the two quadrature components of a signal to different idlers, is simultaneously achieved in a specially designed fiber on the three modes LP_{01} and $LP_{11a,b}$.

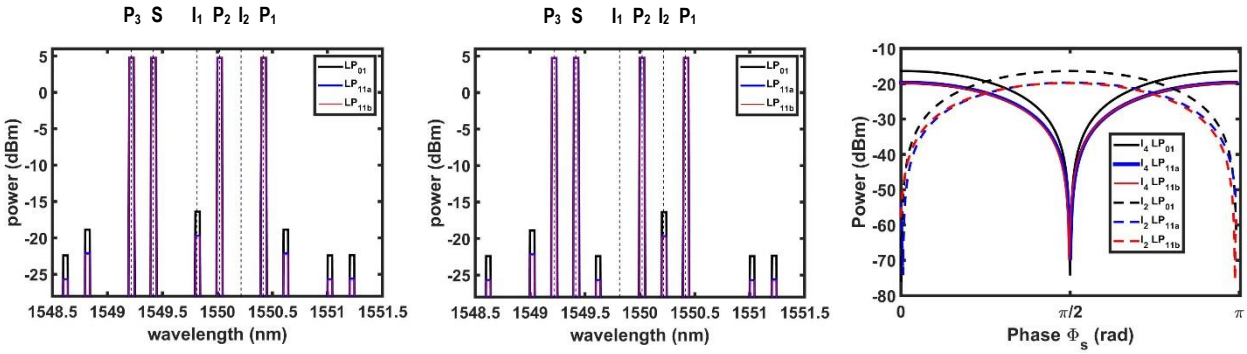

(a) (b) (c)

Fig. 2. (a) Optical spectra at the output of the fiber for $\varphi_s = 0$, (b) $\varphi_s = \pi/2$. (c) Evolution of the power of I_1 and I_2 as a function of φ_s on the three modes.

4. Summary

We have extended the concept of the PSFC scheme that was studied in the context of single-mode fibers, to an EC-FMF by extending the scheme to the number of the modes of the designed fiber, thus achieving multiple phase sensitive frequency conversions in the same fiber using mode-independent intramodal FWM.

5. References

[1] D.J. Richardson et al., Nature Photon. **7**, 354-362 (2013).
[2] A.E. Willner et al., J. Lightw. Technol. **35**, 660-680 (2014).
[3] R.-J. Essiambre et al., IEEE Photon. Technol. Lett. **25**, 539-542 (2013).
[4] F. Parmigiani et al., OFC (2017), Th1F.4.
[5] J. Slim and M. Gay, submitted at CLEO (2018).
[6] E. Nazemosadat et al., J. Lightw. Technol. **35**, 2810-2817 (2017).
[7] C. Guo et al., J. Opt. Soc. Am. B **35**, 545-551 (2018).
[8] R.P. Webb et al., Opt. Express **19**, 20015–20022 (2011).
[9] F. Da Ros et al., Opt. Express **21**, 28743-28750 (2013).
[10] M. Baillot et al., Opt Express **24**, 26930-26941 (2016).
[11] F. Poletti and P. Horak, J. Opt. Soc. Amer. B **25**, 1645-1654 (2008).

129.20.219.154 {ts '2018-06-28 08:55:15'}

Design of an Elliptical-Core Few-Mode Fiber for Mode-Independent Wavelength Conversion

Joseph Slim, Mathilde Gay, and Christophe Peucheret
Univ Rennes, CNRS, FOTON – UMR 6082, F-22305 Lannion, France
joseph.slim@univ-rennes1.fr

Abstract: An elliptical-core graded-index fiber that allows simultaneous intramodal wavelength conversion of mode-multiplexed signals is proposed. The fiber breaks the degeneracy between the LP_{11a} and LP_{11b} modes and prevents detrimental intermodal processes.
OCIS codes: (060.4370) Nonlinear Optics, fibers; (190.4380) Nonlinear Optics, four-wave mixing

1. Introduction

While the main benefit of optical communications is to achieve high data transmission capacities, the processing of the data generally needs to be performed in the electrical domain, thus potentially requiring multiple optical-to-electrical-to-optical conversions. However, some processing functionalities such as wavelength conversion or regeneration could be performed more efficiently directly in the optical domain, as investigated in the field of all-optical signal processing (AOSP) [1].

Mode-division multiplexing (MDM) is currently being investigated as a mean to scale up the capacity of optical communication systems beyond the current limits of single-mode fibers [2]. Most of the research efforts have been so far dedicated to the demonstration of mode-multiplexing devices and point-to-point links. However, it is clear that MDM systems could also benefit from the implementation of AOSP functionalities.

Parametric processes based on four-wave mixing (FWM) are particularly attractive for the wavelength conversion of complex optical signals exploiting the phase and amplitude dimensions (e.g. quadrature-amplitude modulation – QAM). Intermodal FWM has been investigated in a few-mode fiber (FMF) [3], and elliptical-core few-mode fiber (EC-FMF) [4]. In some scenarios, one may need to simultaneously wavelength-convert signals carried by all the modes supported by the transmission FMF. The use of photonic lanterns has been proposed to convert the MDM signals into single mode tributaries, followed by parallel single-mode wavelength conversions and single-to-multimode conversion [5]. The scheme is however cumbersome, and it would be beneficial to perform simultaneous multimode wavelength conversions in a single nonlinear medium for all the spatial modes of a FMF, which in fact appears to be quite challenging, because the phase matching condition needs to be satisfied for all the modes. However, mode-independent single pumped parametric amplifiers based on intramodal FWM has been investigated in a FMF [6] and EC-FMF [7], which enables many applications such as wavelength conversion and phase-sensitive amplification.

We present here the design of a highly nonlinear dispersion-shifted EC-FMF that breaks the degeneracy between the LP_{11a} and LP_{11b} modes and allows simultaneous intramodal wavelength conversion for the three modes, LP_{01} and $LP_{11a,b}$, in the same fiber, achieving a bandwidth conversion larger than 60 nm.

2. Fiber design

The proposed FMF is an elliptical graded-index core double-clad fiber. Figure 1(a) shows the refractive index profiles of the proposed fiber along the major and minor axis, with the resulting mode profiles shown in Fig. 1(b). The fiber has a central core doped with germanium with an alpha index profile, and a low index trench in the cladding. It is designed in such a way that the inverse group velocity differences between two modes $\Delta\beta_1$ are sufficiently large to prevent all intermodal processes [6], as shown in Fig. 2(a).

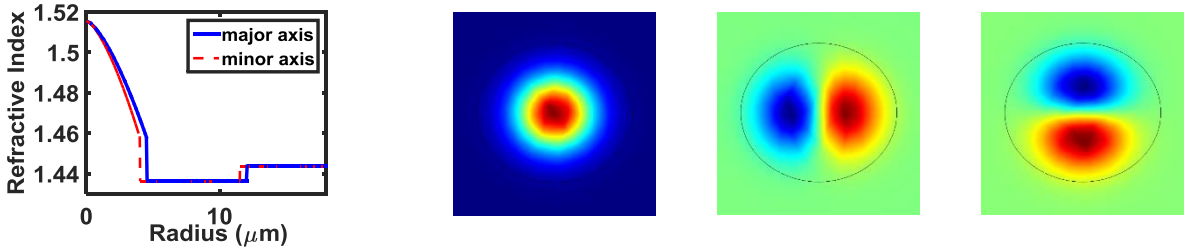

Fig. 1. (a) Refractive index profiles and (b) mode profiles of the three modes LP_{01}, LP_{11a}, and LP_{11b}.

The dispersions of the three modes LP_{01}, LP_{11a} and LP_{11b}, shown in Fig. 2(b), are calculated using a finite-element mode-solver (COMSOL), taking material dispersion properties into account, given by Sellmeier equations. The zero-dispersion wavelengths (ZDWs) of the three modes are shifted to 1.55 μm in the C-band, which makes it possible to simultaneously satisfy the phase matching condition for three intramodal FWM processes.

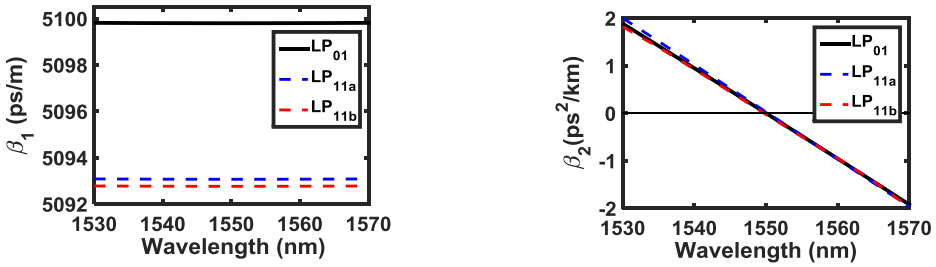

(a) (b)

Fig. 2. (a) Inverse group velocity of the three modes; (b) dispersion of the three modes.

3. Few-mode wavelength conversion

The propagation is simulated in the proposed fiber using the set of coupled nonlinear propagation equations [8]:

$$\frac{\partial A_p}{\partial z} = \frac{-\alpha}{2} A_p + i\,(\beta_{0p} - \beta_r)A_p - (\beta_{1p} - \frac{1}{v_{gr}})\frac{\partial A_p}{\partial t} + i\sum_{n\geq 2}\frac{\beta_{np}}{n!}\left(i\frac{\partial}{\partial t}\right)^n A_p + i\sum_{lmn=1}^{M} f_{lmnp}\frac{\gamma}{3}\left[\,(A_n^T A_m)A_l^* + 2(A_l^H A_m)A_n\right] \quad (1)$$

where A_p is the slowly varying envelope of the pth spatial mode, and M the number of spatial modes. β_{0p}, β_{1p} and β_{2p} represent the propagation constant, inverse group velocity and group-velocity dispersion (GVD), respectively. β_r and v_{gr} are the references propagation constant and group velocity, respectively. The nonlinear parameter γ is defined relatively to the fundamental spatial mode, with the effective area $A_{eff}^{01,01} = 14.8\ \mu m^2$, leading thus to nonlinear overlap factors $f_{01,01} = 1$, $f_{11a,11a} = 0.687$, $f_{11b,11b} = 0.676$, $f_{01,11a} = 0.471$, $f_{01,11b} = 0.454$ and , $f_{11a,11b} = 0.229$ that define the nonlinear coupling among spatial modes [8]. The fiber length is 1 km with 0.22 dB/km loss for all the modes. By fixing three pumps on the three modes near their ZDWs, the phase mismatches (Δβ) for the three intramodal and all intermodal processes in the fiber are shown in Fig. 3(a), with an expansion to the intramodal Δβ shown in Fig. 3(b). Large intramodal and low intermodal four-wave mixing effects are expected. Three signals propagate in the fiber on the three modes with a power of 0.0039 W each, while the power of each pump is set to 0.063 W. Fig. 3(c) shows the conversion efficiencies of the three intramodal processes, with values higher than -12 dB over a bandwidth larger than 60 nm for all three modes.

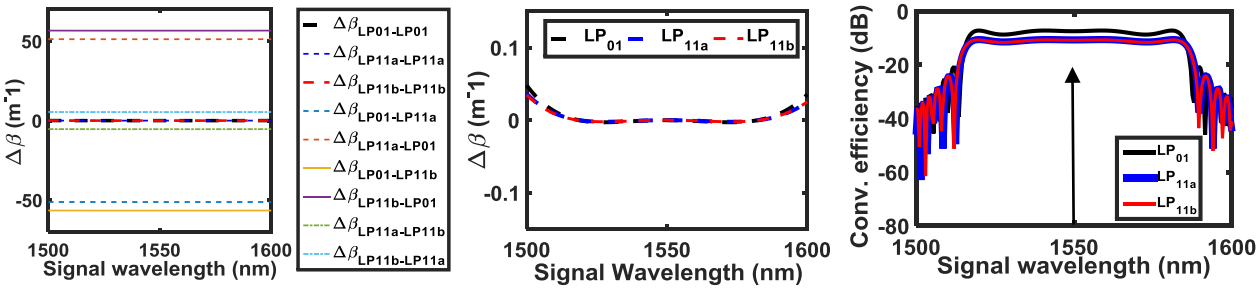

(a) (b) (c)

Fig. 3. (a) Phase mismatch of all intramodal and intermodal processes; (b) expansion to the phase mismatch of the intramodal processes; (c) conversion efficiencies of the three intramodal processes on the three modes. The arrow indicates the wavelength of the pumps

4. Summary

We have designed a highly nonlinear dispersion-shifted EC-FMF that breaks the degeneracy between the LP_{11a} and LP_{11b} modes, and allows the simultaneous wavelength conversion of the three modes LP_{01}, LP_{11a} and LP_{11b} over more than 60 nm bandwidth in the same fiber.

5. References

[1] A.E. Willner et al., J. Lightw. Technol. **35**, 660-680 (2014).
[2] D.J. Richardson et al., Nature Photon. **7**, 354-362 (2013).
[3] R.-J. Essiambre et al., IEEE Photon. Technol. Lett. **25**, 539-542 (2013).
[4] F. Parmigiani et al., OFC (2017), Th1F.4.
[5] J. Xu et al., Opt. Express **24**, 8926-8939 (2016).
[6] E. Nazemosadat et al., J. Lightw. Technol. **35**, 2810-2817 (2017).
[7] C. Guo et al., J. Opt. Soc. Amer. B **35**, 545-551 (2018).
[8] S. Mumtaz et al., J. Lightw. Technol. **31**, 398-406 (2013).

Design of a Few-Mode Fiber for Bandwidth Enlarged Intermodal Four-Wave Mixing

Joseph Slim, Mathilde Gay, Christophe Peucheret
Univ Rennes, CNRS, FOTON - UMR 6082, F-22305 Lannion, France
Author e-mail address: joseph.slim@univ-rennes1.fr

Abstract: *An elliptical core graded index dispersion shifted few mode fiber is designed in order to provide low dispersion and low differential mode delay between its modes, allowing bandwidth enlarged intermodal four wave mixing.*
Keywords: *Fiber based switching and nonlinear optical processing; Optical signal processing techniques for optical communications; Fiber based devices for space division multiplexing.*

I. INTRODUCTION

Mode-division multiplexing (MDM) is being investigated as a mean to scale up the capacity of optical communication systems, by exploiting spatially distinct channels in few-mode fibers (FMFs) [1]. While nonlinear effects need to be minimized in MDM transmission, they can be useful for all-optical signal processing (AOSP) applications, such as parametric amplification and wavelength conversion, based on intramodal or intermodal four-wave mixing (FWM).

In the intramodal case, the interacting waves occupy the same mode, and the FWM process is then limited within the same mode. Some FMFs have been designed to enable wide-bandwidth and efficient simultaneous intramodal FWM processes on multiple modes for parametric amplification [2] or wavelength conversion [3]. This is achieved by tailoring the refractive index profile of the fiber in a way to obtain close zero-dispersion wavelengths (ZDWs) for all the modes, while shifting them to the C-band. However, intermodal FWM between different spatial modes has always been limited between two frequency separation of the modes [4,5], given that the phase matching condition in this case depends not only on the group velocity dispersion (GVD) of the modes, but also on their inverse group velocities (IGVs), which limits the bandwidth of the conversion efficiency. Nevertheless, a step-index multimode fiber (MMF) was proposed for bandwidth enhancement for the intermodal phase conjugation (PC) process when modes LP_{01} and LP_{02} are employed [6], and a graded-index MMF was proposed for bandwidth enhancement for the intermodal Bragg scattering (BS) process when modes LP_{01} and LP_{11} are employed [7], only for signal to pump wavelength detuning belonging to the same mode.

We report here the design of a dispersion-shifted elliptical-core few-mode fiber (EC-FMF) that breaks the degeneracy between the modes LP_{11a} and LP_{11b}, and exhibits low GVD and low differential mode delay (DMD) between its modes LP_{01}, LP_{11a} and LP_{11b}. The fiber breaks the main intermodal FWM condition that requires operating over a specific frequency separation to obtain similar IGVs of the modes, and allows intermodal FWM over a broad bandwidth for both PC and BS processes simultaneously.

II. FIBER DESIGN

The proposed FMF is an elliptical graded-index core double-clad fiber. Figure 1(a) shows the refractive index profiles of the proposed fiber along the major and minor axes. The fiber has a central core doped with germanium with an alpha-law index profile, and a low index trench in the cladding.

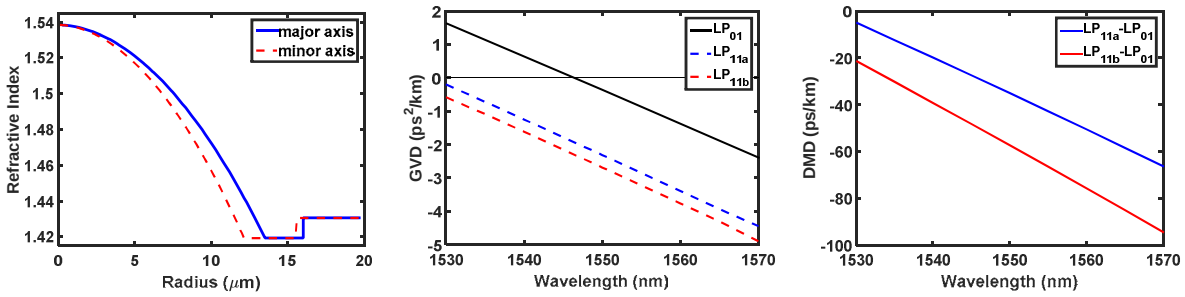

Fig. 1. (a) Refractive index profiles, (b) group velocity dispersion of the three modes and (c) differential mode delay of the modes LP_{11a} and LP_{11b} with respect to LP_{01}.

Figure 1(b) shows the GVD (β_2) of the three modes calculated using a finite-element mode-solver (COMSOL), where the GVDs of the two modes LP_{11a} and LP_{11b} are shifted to the anomalous regime, achieving then a small difference between the GVDs of the modes LP_{01}-LP_{11a} and LP_{01}-LP_{11b}. Similarly, the small DMD resulting from the IGV differences ($\Delta\beta_1$) of the modes LP_{11a} and LP_{11b} with respect to LP_{01}, can be visualized in Fig. 1(c). The small differences between the GVDs of the modes and the small DMD, will make it possible to obtain a wider band of intermodal FWM processes between the modes LP_{01}-LP_{11a} and LP_{01}-LP_{11b}.

©IEICE

III. INTERMODAL FWM

A. Theory

Assuming two pumps (P1) and (P2) on the modes LP_{01} and LP_{11a}, respectively, with a signal (S) on the mode LP_{01}, the two intermodal FWM processes that are to be studied are

$$\omega_I = \omega_{P1} - \omega_S + \omega_{P2} \quad (1)$$

$$\omega_I = -\omega_{P1} + \omega_S + \omega_{P2} \quad (2)$$

where Eq. (1) and Eq. (2) refer to the PC and BS processes, respectively. The corresponding phase matching conditions of each of the processes can be expressed from the propagation constants of the interacting waves. For instance, for PC

$$\Delta\beta\,(\mathrm{PC}) = \beta^{(01)}(\omega_{P1}) - \beta^{(01)}(\omega_S) + \beta^{(11a)}(\omega_{P2}) - \beta^{(11a)}(\omega_I) \quad (3)$$

By using Taylor series expansions of the propagation constants of each mode around a frequency ω_0, the phase matching condition can be expressed as,

$$\beta_1^{(01)}\left[\Delta\omega_{P1} - \Delta\omega_S\right] + \beta_1^{(11a)}\left[\Delta\omega_{P2} - \Delta\omega_I\right] = \frac{\beta_2^{(01)}}{2}\left[(\Delta\omega_S)^2 - (\Delta\omega_{P1})^2\right] + \frac{\beta_2^{(11a)}}{2}\left[(\Delta\omega_I)^2 - (\Delta\omega_{P2})^2\right] \quad (4)$$

where the constant β_1 is the IGV and β_2 is the GVD. Higher-order terms such as third-order and fourth-order dispersion are not shown in the equation, but will be considered later in the calculations. Eq. (4) shows that phase matching of the intermodal PC process is achieved when the difference between the IGVs and the GVDs of the two modes are small enough to satisfy the equalization, which is confirmed by the design of the fiber explained previously. A similar phase matching condition and same reasoning can be applied for the BS process.

The propagation is simulated in the proposed fiber using the set of coupled nonlinear propagation equations [8]:

$$\frac{\partial \mathbf{A}_p}{\partial z} = \frac{-\alpha}{2}\mathbf{A}_p + i\left(\boldsymbol{\beta}_{0p} - \beta_r\right)A_p - \left(\boldsymbol{\beta}_{1p} - \frac{1}{v_{gr}}\right)\frac{\partial \mathbf{A}_p}{\partial t} + i\sum_{n\geq 2}\frac{\boldsymbol{\beta}_{np}}{n!}\left(i\frac{\partial}{\partial t}\right)^n \mathbf{A}_p + i\sum_{lmn=1}^{M} f_{lmnp}\frac{\gamma}{3}\left[(\mathbf{A}_n^T\mathbf{A}_m)A_l^* + 2(\mathbf{A}_l^H\mathbf{A}_m)\mathbf{A}_n\right] \quad (5)$$

where A_p is the slowly varying envelope of the pth spatial mode, and M the number of spatial modes. β_{0p} is the propagation constant. β_{1p} and β_{2p} have been defined previously as the IGV and the GVD. β_r and v_{gr} are the references propagation constant and group velocity, respectively. The nonlinear parameter γ is defined relatively to the fundamental spatial mode, with the nonlinear overlap factors f_{lmnp} that define nonlinear coupling among spatial modes [8]. Fiber losses are included by the loss parameter α, and Eq. (5) can be solved numerically using the split-step Fourier method.

B. Intermodal FWM (LP_{01}-LP_{11a})

A pump P1 and a signal S propagate on the mode LP_{01}, with another pump P2 on the mode LP_{11a}. By fixing the wavelengths of P1 and S, and sweeping the wavelength of P2 across the C-L bands, the bandwidth of the conversion efficiency of the two intermodal FWM processes PC and BS will be studied. Figure 2(a-b) show the phase mismatch for the PC and BS processes respectively, for different wavelength separations between P1 and S ($\Delta\lambda_{P1\text{-}S}$) ranging from 0.1 nm to 0.5 nm when λ_{P1} is fixed at 1540 nm, while sweeping λ_{P2}. The phase matching is completely satisfied when λ_{P2} is 1565.19 nm for PC and 1564.67 nm for the BS process. Moreover, the closer λ_S is to λ_{P1}, the smaller is the phase mismatch. By fixing λ_{P2} at 1565 nm, and assuming continuous waves (CWs), the optical spectrum at the output of the fiber is shown in Fig. 3(a), for $\Delta\lambda_{P1\text{-}S}$ = 0.5 nm, where the propagation was calculated using Eq. (5), with a power of 100 mW for the pumps P1 and P2, and 3.9 mW for S, using a fiber length of 1 km, and 0.22 dB/km loss for all modes. The nonlinear parameter γ is defined relatively to the fundamental spatial mode, with an effective area $A_{eff}^{01,01}$ = 32 μm², leading to the nonlinear overlap factors $f_{01,01} = 1$, $f_{11a,11a} = 0.75$, $f_{01,11a} = 0.5$. Figure 3(b) shows the conversion efficiency for both processes when $\Delta\lambda_{P1\text{-}S}$ is fixed to 0.5 nm, while sweeping λ_{P2}. The full-width at half-maximum (FWHM) bandwidth of the conversion efficiency reaches 5 nm for both PC, and BS process. It confirms that the phase matching remains good enough to reduce the constraint of limited frequency separation between the modes met in previous work. The small wavelength shift between the conversion efficiencies of the two processes comes from the small difference between the phase matching wavelengths (as depicted in Fig. 2(a-b)). The same kind of calculation as in Fig. 3(b) is performed for different values of $\Delta\lambda_{P1\text{-}S}$ while sweeping λ_{P2}; the resulting conversion efficiency bandwidth is plotted in Fig. 3(c). It reaches 23 nm for both PC and BS processes when $\Delta\lambda_{P1\text{-}S}$ is reduced to 0.1 nm owing to a better phase matching in this case as depicted in Fig. 2(a-b), relaxing even more the frequency separation constraint between modes.

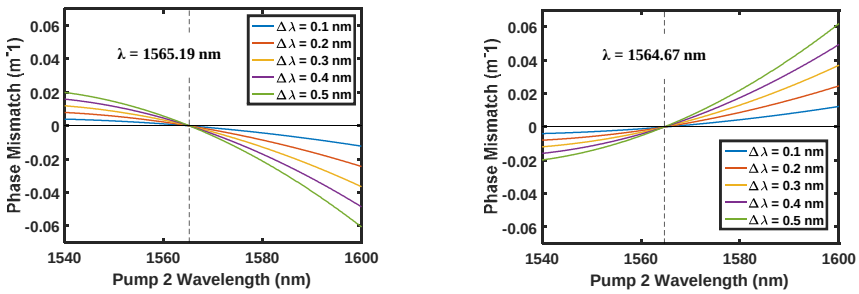

Fig. 2. (a) Phase mismatch for PC process and (b) for BS process for different $\Delta\lambda_{P1\text{-}S}$ ranging from 0.1 nm to 0.5 nm

©IEICE

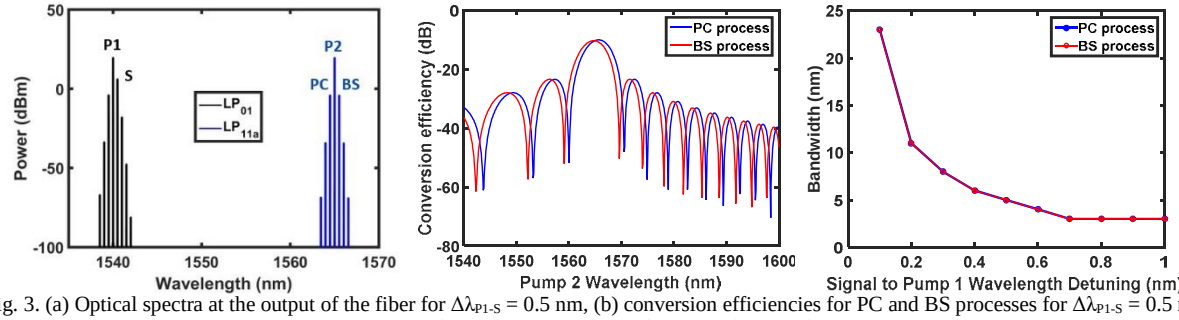

Fig. 3. (a) Optical spectra at the output of the fiber for $\Delta\lambda_{P1\text{-}S}$ = 0.5 nm, (b) conversion efficiencies for PC and BS processes for $\Delta\lambda_{P1\text{-}S}$ = 0.5 nm and (c) FWHM bandwidth of the two processes as a function of $\Delta\lambda_{P1\text{-}S}$, for the case LP_{01}-LP_{11a}

C. Intermodal FWM (LP_{01}-LP_{11b})

Similarly, the bandwidth of the conversion efficiencies of the PC and BS processes are studied for the case of LP_{01}-LP_{11b}, where a pump P3 on the mode LP_{11b} is swept across the C-L bands in this case, and the phase matching is completely satisfied at λ_{P3} around 1570 nm. The optical spectrum is shown in Fig. 4(a) for $\Delta\lambda_{P1\text{-}S}$ = 0.5 nm, where the nonlinear overlap factors are given by $f_{01,01}$ = 1, $f_{11b,11b}$ = 0.72, $f_{01,11b}$ = 0.49. The conversion efficiencies are shown in Fig. 4(b), where the FWHM bandwidth reaches 4 nm for both processes, when $\Delta\lambda_{P1\text{-}S}$ = 0.5 nm. While the bandwidth reached 23 nm for $\Delta\lambda_{P1\text{-}S}$ = 0.1 nm in the previous case, it now reaches 18 nm, as shown in Fig. 4(c). The bandwidths in this case are smaller than for LP_{01}-LP_{11a}, due to the dispersion parameters. For instance, the DMD resulting from the IGV differences between the modes LP_{01}-LP_{11b} shown in Fig. 1(c) is higher than the DMD between LP_{01}-LP_{11a}. Therefore, the smaller difference between the GVDs and IGVs of the modes LP_{01}-LP_{11a}, results in a broader bandwidth.

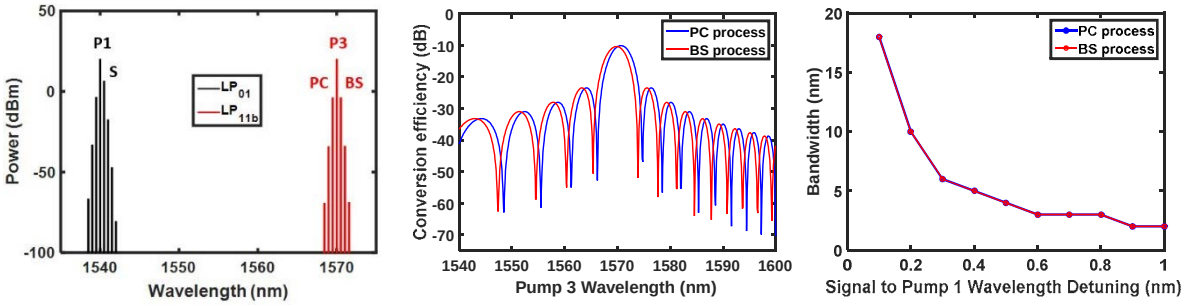

Fig. 4. (a) Optical spectra at the output of the fiber, (b) conversion efficiencies for both processes and (c) FWHM bandwidth for the case LP_{01}-LP_{11b}

IV. CONCLUSIONS

We have designed a dispersion-shifted EC-FMF that shows low dispersion and low DMD between its modes, and allows bandwidth-enlarged intermodal FWM between the modes LP_{01}-L_{11a} and LP_{01}-LP_{11b}, for both PC and BS processes.

ACKNOWLEDGMENT

This work was supported by Presidential Grant of University of Rennes 1

REFERENCES

[1] D. J. Richardson, J. M. Fini, and L. E. Nelson, “Space-division multiplexing in optical fibres,” Nature Photon., vol. 7, pp. 354–362, April 2013.
[2] E. Nazemosadat, A. Lorences-Riesgo, M. Karlsson, and P. A. Anderkson, "Design of highly nonlinear few-mode fiber for C-band optical parametric amplification," J. Lightw. Technol., vol. 35, pp. 2810-2817, July 2017.
[3] J. Slim, M. Gay, and C. Peucheret, "Design of an elliptical-core few-mode fiber for mode-independent wavelength conversion," CLEO PR (2018), W4E.4.
[4] R.-J. Essiambre, M. A. Mestre, R. Ryf, A. H. Gnauck, R. W. Tkach, A. R. Chraplyvy, Y. Sun, X. Jiang, and R. Lingle, Jr., "Experimental investigation of inter-modal four-wave mixing in few-mode fibers," IEEE Photon. Technol. Lett., vol. 25, pp. 539–542, March 2013.
[5] S. M. M. Friis, I. Begleris, Y. Jung, K. Rottwitt, P. Petropoulos, D. J. Richardson, P. Horak, and F. Parmigiani, “Inter-modal four-wave mixing study in a two-mode fiber,” Opt. Express, vol. 24, pp. 30338-30349, December 2016.
[6] M. Guasoni, F. Parmigiani, P. Horak, D. J. Richardson, “Novel Fiber Design for Wideband Conversion and Amplification in Multimode Fibers,” ECOC (2017), P1.SC1.12.
[7] O. F. Anjum, P. Horak, Y. Jung, M. Suzuki, Y. Yamamoto, T. Hasegawa, P. Petropoulos, D. J. Richardson, F. Parmigiani, “Bandwidth enhancement of inter-modal four wave mixing Bragg scattering by means of dispersion engineering,” APL Photonics, vol. 4, pp. 022902, December 2018.
[8] S. Mumtaz, R-J. Essiambre, and G. P. Agrawal, J. Lightw. Technol., vol. 31, pp. 398-406, February 2013.

©IEICE

UNIVERSITÉ DE RENNES 1

Titre : Traitement du signal optique pour les systèmes à multiplexage spatiale

Mots clés : télécommunication par fibre optique, multiplexage spatiale, traitement du signal tout-optique, optique non linéaire, mélange à quatre ondes

Résumé : Bien que l'avantage principal des communications optiques est de permettre la transmission des capacités élevées en multiplexant les longueurs d'onde, le traitement des données, par exemple en vue de régénération ou de routage, doit être effectué dans le domaine électrique, nécessitant ainsi des conversions optique-électrique-optique. Cependant, certaines fonctions de traitement pourraient être effectuées plus efficacement directement dans le domaine optique, ce qui est connu par le traitement de signal tout-optique. Comme des nouvelles techniques exploitant la dimension spatiale dans les fibres multimodes ont été proposées afin d'augmenter la capacité de transmission, une meilleure compréhension des effets non linéaires associés aux interactions multimodes est donc souhaitable. Cette thèse visait à explorer le traitement du signal tout-optique dans le multiplexage modal. En particulier, l'objectif était de démontrer comment les effets non linéaires dans les fibres multimodes pouvaient être utilisés pour manipuler les propriétés des signaux, de manière indépendante ou dépendante du mode. Deux types de fibres ont été conçus. La première permet de réaliser certaines fonctions de traitement de signal tout-optique pour tous les modes de la fibre individuellement et simultanément, en utilisant l'effet non linéaire mélange à quatre ondes intramodal. La deuxième fibre a été conçue de manière à realiser du traitement de signal tout-optique entre différents modes de la fibre, en utilisant le mélange à quatre ondes intermodal.

Title : Optical Signal Processing for Space Division Multiplexed Systems

Keywords : optical fiber communication, space-division multiplexing, all-optical signal processing, nonlinear optics, four-wave mixing

Abstract : While the main advantage of optical communications is to enable transmission of ultra-high capacities by multiplexing dozens of wavelength channels operating at high bit rates, the processing of the data, for instance in view of its regeneration or routing, needs to be performed in the electrical domain, thus requiring optical-to-electrical-to-optical conversions. However, some processing functionalities could be performed more efficiently directly in the optical domain, which is known as all-optical signal processing. As new techniques exploiting the spatial dimension in multimode fibers have been proposed in order to further increase the transmitted capacity, a better understanding of nonlinear effects associated with multimode interactions is desirable. This thesis aimed to explore paths for all-optical signal processing in mode-division multiplexing. In particular, the target was to demonstrate how nonlinear effects in multimode fibers could be used to manipulate the properties of optical signals, either in a mode independent way, or mode dependent way. Two types of fibers were designed. The first one allows to perform some all-optical signal processing functionalities for all the modes of the fiber individually and simultaneously, by using the intramodal four-wave mixing nonlinear effect. The second fiber was designed in a way to perform all-optical signal processing between different modes of the fiber, using intermodal four-wave mixing.